National Library
of Canada

Acquisitions and
Bibliographic Services Branch

395 Wellington Street
Ottawa, Ontario
K1A 0N4

Bibliothèque nationale
du Canada

Direction des acquisitions et
des services bibliographiques

395, rue Wellington
Ottawa (Ontario)
K1A 0N4

Your file Votre référence

Our file Notre référence

NOTICE

The quality of this microform is heavily dependent upon the quality of the original thesis submitted for microfilming. Every effort has been made to ensure the highest quality of reproduction possible.

If pages are missing, contact the university which granted the degree.

Some pages may have indistinct print especially if the original pages were typed with a poor typewriter ribbon or if the university sent us an inferior photocopy.

Reproduction in full or in part of this microform is governed by the Canadian Copyright Act, R.S.C. 1970, c. C-30, and subsequent amendments.

AVIS

La qualité de cette microforme dépend grandement de la qualité de la thèse soumise au microfilmage. Nous avons tout fait pour assurer une qualité supérieure de reproduction.

S'il manque des pages, veuillez communiquer avec l'université qui a conféré le grade.

La qualité d'impression de certaines pages peut laisser à désirer, surtout si les pages originales ont été dactylographiées à l'aide d'un ruban usé ou si l'université nous a fait parvenir une photocopie de qualité inférieure.

La reproduction, même partielle, de cette microforme est soumise à la Loi canadienne sur le droit d'auteur, SRC 1970, c. C-30, et ses amendements subséquents.

Canada

UNIVERSITY OF ALBERTA

PIPE FLOW EXPERIMENTS FOR THE ANALYSIS OF TWO–PHASE LIQUID–LIQUID PRESSURE DROP IN HORIZONTAL WELLS

BY

WILLIAM LEONARD PLAXTON

A THESIS

SUBMITTED TO THE FACULTY OF GRADUATE STUDIES AND RESEARCH

IN PARTIAL FULFILLMENT OF THE REQUIREMENTS FOR THE DEGREE OF

MASTER OF SCIENCE

IN PETROLEUM ENGINEERING

DEPARTMENT OF MINING, METALLURGICAL AND PETROLEUM ENGINEERING

EDMONTON, ALBERTA

FALL, 1995

National Library of Canada
Acquisitions and Bibliographic Services Branch
395 Wellington Street
Ottawa, Ontario
K1A 0N4

Bibliothèque nationale du Canada
Direction des acquisitions et des services bibliographiques
395, rue Wellington
Ottawa (Ontario)
K1A 0N4

Your file Votre référence

Our file Notre référence

THE AUTHOR HAS GRANTED AN IRREVOCABLE NON-EXCLUSIVE LICENCE ALLOWING THE NATIONAL LIBRARY OF CANADA TO REPRODUCE, LOAN, DISTRIBUTE OR SELL COPIES OF HIS/HER THESIS BY ANY MEANS AND IN ANY FORM OR FORMAT, MAKING THIS THESIS AVAILABLE TO INTERESTED PERSONS.

L'AUTEUR A ACCORDE UNE LICENCE IRREVOCABLE ET NON EXCLUSIVE PERMETTANT A LA BIBLIOTHEQUE NATIONALE DU CANADA DE REPRODUIRE, PRETER, DISTRIBUER OU VENDRE DES COPIES DE SA THESE DE QUELQUE MANIERE ET SOUS QUELQUE FORME QUE CE SOIT POUR METTRE DES EXEMPLAIRES DE CETTE THESE A LA DISPOSITION DES PERSONNE INTERESSEES.

THE AUTHOR RETAINS OWNERSHIP OF THE COPYRIGHT IN HIS/HER THESIS. NEITHER THE THESIS NOR SUBSTANTIAL EXTRACTS FROM IT MAY BE PRINTED OR OTHERWISE REPRODUCED WITHOUT HIS/HER PERMISSION.

L'AUTEUR CONSERVE LA PROPRIETE DU DROIT D'AUTEUR QUI PROTEGE SA THESE. NI LA THESE NI DES EXTRAITS SUBSTANTIELS DE CELLE-CI NE DOIVENT ETRE IMPRIMES OU AUTREMENT REPRODUITS SANS SON AUTORISATION.

ISBN 0-612-06524-3

Canada

UNIVERSITY OF ALBERTA

RELEASE FORM

NAME OF AUTHOR:	WILLIAM LEONARD PLAXTON
TITLE OF THESIS:	Pipe Flow Experiments for the Analysis of Two–Phase Liquid–Liquid Pressure Drop in Horizontal Wells
DEGREE FOR WHICH THESIS WAS PRESENTED:	MASTER OF SCIENCE
YEAR THE DEGREE WAS GRANTED:	FALL, 1995

Permission is hereby granted to the UNIVERSITY OF ALBERTA LIBRARY to reproduce single copies of this thesis and to lend or sell such copies for private, scholarly or scientific research purposes only.

The author reserves other publication rights, and neither the thesis nor extensive extracts from it may be printed or otherwise reproduced without the author's written permission.

(SIGNED) ..B Plaxton.....

PERMANENT ADDRESS:

1607, 12121 Jasper Ave.
Edmonton, Alberta
Canada T5N 3X7

DATED: ....april 24/95.....

UNIVERSITY OF ALBERTA

FACULTY OF GRADUATE STUDIES AND RESEARCH

The undersigned certify that they have read and recommend to the Faculty of Graduate Studies and Research, for acceptance, a thesis entitled PIPE FLOW EXPERIMENTS FOR THE ANALYSIS OF TWO–PHASE LIQUID–LIQUID PRESSURE DROP IN HORIZONTAL WELLS submitted by WILLIAM LEONARD PLAXTON in partial fulfillment of the requirements for the degree of MASTER OF SCIENCE in PETROLEUM ENGINEERING.

.....
Professor S.M. Farouq Ali (Supervisor)

.....
Professor R.G. Bentsen

.....
Professor J.M. Whiting (Chairman)

.....
Professor R. Rajaratnan (External Examiner)

DATED: April 24, 95

ABSTRACT

Recently, there has been a great deal of interest in the importance of wellbore pressure drop in horizontal wells. The pressure drop is important in horizontal well performance in certain situations, including low drawdown, overlying gas and/or underlying water zones, etc. Several contemporary studies have dealt with numerical or analytical solutions to the problem of determining wellbore pressure drop for single–phase wellbore flow. At the same time, ever increasingly sophisticated multiphase pipe flow models are being developed.

This study examines for the first time the effect of influx into a two–phase flow system, as occurs in many horizontal wells. The purpose of the present research was to analyze the pressure drop behaviour of two–phase oil–water flow in a physical pipe model with influx. A closed–loop pipe flow model was designed and constructed for the purpose of these experiments. Varying turbulent oil–water pipe flow and influx flow rates were generated using the apparatus, with the experiments recorded using photographic and video equipment. Comparative modeling of the experimental pressure drop and holdup data was performed using a recent and widely accepted pipe flow correlation model. A pipe flow correlation method was developed for analysis of oil–water flows. The significance of the influx disturbance with respect to wellbore pressure drop was examined. An analysis of the experimental results leads to the adaptation and development of field–scale predictive models for horizontal wellbore pressure drop and specific inflow profile.

Based on the experimental results, it is concluded that: the pipe flow correlation method examined provides adequate pressure gradient predictions for oil–water flows; an accelerational model of pressure drop across a single perforation is inadequate in its prediction capability; and at sufficiently high perforation–to–axial flow velocity ratios, the dominant factor determining the pressure drop across a single perforation is a constriction–disruption, or venturi–type effect.

ACKNOWLEDGEMENTS

I wish to express my gratitude and appreciation to Dr. S.M. Farouq Ali for his guidance and support throughout the course of this study.

I would also like to thank Mr. Quang Doan for his great support and encouragement, and for frequently sharing his academic wisdom.

Mr. Robert Smith provided a great deal of assistance in the design and construction of the physical model, for which I am extremely grateful.

The completion of this study would not have been possible without the financial support of Norcen Energy Resouces Ltd. and the Society of Petroleum Engineers Canadian Section.

Others who have aided me at various times during the course of this study include: Dr. W. Finlay, Dr. K. Nandakumar, Dr. J. Masliyah, Dr. R. Bentsen, Ms. Sara Thomas, John Czuroski, and Indranil Barman.

Finally, I would like to express thanks for the love, encouragement and support of my family and my girlfriend, Liane.

TABLE OF CONTENTS

ABSTRACT iv
ACKNOWLEDGEMENTS v
LIST OF TABLES viii
LIST OF FIGURES ix
NOMENCLATURE xiii
1. INTRODUCTION 1
2. STATEMENT OF THE PROBLEM 2
2.1 Experimental Objectives 2
3. LITERATURE REVIEW 4
3.1 Pressure Drop in Horizontal Wells 4
3.1.1 Influence of Fluid Entry Profile 4
3.1.2 Practical Numerical Models 5
3.1.3 Physical Models 9
3.1.4 Pressure Drop and Reservoir Simulation 12
3.1.5 Field Experience and Case Studies 14
3.2 Two–phase Pipe Flow 15
4. EXPERIMENTAL PROCEDURE 24
4.1 Objectives and Strategy of the Experimental Program 24
4.2 Model Design 25
4.3 Preparation and Calibration of Equipment 28
4.4 Experimental Procedure 32
5. DISCUSSION OF EXPERIMENTAL RESULTS 34
5.1 Pressure Gradient Data 34
5.1.1 Theory 34
5.1.2 Single–Phase Flow Data 38
5.1.3 Two–Phase Liquid–Liquid Flow 40
5.1.3.1 Numerical Predictive Approach 43
5.1.3.2 Hall and Hewitt's Correlation Method 52
5.1.3.3 Beggs and Brill Correlation Method 55
5.2 Pipe Flow With Confluent Influx 57
5.2.1 Single–Phase Pipe Flow With Flow Through A Single Perforation 57
5.2.2 Open–Hole Completion 60

5.2.3 Liquid–Liquid Pipe Flow With Flow Through A Single Perforation 62
5.2.4 Experimental Data and Model Predictions 66
5.2.5 Field–Scale Prediction Methods 73
5.2.5.1 Simple Constant Influx Open–Hole Model 73
5.2.5.2 Reservoir–Coupled Cased and Perforated Model 75
5.2.5.3 Reservoir–Coupled Open–Hole Model 79
5.2.5.4 Modified Coupled Open Hole Model 87
5.3 Holdup Data 91
6. FLOW REGIME OBSERVATIONS 99
6.1 Oil–Water Pipe Flow 99
6.2 Oil–Water Flow With Influx Flow Through A Perforation 103
7. SUMMARY AND CONCLUSIONS 110
8. RECOMMENDATIONS FOR FURTHER RESEARCH 112
APPENDIX A 121
A.1 Semi–Infinite Well Case 124
A.1.1 Laminar Flow 124
A.1.2 Turbulent Flow 125
A.2 Finite Well Case 129
A.2.1 Laminar Flow 129
A.2.2 Turbulent Flow 131
APPENDIX B 136
APPENDIX C 144
C.1 Colebrook and White Correlation C Program Listing 144
C.2 Gemmell and Epstein[40] Stratified Model 145
C.3 Field–Scale Predictive Models 151
C.3.1 Non–Reservoir–Coupled Constant Influx Model 151
C.3.2 Landman and Goldthorpe4 Cased and Perforated Model 152
C.3.3 Landman[8] Hypergeometric Model 153

LIST OF TABLES

Table 1: Dimensions of Model Apparatus 26
Table 2: Single–Phase Water Pressure Gradients 39
Table 3: Comparison of Correlations with Measured Values for Single–phase Experiments 40
Table 4: Oil–Water Pipe Flow Experimental Data 42
Table 5: Well and Production Data Used In Figures 33 – 35 73
Table 6: Well and Production Data Used in Figure 36 76
Table 7: Well and Production Data Used in Figures 37 – 40 77
Table 8: Well and Production Data Used in Figures 41 – 46 80
Table 9: Well and Production Data Used in Figures 47 – 50 88
Table 10: Flow Regime Data and Observations, Oil–Water Pipe Flow Experiments 100

LIST OF FIGURES

Figure 1(a): Uniform Flux Entry Profile 5
Figure 1(b): Triangular Profile, Decreasing Towards Producing End 5
Figure 1(c): Triangular Profile, Increasing Towards Producing End 5
Figure 2: Calibration Data for Progressing Cavity Pump #1 29
Figure 3: Calibration Data for Progressing Cavity Pump #2 29
Figure 4: Layout of Physical Apparatus Used for Experiments 31
Figure 5: Test Section Detail of Model Apparatus 31
Figure 6: Control Volume for Pipe Flow 34
Figure 7: Oil–Water Pressure Gradient Data from Pipe Flow Experiments 38
Figure 8: Oil–Water Pressure Gradient Data With Water Rate As Cross Parameter 41
Figure 9: Discretization of Pipe Cross Section 43
Figure 10: Nodal Representation of Pipe Cross Section 45
Figure 11: Critical Parameters Defining Relationship Between Interface and Pipe Wall 48
Figure 12: Measured and Predicted Oil–Water Pipe Flows, Oil Flow Rate = 6.08e–5 m^3/s 50
Figure 13: Measured and Predicted Oil–Water Pipe Flows, Oil Flow Rate = 9.20e–5 m^3/s 50
Figure 14: Measured and Predicted Oil–Water Pipe Flows, Oil Flow Rate = 1.31e–4 m^3/s 51
Figure 15: Measured and Predicted Oil–Water Pipe Flows, Oil Flow Rate = 1.70e–4 m^3/s 51
Figure 16: Measured and Predicted Oil–Water Pipe Flows, Oil Flow Rate = 2.01e–4 m^3/s 52
Figure 17: Best Fit Curve Drawn Through Measured Data for Oil–Water Experiments 54
Figure 18: Correlation of Martinelli Parameters for Oil–Water Pipe Flow Experiments 54
Figure 19: Comparison of Measured Pressure Gradient Data With Beggs and Brill[6] Correlation 56
Figure 20: Pipe Flow With Influx Flow Through Single Perforation 58
Figure 21: Pipe Section With Segment of Continuous Influx 61

Figure 22: Measured and Predicted Pressure Gradients for Oil–Water Experiments With Flow Through A Single Perforation (Oil Rate = 6.08 e–5 m^3/s) 66
Figure 23: Measured and Predicted Pressure Gradients for Oil–Water Experiments With Flow Through A Single Perforation (Oil Rate = 9.20 e–5 m^3/s) 67
Figure 24: Measured and Predicted Pressure Gradients for Oil–Water Experiments With Flow Through A Single Perforation (Oil Rate = 1.31 e–4 m^3/s) 67
Figure 25: Measured and Predicted Pressure Gradients for Oil–Water Experiments With Flow Through A Single Perforation (Oil Rate = 1.70 e–4 m^3/s) 68
Figure 26: Measured and Predicted Pressure Gradients for Oil–Water Experiments With Flow Through A Single Perforation (Oil Rate = 2.01 e–4 m^3/s) 68
Figure 27: Measured and Predicted Pressure Drops Across A Single Perforation, Oil–Water Pipe Flow Experiments (Oil Flow Rate = 6.08 e–5 m^3/s) 69
Figure 28: Measured and Predicted Pressure Drops Across A Single Perforation, Oil–Water Pipe Flow Experiments (Oil Flow Rate = 9.20 e–5 m^3/s) 70
Figure 29: Measured and Predicted Pressure Drops Across A Single Perforation, Oil–Water Pipe Flow Experiments (Oil Flow Rate = 1.31 e–4 m^3/s) 70
Figure 30: Measured and Predicted Pressure Drops Across A Single Perforation, Oil–Water Pipe Flow Experiments (Oil Flow Rate = 1.70 e–4 m^3/s) 71
Figure 31: Measured and Predicted Pressure Drops Across A Single Perforation, Oil–Water Pipe Flow Experiments (Oil Flow Rate = 2.01 e–4 m^3/s) 71
Figure 32: Pipe Flow With Rapid Flow Through Single Perforation 72
Figure 33: Predicted Field–Scale Pressure Profiles Assuming Constant Influx, With Fluid Viscosity As A Cross Parameter 74
Figure 34: Predicted Field–Scale Pressure Profiles Assuming Constant Influx, With Fluid Flow Rate As A Cross Parameter 74
Figure 35: Predicted Field–Scale Pressure Profiles Assuming Constant Influx, With Well Length As A Cross Parameter 75
Figure 36: Field–Scale Prediction Model Comparison 76
Figure 37: Field–Scale Pressure Profile Predictions for Cased and Perforated Horizontal Wells With Viscosity As A Cross Parameter 77

Figure 38: Field–Scale Pressure Profile Predictions for Cased and Perforated Horizontal Wells With Well Diameter As A Cross Parameter 78
Figure 39: Field–Scale Pressure Profile Predictions for Cased and Perforated Horizontal Wells With Permeability As A Cross Parameter 78
Figure 40: Field–Scale Pressure Profile Predictions for Cased and Perforated Horizontal Wells With The Perforation Density As A Cross Parameter 79
Figure 41: Field–Scale Pressure and Specific Inflow Profile Predictions for Open Hole Horizontal Wells With Well Diameter As A Cross Parameter 81
Figure 42: Field–Scale Pressure and Specific Inflow Profile Predictions for Open Hole Horizontal Wells With Well Length As A Cross Parameter..... 82
Figure 43: Field–Scale Pressure and Specific Inflow Profile Predictions for Open Hole Horizontal Wells With Permeability As A Cross Parameter 83
Figure 44: Field–Scale Pressure and Specific Inflow Profile Predictions for Open Hole Horizontal Wells With Viscosity As A Cross Parameter 84
Figure 45: Field–Scale Pressure and Specific Inflow Profile Predictions for Open Hole Horizontal Wells With Flow Rate As A Cross Parameter..... 85
Figure 46: Field–Scale Pressure and Specific Inflow Profile Predictions for Open Hole Horizontal Wells With The Blasius Exponent α As A Cross Parameter 86
Figure 47: Comparison of Landman Hypergeometric and Modified Predictive Methods for Open Hole Completed Horizontal Wells With Viscosity As A Cross Parameter..... 88
Figure 48: Comparison of Landman Hypergeometric and Modified Predictive Methods for Open Hole Completed Horizontal Wells With Well Diameter As A Cross Parameter 89
Figure 49: Comparison of Landman Hypergeometric and Modified Predictive Methods for Open Hole Completed Horizontal Wells With Well Length As A Cross Parameter..... 89
Figure 50: Comparison of Landman Hypergeometric and Modified Predictive Methods for Open Hole Completed Horizontal Wells With Permeability As A Cross Parameter 90
Figure 51: Measured Holdup Data For Oil–Water Pipe Flow Experiments 92
Figure 52: Pipe Geometry Parameters 94
Figure 53: Correlation of Martinelli Holdup Parameter by Hall and Hewitt[50] 96
Figure 54: Comparison of Measured and Predicted Holdup Values in the Form of the Martinelli Parameter, X..... 97

Figure 55: Experimental Oil–Water Flow Pattern Map Based on Observations of Russell, Hodgson and Govier36 and Reproduced from Govier and Aziz[29] 99
Figure 56: Oil–Water Experimental Flow Pattern Map Along With Classification and Description of Patterns 101
Figure 57: Experimental Oil–Water Flow Pattern Data 102
Figure 58: Oil–Water Flow Experiment 1, With No Flow Through Perforation 104
Figure 59: Oil–Water Flow Experiment 1, With Water Flow Through Perforation at 2.35 m/s 104
Figure 60: Oil–Water Flow Experiment 1, With Water Flow Through Perforation at 3.26 m/s 104
Figure 61: Oil–Water Flow Experiment 2, With No Flow Through Perforation 105
Figure 63: Oil–Water Flow Experiment 5, With No Flow Through Perforation 105
Figure 64: Oil–Water Flow Experiment 5, With Water Flow Through Perforation at 3.26 m/s 106
Figure 65: Oil–Water Flow Experiment 7, With No Flow Through Perforation 106
Figure 66: Oil–Water Flow Experiment 7, With Water Flow Through Perforation at 2.35 m/s 106
Figure 67: Oil–Water Flow Experiment 7, With Water Flow Through Perforation at 3.26 m/s 108
Figure 68: Oil–Water Flow Experiment 14, With No Flow Through Perforation 108
Figure 70: Oil–Water Flow Experiment 18, With No Flow Through Perforation 109
Figure 71: Oil–Water Flow Experiment 18, With Water Flow Through Perforation at 3.26 m/s 109
Figure A1: Influx and Well Flow in Horizontal Well 122
Figure A2: Turbulent Flow in a Semi–Infinite Horizontal Well 129
Figure A3: Numerical Solution for Turbulent Flow in Finite Horizontal Well 135
Figure B1: Bipolar Co-oridinate Transformation using Conformal Mapping 136
Figure B2: Typical Node in the Numerical Grid 142

NOMENCLATURE

a	constant
A	cross sectional area of pipe or wellbore, m^2
b	constant
c	constant
C	constant
C	input volume fraction
d	perforation diameter, m
D	wellbore or pipe diameter, m
E	in situ volume fraction
f	friction factor
F	momentum force, N
g	acceleration due to gravity, m/s^2
h	height of interface between phases, m
h	step length
H	holdup ratio
i,j	nodal coordinates, pipe cross section
l	constant
I	momentum, N
J_s	specific productivity index, $m^3/(s.m.Pa)$
k	permeability, m^2
K	constant of integration
K	coefficient
L	length of wellbore, m
LHS	left–hand side of equation
log	base 10 logarithm
ln	natural logarithm
$\dot{m}$	mass flow rate, kg/s
n	constant
n	number of perforations or segments
P	pressure, Pa
ΔP	pressure drop, Pa
q	volumetric flow rate, m^3/s

Q	total volumetric flow rate, m^3/s
R	pipe or wellbore radius, m
R^2	correlation coefficient, least squares fit
Re	Reynolds number
RHS	right–hand side of equation
S	perimeter of section of duct, m
S	source term
t	time, s
u	velocity in the direction of flow, m/s
U	average velocity in the direction of flow, m/s
V	in situ volume, m^3
vfrf	volumetric flow rate factor
w	width of interface between phases, m
w	Cartesian co-ordinate plane
x	Cartesian co-ordinate in the direction of the well axis, m
y	Cartesian co-ordinate in the direction of the well height, m
z	Cartesian co-ordinate in the direction of the well width, m

Subscripts:

0	initial
0,1, 2,3,4	relative node locations for pipe cross section discretization
1	designates a position upstream of a perforation or zone of influx
2	designates a position downstream of a perforation or zone of influx
a	accelerational
A	designates a phase, normally the less dense phase
B	designates a phase, normally the more dense phase
c	corrector
e	constant pressure boundary
eq	equivalent
full	flowing full of designated phase
F	frictional
G	gaseous
i	interface
L	liquid
m	mixture, or averaged quantity

M	accelerational confluence
O	oil phase
p	perforation
p	predictor
s	superficial
s	open-hole influx
tp	two-phase
w	wall friction
w	well boundary
W	water phase

Greek Symbols:

α	Blasius equation exponent
γ	angle subtended by the intersection of the interface and pipe walls, radians
Δ	difference
ε	the effective height of the roughness elements of a pipe, m
λ	pressure gradient, Pa/m
μ	fluid viscosity, Pa.s
ρ	fluid density, kg/m^3
τ	shear stress, N
ϕ	Martinelli pressure gradient parameter
η	substitute variable for predictor–corrector method
ξ	substitute variable for predictor–corrector method
Φ	bipolar co-ordinate
Ψ	bipolar co-ordinate
θ	angle between pipe or wellbore and horizontal, radians
X	Martinelli holdup parameter
ω	bipolar co-ordinate plane

Other:

"tilde", as in the ~ above a symbol, refers to a dimensionless quantity.

1. INTRODUCTION

Horizontal wells have gained wide acceptance in the petroleum industry in recent years. Many studies have been carried out that examine the superior recovery performance of horizontal wells, especially in comparison with their conventional counterparts. In their analytical models, researchers originally treated the horizontal wellbore as being analogous to a vertical fracture having infinite or near infinite conductivity. Dikken[3] was the first to demonstrate the potential limitations to production imposed by pressure drop across horizontal wells. That study initiated a great deal of interest in wellbore hydraulics that has carried forward until the present.

A pressure drop in a horizontal well will always occur as a necessity for flow. Whether the condition in a particular well will be problematic is another matter, and that is not the focus of this study. This study is an attempt to contribute to the understanding of horizontal wellbore hydraulics. The study is expressly concerned with the mechanisms of the pressure gradient, in both single–phase liquid and two–phase liquid–liquid flow, and with or without confluent influx from flow through a single perforation. For this purpose a scaled pipe model was designed and constructed, and a series of experiments was carried out. Also, a small number of numerical programs were developed in order to make comparisons with the experimental data and to aid with the analysis.

2. STATEMENT OF THE PROBLEM

The broad objectives of this research are to examine experimentally the effects of varying two phase (liquid–liquid) flow conditions within a section of a horizontal well. Of specific interest is the measurement of the holdup of the more dense liquid phase and especially the pressure drop across the horizontal well section. Most of the currently available horizontal well solutions do not consider the along–wellbore pressure drop. Recently, the importance of this parameter to horizontal well production has been much discussed, leading to several theoretical studies of the problem. The problem cannot be reasonably studied in an actual horizontal well, although a compilation of available data would prove useful. Similarly, when influx is included and a mechanistic basis is desired, the problem proves to be a difficult one to solve numerically for multiphase flow. This leaves an experimental program as the most reasonable approach given the time frame and funding constraints.

2.1 Experimental Objectives:

Objectives of the research are to include the following:

1. Design and construct a suitable experimental apparatus, including a scaled physical model of a representative section of a horizontal well, to be used for the present series of experiments as well as for future related research.

2. Perform a series of experiments under varying rate conditions. Photography and video media are to be used to record the visual aspects of the experiments. This will allow a presentation of the flow regimes and the mixing effect of influx. Stabilized rate and pressure data are to be recorded. Holdup of the more dense phase is also to be measured.

3. Analyze the results of the experiments. Compare the data with other similar pipe flow studies where applicable. Compare the data with the results of single phase (and possibly, two phase liquid–liquid) simulations.

4. Present conclusions, based on the analysis of the results, regarding the effects of varying phase rates and influx on the holdup and the pressure drop across the well

section. Comment on the validity of the results, their usefulness in practical application, and the relative importance of along–wellbore pressure drop under two–phase liquid–liquid flow conditions.

5. Present recommendations for further research, including suggestions for modifications and improvements to the model design for more extensive studies.

3. LITERATURE REVIEW

There are two main subject areas in the published literature that are of interest in relation to the subject at hand. The first of these is the recent research specifically dealing with the effects and mechanisms of pressure drop in horizontal wells. The second group includes mostly two–phase pipe flow research. Both groups include physical, theoretical and numerical modeling and, to a lesser extent, field case studies. Much of the vast literature occurring outside of these narrow groups, such as research conducted in multiphase flow in conventional (vertical or deviated) wellbores, and productivity and pressure transient analysis studies of horizontal wells, have not been included here.

3.1 Pressure Drop in Horizontal Wells

3.1.1 Influence of Fluid Entry Profile

Joshi[1] illustrated various possible fluid entry profiles along the length of a horizontal well (Figure 1). Three different fluid entry profiles were modeled: (a) uniform influx profile along the well; (b) triangular profile with the influx decreasing towards the producing end of the well; and (c) triangular profile with the influx increasing towards the producing end of the well. Case (a) is a simplification of the influx profile anticipated in theory for horizontal wells that are treated as line sources with infinite conductivity, in homogeneous, isotropic reservoirs with constant productivity index. (The actual profile would be slightly parabolic with higher influx at the well ends due to the effects of partial penetration of the well lengthwise in the reservoir).

Case (b) is often cited as the expected fluid entry profile in horizontal wells where there was skin damage due to drilling. The idea is that during drilling fines from the drilling mud are continuously flowing into the surrounding formation because of the over–pressure condition used to control the well. The flux of the fines into the reservoir causes skin damage, the degree of which would logically be decreasing linearly toward the toe of the well. However, a profile more like Case (c) is far more frequently encountered in published production profiles; i.e., typically more production tends to come from the heel or producing end of horizontal wells. This behaviour clearly contradicts the expected pattern if only skin damage from drilling mud fines is considered. It is therefore likely that other mechanisms are at work. It seems plausible, for example, that the greatest fluid influx would occur nearest to the pump in an artificial lift condition[2]. More importantly,

the Case (b) fluid entry profile would result from a significant pressure drop along the horizontal wellbore, in comparison with the other two profiles.

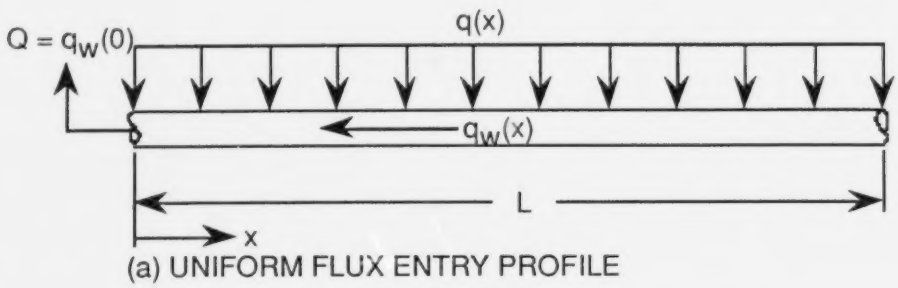

Figure 1(a): Uniform Flux Entry Profile

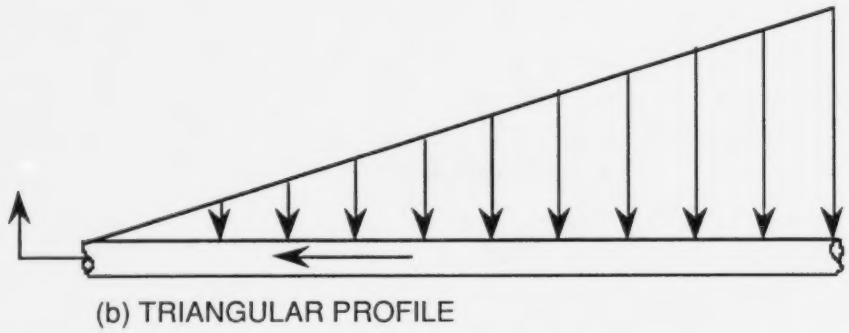

Figure 1(b): Triangular Profile, Decreasing Towards Producing End

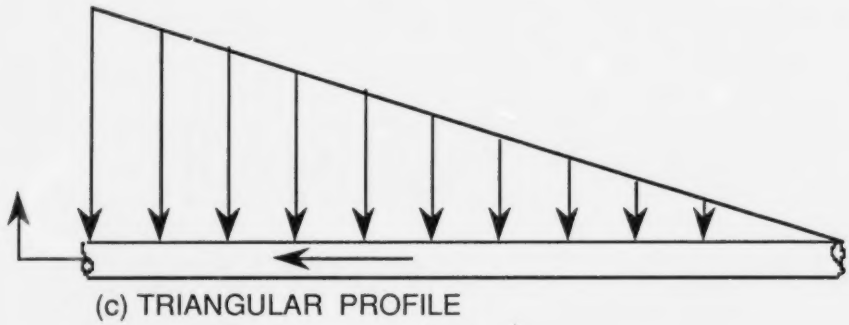

Figure 1(c): Triangular Profile, Increasing Towards Producing End

3.1.2 Practical Numerical Models

In his paper entitled "Pressure Drop in Horizontal Wells and Its Effect on Their Production Performance", Dikken[3] presented the first (semi–)analytical model to predict the frictional pressure drop in a horizontal well due to turbulent single–phase wellbore

flow. A second order differential equation coupling single–phase turbulent well flow with stabilized and isothermal reservoir flow was derived and solved for various boundary conditions, thus predicting the frictional pressure gradient along the horizontal wellbore for an open–hole completion. The formulation used is dependent on a simple correlation for the turbulent pipe flow friction factor, provided by Blasius, (as cited in Dikken[3])

$$f = 0.3164\,\mathrm{Re}^{-\alpha} \qquad (3\text{–}1)$$

Here α is used to describe the degree of roughness of the pipe, with $\alpha = 0$ for the limiting case of a rough surface and $\alpha = 0.25$ for a smooth surface. The parameter Re is the Reynolds number. Dikken concluded that the reduced drawdown due to turbulent flow along the wellbore may result in the total production rate reaching a certain critical value as a function of wellbore length, with the consequence of achieving no further gain in production rate beyond it. Thus, the important conclusion was reached that under certain conditions absolutely no benefit may be obtained by drilling horizontally beyond this critical well length.

Dikken's[3] paper was the origin of the current focus on pressure drop and hydraulics in horizontal wells in the published literature. Landman and Goldthorpe[4] demonstrated the potential problems where horizontal wells are used to minimize water or gas coning. The pressure drop across the well length causes preferential influx into the well closer to the production end, and therefore premature breakthrough. The authors provided a simple single–phase numerical solution to the problem of frictional pressure drop in horizontal wells. Their approach allows for any number and size of cylindrical perforations intercepting the wellbore. The distribution of the perforations may also be varied. The model couples the Darcy flow into each perforation with the one dimensional momentum equations for pipe flow. A correlation for turbulent pipe flow wall friction factor was used which incorporates the relative roughness of the well, and is therefore better suited than the Blasius formula used by Dikken in that the roughness may be modeled quantitatively. The authors used the model to determine the optimal perforation distribution under differing production requirements. Also provided was a comparison with Dikken's pressure drop results. The model does not include a provision for either laminar flow or pressure drop due to the accelerational force. The Landman and Goldthorpe[4] model has been coded by this author in Mathematica for this study, and extended to include these features. The main limitation of this type of model is the computational work required for problems involving large numbers of perforations, since the program must invert an nxn matrix, with n equaling the number of perforations used.

The Landman and Goldthorpe[4] model was later extended by Marett and Landman[5] to include the pressure field due to individual perforations distributed along an inclined well in an anisotropic homogeneous reservoir bounded by no–flow or constant pressure boundaries. The original model was adapted to allow the well length to be made up of two or more sections of varying inclination, radius, perforation size and density, phase angle, etc. Perforation skin factors and multiphase flow within the wellbore may also be included. Multiphase flow was incorporated by employing the Brill and Beggs[6] two–phase flow pressure drop correlation. The study demonstrated a method of horizontal well design and completion optimization given knowledge of certain parameters. For example, vertically oriented perforation phasing was found to be beneficial for many cases, as was increasing the shot density towards the toe of a horizontal well in order to overcome the loss of pressure drawdown. Various methods of varying the completion design of a horizontal well to optimize production for tertiary recovery were examined earlier by Doan[7].

Dikken's model for a horizontal well was extended by Landman[8], who showed that the predictor–corrector numerical method used by Dikken to solve for the well rate of a finite length horizontal well under a turbulent flow condition is unnecessary. This extended model allows for adaptation to perforated wells, with or without selectively perforated intervals, but does not require as much computational effort as the Landman and Goldthorpe model mentioned above. The model is semi–analytical, allowing easy incorporation into a reservoir simulator if the specific inflow to the well is made constant. The second order non–linear ordinary differential equation defined by Dikken is solved for the case of a constant productivity index using an implementation of the Gauss hypergeometric function. Two out of three of the productivity index, the total flow rate and the drawdown must be specified beforehand, and the third parameter is solved for as part of the solution. The productivity index may be provided via any of the commonly used equations for horizontal wells. This routine has also been coded as a part of the current study. Landman demonstrated that Dikken's method may also be extended to the more realistic case of variable productivity index (i.e., variable with respect to distance along the wellbore) if a shooting numerical method is used to solve the resulting second–order boundary–value problem. An explanation of shooting methods is provided by Gerald and Wheately[66].

Joshi[1] devoted the last chapter of his text on horizontal well technology to pressure drop in a horizontal well. Several simple calculations were made to determine the pressure drop under different conditions. The examples demonstrated that the pressure drop developed along a horizontal wellbore is generally insignificant with respect to the

drawdown of the well. Joshi's calculations were conservative in that the entire volume of pumped (or flowing) fluid entered the well from its distant end, thus allowing for the maximum possible pressure drop occurring from stabilized, fully developed horizontal pipe flow. However, the assumption of fully developed pipe flow adequately modeling an actual horizontal well is questionable. Influx from perforations in a cemented and perforated horizontal well will cause a flow disturbance and may prevent the main flow (perpendicular to the influx, running along the well) from becoming fully developed. Friction factors in the developing flow region can be several times larger than those determined assuming a fully developed flow condition. Thus, the calculated pressure drops using this assumption could be too low.

Joshi noted that Dikken's usage of the Blasius equation for the turbulent flow friction factor in a pipe is disputable. Joshi argued that, since the Blasius exponent $\alpha = 0$ corresponds with a Moody's friction factor of 0.3164, which is more than three times the highest value available on the Moody's chart of friction factors for rough pipes, a degree of roughness coinciding with $\alpha = 0$ is highly unrealistic at best, given that the condition is fully developed pipe flow. But this is not the condition in a horizontal well, and Dikken perhaps considered that the radial inflow at the completions will result in values for α that are closer to zero than to 0.25. Joshi, on the other hand, recommended estimating the roughness from Moody's chart, or taking it from the liner manufacturer's data if available. This approach neglects the effects of influx on the friction factor, and thus on the pressure drop.

An approach very similar to that of Dikken's was taken by Novy[9]. Flow in the reservoir and in the wellbore was linked via a volume balance resulting in a boundary value problem. The solution for the case of laminar liquid flow is analytical, and was provided. For all other cases considered, i.e., turbulent single–phase liquid and gas flows, the calculations were made numerically, using a routine provided in the IMSL Fortran library. The method used to determine the friction factor for the wellbore flow is a correlation that generates Moody friction factors for any degree of dimensionless pipe roughness, as had been recommended by Joshi[1]. Novy demonstrated that Dikken's results were probably pessimistic at the rough pipe wall limit, due to the use of a non–standard form of the Blasius equation for the friction factor. To account for the effect of radial influx on the friction factor, Novy relied upon the experimental findings of Kinney[10] and Olson and Eckert[11], and found that this effect was negligible for the cases considered.

A more general semi–analytical model coupling horizontal wellbore and reservoir fluid flows was developed by Ozkan *et al.*[12]. The paper notes several significant shortcomings of Dikken' s model: the assumptions of steady flow in the reservoir and

constant productivity index per unit wellbore length precludes general use of the model for horizontal well performance and transient pressure behaviour; the assumption of negligible pressure gradients in the reservoir parallel to the well axis results in an underestimation of the reservoir pressure drop, and therefore an exaggeration of the impact of wellbore pressure drop; finally, the flow resistance term used by Dikken is the result of a specific and not well validated correlation for the friction factor (this is the most frequent criticism of Dikken's approach). The model presented addresses these areas while still remaining isothermal and single–phase. The most interesting and unique aspect of their model is the treatment of the transient response of the horizontal well within the reservoir. The authors also point out the inadequacy of the current approach of modeling horizontal wellbore flow behaviour using pipe flow correlations. Pipe flow models cannot account for frictional losses generated by open–hole completions or other completion techniques. Hence, the need exists for further physical and numerical modeling of the effect of the influx on wellbore friction. This model was extended by Sarica *et al.*[13] for use with gas reservoirs, using the pseudopressure function. Allowance for produced fluid compressibility was shown to necessitate the inclusion of the accelerational component of the momentum equation for accurate pressure gradient predictions.

Tiefenthal[14] presented a numerical model for the prediction of two–phase (oil–water or oil–gas) or three–phase super–critical (i.e., subsequent to gas breakthrough) production rates from horizontal wells drilled in reservoirs located above active aquifers and/or beneath a gas cap. The model is based on an extension of the two–phase gravity drainage model for critical rates in two–phase cases as presented by Konieczek[15]. Tiefenthal notes that to achieve a prediction accuracy beyond a "first approximation", the effect that the pressure gradients within the aquifer or gas cap have on the cone shape must be considered, especially when the expected friction losses in the wellbore will be the same order of magnitude as that of the drawdown.

3.1.3 Physical Models

Ihara[16], and Ihara, Brill and Shoham[17] designed and constructed a coupled reservoir/horizontal well physical model. The focus of the study was the two–phase flow behaviour of a horizontal well and its interaction with the reservoir. Also developed by the author was a simulator to model this flow behaviour, using "mechanistic" calculations. The well model consisted of 1-in. (0.0254 m) pipe with a horizontal (7.92 m) and vertical (2.74 m) section. The reservoir was not represented by porous media but by a tank with compressed air for the driving force. Air and water were mixed and then produced through

manifolds to various completions in the horizontal section. Air and water flow rates, the pressure drop along the horizontal section, the drawdown from the tank to the horizontal section, and the tank and separator absolute pressures were measured during steady–state flow. Void fraction and liquid holdup were not measured.

The simulations demonstrated the following:

1. The assumption of infinite wellbore conductivity is frequently invalid, especially with two–phase gas–liquid flow. If the pressure drop along the wellbore is significant with respect to the drawdown, influx along the wellbore will be affected such that the influx will decrease upstream until a point is reached beyond which no influx occurs. This means that the effective, or producing, well length can be significantly shorter than the drilled length.
2. The effect on influx of different reservoir permeabilities. Higher permeabilities lead to greater influx near the producing end of the horizontal well, resulting in production being independent of the well length.
3. A larger diameter wellbore or tubing means a much smaller pressure drop along the wellbore, and thus a more uniform fluid influx.
4. Large producing gas–oil ratios result in a more significant well pressure drop. This is due to increased flowing friction associated with continuously expanding gas in the horizontal wellbore in the direction of flow.
5. For the case examined, increasing the perforation shot density to greater than two shots per foot contributed very little to increasing oil production. This is an indication of the limit of reservoir flow into the wellbore due to perforations.

Ihara and Shimizu[18] examined the effects of accelerational pressure drop in a horizontal wellbore. "Accelerational pressure drop" refers to the additional pressure drop resulting from influx via the perforations or slots of the completion used. A well model experimental program and simulation development was performed in the study. Experiments were run with both one and two–phase (air and water) flows, within the wellbore and as influx. The computer modeling employed homogeneous fluid flow instead of separate constituent flows. The results of the study demonstrated an increased pressure drop due to confluent fluid influx; the magnitude of the pressure drop varied with confluent influx position, rate, water concentration, and main (wellbore) flow rate and concentration. The effects on liquid holdup were also measured. Good agreement was reached between the experimental results and those from the computer model.

Three different approaches to completion design were investigated by Brekke and Lien[19] for optimization of horizontal well oil production via reduction of along the wellbore pressure loss. The field case used for the model is a (relatively) thin, highly permeable oil

rim underlain by an active aquifer and located beneath a large gas cap, thus requiring a limited drawdown to delay water and gas coning. The completion techniques examined included: reducing the perforation or flow opening density and reducing the drag for the remaining perforations or flow openings in order to reduce the flowing friction along the wellbore; redistributing the pressure loss by inserting a production tubing stinger a certain distance into the horizontal well; or creating an optimal sand face pressure profile by introducing flow restrictions between the sandface and the liner. All three methods were found to improve significantly the rate of recovery of oil in their simulations.

Su and Gudmundsson[20] measured the friction factor of perforation roughness in pipes scaled similarly to casing used in horizontal wells. The experiments were conducted using single–phase oil for flow velocities corresponding to Reynolds numbers between 30,000 and 100,000. Flow through the perforations was not considered, but was to be included in a later study. It was found that pipe roughness increased linearly with perforation density and also with the perforation/casing diameter ratio. Perforation phasing and cavity depth were found not to have a significant effect on the friction factor. A useful empirical method of estimating the friction factor in horizontal wells with perforation roughness was obtained.

Very interesting and elaborate experiments were conducted by Ihara *et al.*[21] to study the effects of open completion pipe roughness and influx on the single–phase pressure gradient behaviour of horizontal wells. A flow loop was constructed utilizing a rectangular (90 mm wide by 30 mm high) test section, with transparent acrylic resin side panels (allowing both visual observation of the flow and laser–Doppler measurements of velocity), and top and bottom panels of a porous material with box–shaped porous media blocks located above and below. A smooth walled inlet channel with the same dimensions as the test section was located just upstream of the test section, for comparison of pressure gradients. The inlet channel and the test section were connected lengthwise within the flow loop, providing single–phase axial flow conditions. The influx rate into the test section is controlled via the pressure in the porous blocks. High flow rate experiments were conducted without influx flow to enable the determination of the friction factor of the rough porous wall, and with the influx flowing at different rates to determine the pressure loss associated with the influx disturbance—both under varying axial flow rate conditions. A one–dimensional model for the pressure loss was developed, in which the authors defined a dimensionless pressure gradient term made up of two parts: the loss due to friction and the loss due to the accelerational confluence (i.e. the disturbance caused by the influx flow), as illustrated below.

$$\tilde{\lambda} = 2\frac{\Delta P/L}{\rho u_0^2} D_{eq} \qquad (3\text{–}2)$$

$$\tilde{\lambda} = \tilde{\lambda}_M + \tilde{\lambda}_F \qquad (3\text{–}3)$$

where:

$\Delta P/L$	is the dimensional pressure gradient across the test section
D_{eq}	is the equivalent circular diameter of the (rectangular) test section
ρ	is the density of the fluid
u_0	is the axial velocity at the entrance of the test section, and
$\tilde{\lambda}$, $\tilde{\lambda}_M$, $\tilde{\lambda}_F$	are the total, accelerational confluence and frictional dimensionless pressure gradient terms, respectively.

Pressure gradients were found to increase quite uniformly in the test channel with increasing constant influx rates. The frictional component of the dimensionless pressure gradient was obtained by comparing the pressure gradients measured in the inlet (smooth) and test channels. By subtracting the friction loss of the test channel, the magnitude of the accelerational pressure drop due to the confluence was evaluated. The pressure gradient across the test section due to the accelerational confluence was seen to increase almost linearly with the influx velocity, and the total pressure gradient was found to depend weakly on the Reynolds number of axial flow.

3.1.4 Pressure Drop and Reservoir Simulation

Among the first attempts to adequately simulate multiphase flow in a horizontal wellbore while incorporating the pressure drop along the well were those provided by Stone, Edmunds and Kristoff[22] and Islam and Chakma[23]. The former study modeled the dynamics of gravity drainage in a heavy oil reservoir, using Darcy's law to describe fluid flow in the reservoir and momentum, mass and energy balances of emulsion (oil and water) and gas in the wellbore. A simple productivity index model was used to model the radial inflow into the horizontal wellbore. In the latter study, a series of experiments were performed to model three–phase fluid flows in horizontal wellbores with influx, for three mineral oils of viscosity 10, 400 and 1000 mPa.s, respectively, and one crude oil (1000 mPa.s). The presence of perforations was shown to affect the wellbore flow regime to a

great extent, such that pipeline correlations and simulations should not (it was argued) be relied upon for predictions of realistic horizontal wellbore flow behaviour. Also demonstrated, through a coupling of their numerical model with a three–phase compositional reservoir simulator, was the effect of wellbore pressure drop upon oil production estimates for several cases. In particular, the elimination of the pressure drop in the well leads to overestimation of the oil production rate. This is accentuated in cases with overlying gas and/or underlying water zones, as breakthrough is hastened by the inclusion of the along–wellbore pressure drop.

Folefac *et al.*[24] and Folefac, Issa and Wall[25] coupled a drift–flux model for two–phase gas–liquid horizontal wellbore flow with a reservoir simulator. The focus of this study was the influence of wellbore diameter and specific productivity on well pressure gradient. The drift–flux assumption, as described in Wallis[26], means that one phase must be discontinuous and carried within the other (continuous) phase.

Briggs[27] described a method for preparing input data for reservoir simulators allowing for the calculation of multiphase pressure drops in horizontal and near–horizontal wells. The method utilizes the Beggs and Brill[6] correlation for multiphase flow in pipes. The correlation relies on a multiphase friction factor determined by adjusting upward the friction factor for smooth pipes. The effects of well roughness, diameter and gas–oil ratio were examined, and a comparison was made using data from a well that had been production logged. The pressure gradient calculation matched the production log data fairly well.

A more typical approach to the modeling of both the flow within the horizontal wellbore and the flow in the immediate vicinity of the well for the purpose of reservoir simulation was taken by Collins *et al.*[28]. The wellbore was represented by cylindrical grid blocks which have as additional parameters permeabilities and relative permeabilities in order to incorporate the pressure drop and liquid holdup predicted by multiphase pipe flow correlations. The correlations used are those provided by Govier and Aziz[29]. The detailed simulation of flow around the wellbore is handled using a system of fine elliptical and hyperbolic grids. The effect of the inclusion of the detailed inner and outer wellbore flows is demonstrated to be a significant difference in cumulative production, and especially a difference in the nature of the influx or production profile, agreeing with the results of many workers.

A high level of discrepancy between several of the most well–known and used reservoir simulators with regards to the pressure drop along a horizontal wellbore has been reported by Nghiem *et al.*[30]. The paper reports the results of comparisons of simulation runs performed by fourteen organizations on a problem involving production from a

horizontal well in a reservoir where coning tendencies were important. All the participating simulators used some form of multiphase correlation for the calculation of the wellbore pressure drop. The simulators offered remarkably similar results for all aspects of production behaviour, with the notable exception of wellbore pressure drop. The study was not able to identify superior prediction performance for wellbore hydraulics in any of the simulators compared. It was noted that runs with, and without the wellbore hydraulics included often give comparable cumulative production results over long times, but that the inclusion of these calculations and the resultant pressure drop along the wellbore yield a substantially different drainage pattern along the wellbore.

3.1.5 Field Experience and Case Studies

The results of an on–going long term production test of an offshore horizontal well in the Troll field, offshore Norway, were reported by Lein *et al.*[31]. The well was positioned in a 22 m oil column located between a large gas cap and an active aquifer. After 6 months of production, the water–cut had stabilized at about 30% and no gas breakthrough had occurred. The production rate was about four times the average from offset vertical wells. Significant friction losses were anticipated during production at upwards of 4000 sm^3/d. This was allowed for in the numerical model set–up for the production test evaluation. This was one of the first documented attempts of including the effects of pressure drop along a horizontal well in a numerical simulation.

Korady, Renard and Lemonnier[32] described a method for coupling a modern hydraulic pipeline model with a three–phase, three–dimensional and fully implicit reservoir simulator, for the purpose of accurately predicting the effects of multiphase pressure gradient on the production behaviour. The pipeline correlation model used was modified slightly to allow for the roughness of the wellbore from perforations and influx. This modification was made by introducing a source term to represent the local perturbation due to the influx and its associated additional pressure drop. The resulting model was validated by comparison with Dikken's[3] model. The authors performed case studies with their model to demonstrate the implications of the pressure gradient on short and long term production strategies in different situations. They found that the pressure drop in the well could influence the well rate and water and/or gas cresting behaviour of the system significantly, especially in high productivity reservoirs.

The importance of friction pressure loss in horizontal wells of the Troll field was further studied by Seines *et al.*[33]. This included a full–scale section of liner being lab tested to determine its effective absolute roughness. Flow was directed both along and

perpendicular to the liner over a large range of conditions. The experiments resulted in absolute effective roughness values between 0.4 and 0.8 mm for the given section of liner. An analytical model for pressure loss was developed and incorporated into a commercially available three–dimensional, three–phase reservoir simulator. The multiphase flow condition was treated simply as a homogeneous flow, with average values used for density and viscosity. This assumption is somewhat reasonable under expected flowing conditions in horizontal wells in the Troll field, i.e., at very high liquid and gas rates. Simulation results demonstrated that: variation of liner roughness between the two extremes considered reasonable affected cumulative production over a one year time period by 10%; the maximum initial rate that could be achieved was 50% higher for a 6-in. (0.152 m) ID liner than for a 4-in. (0.102 m) liner; for the cases examined, the length of horizontal well that contributed 90% of the total initial inflow varied from 430 to 630 m (total length of horizontal well modeled is 800 m), indicating that the last few hundred metres of horizontal well length offered little benefit; however, when longer terms were examined it was noted that as production proceeded, pressure loss became less important and the longer wells began to produce significantly more oil. Also, the impact of pressure loss would typically be much less than for the Troll case for several reasons. Most importantly, the pressure loss would be less where lower production rates occur, and the impact of the loss would be less significant where the ratio of the reservoir drawdown to the along–wellbore pressure gradient is higher.

3.2 Two–phase Pipe Flow

One of the first and most cited papers on two–phase gas–liquid flow was written by Lockhart and Martinelli[34]. The authors developed an empirical correlation for pressure drop and holdup in horizontal flow. The correlation is based on the hypothesis that the pressure gradient for simultaneous flow of two–phases is equal to that which would occur if one of the phases were flowing alone, multiplied by a predictable factor. This factor was correlated as a function of the ratio of single–phase pressure gradient of the liquid to the single–phase pressure gradient of the gas phase for a specified flow regime. The flow regimes considered were laminar–laminar, laminar–turbulent, turbulent–laminar and turbulent–turbulent. Although the physical interpretation of the correlation is that of a separated flow structure, it was based on experimental data encompassing many flow regimes. The Lockhart–Martinelli parameters are defined as follows:

$$X = \sqrt{\frac{\left(\Delta P/L\right)_{L_s}}{\left(\Delta P/L\right)_{G_s}}} \qquad (3\text{–}4)$$

$$\phi_L = \sqrt{\frac{\left(\Delta P/L\right)_{tp}}{\left(\Delta P/L\right)_{L_s}}} \qquad (3\text{–}5)$$

where,

$\left(\Delta P/L\right)_{L_s}$ is the pressure gradient that would occur if the liquid were flowing alone at a velocity equal to its superficial velocity,

$\left(\Delta P/L\right)_{G_s}$ is the pressure gradient that would occur if the gas were flowing alone at a velocity equal to its superficial velocity, and

$\left(\Delta P/L\right)_{tp}$ is the pressure gradient that occurs with both phases flowing in the pipe.

The superficial velocity of either of the phases is simply the volumetric flow rate of that phase divided by the pipe cross sectional area.

Many modifications of the correlation have been proposed, and the Lockhart–Martinelli parameters are still widely used by researchers to describe two–phase flow behaviour, including liquid–liquid flow. A good introduction to the correlation and to many of the modifications is provided in Govier and Aziz[29].

The practical objective of much of the early research work regarding two–phase liquid–liquid flow was to reduce pumping power requirements in oil pipelines. As early as 1949 a process was patented for the introduction of water into heavy oil pipelines in order to reduce their power requirements (Clark and Shapiro[35]). Russell, Hodgson and Govier[36] observed the simultaneous flow of oil and water in a transparent horizontal pilot pipeline 28-ft. (8.53 m) long and 0.806-in. (0.0205 m) in diameter. A wide range of oil and water volumetric flow rates were generated and the flow behaviour, pressure gradient and holdup data were analyzed. The oil used had a viscosity of 18 mPa.s, and stratified flow conditions were observed for the laminar flow rates. It was determined that it was possible to reduce the pressure gradient of a given oil flow by the addition of about 10% water (by volume). However, this reduction was only a factor of 1.2 for Reynolds

numbers ranging between 10 and 400. Outside this region the pressure gradient (and thus the power requirements) were increased by the addition of the water. From the holdup experiments it was concluded that in the laminar region, holdup is a function of input water fraction and viscosity only, while in the turbulent region it is also a function of superficial water velocity.

The simultaneous flow of two immiscibly stratified liquids between two parallel plates, and concentrically in a circular pipe, was analyzed by Russell and Charles[37]. The optimum interface position giving the minimum pressure gradient and power requirement was determined analytically for both the parallel plate and pipe cases for various viscosity ratios of the fluids. A maximum pressure gradient reduction factor approaching 4 was predicted for the parallel plate case for very a high viscosity ratio and for laminar flow. The limitation of their approach is the assumption of the occurrence of a concentric (also referred to as annular) flow regime for two–phase liquid–liquid pipe flow, in which the less viscous water forms a uniform annulus in the region of high shear rate next to the pipe wall. This regime is ideal for pressure gradient reduction, but does not usually occur where there is an appreciable density difference between the two fluids (as is the usual case with oil and water).

The occurrence of a concentric flow regime may be encouraged greatly by either of two methods: by machining a rifle on the inside of the pipe wall, a rotational motion may be imparted on the flowing fluids, thus causing concentric stratification via gravitation; or, by eliminating the density difference between the two fluids. The latter approach was taken by Charles, Govier and Hodgson[38]. They investigated the behaviour of equal density oil–water mixtures in a horizontal pipe experimental apparatus for three different commercial Newtonian oils, of viscosity 6.3, 16.8 and 65 mPa.s, respectively. The density of each oil was modified by the addition of carbon tetrachloride in order to make it equivalent to the water density at the ambient experimental temperature. They found that the resulting oil–water flow patterns were mostly independent of the oil viscosities. They also found that the in situ holdup was higher than the no–slip holdup when the oil phase was in contact with the pipe wall. The best pressure gradient reduction factors were found to be between 1.7 (for the 6.3-mPa.s oil) and 10 (for the 65-mPa.s oil) by varying the input oil–water ratio. An economic analysis of scaling up the experimental method used to raise the oil densities for commercial pipeline purposes was not included.

Charles and Redberger[39] were the first workers to publish a numerical approach to the problem. They analyzed stratified oil–water flow in pipes using a discretization of the Navier–Stokes equations (this technique will be discussed in further detail in a later section). Assumptions included laminar, incompressible and perfectly stratified flow, with

zero fluid velocity at the pipe wall and no slip between the phases at the interface. The authors found maximum values of the pressure gradient reduction factor between 1.12 and 1.31 for oils varying in viscosity between 4 and 1500 mPa.s. Their results matched very well with the experimental data of Russell, Hodgson and Govier[36], as did the results of Gemmell and Epstein[40], who performed very similar numerical work at about the same time. Dimensionless solutions of the velocity profiles were determined for viscosity ratios of 1, 10, 100 and 1000, at eight positions of the horizontal interface, using a two–dimensional finite difference method with a Cartesian grid superimposed on the cross–section. The velocity profiles were used to calculate theoretical hold–up ratios, pressure gradient and power reduction factors. Gemmell and Epstein's[40] numerical pressure gradient data failed to match closely the experimental data of Russell, Hodgson and Govier[36] only where the experimental flow data occurred beyond the laminar flow region for either or both liquid phases. The pressure gradient reduction factors (defined as the ratio of the pressure gradient for the flow of the more viscous phase alone to the pressure gradient of the two–phase system, the volumetric flow rate of the more viscous phase being the same for each case) did not match particularly well with the aforementioned experimental data.

Analytical expressions were derived for the velocity distribution of laminar stratified oil–water flows in rectangular conduits by Charles and Lilleleht[41]. The authors noted the discrepancy in reported pressure gradient reduction factors between the experimental results of Russell, Hodgson and Govier[36] and the numerical results of Charles and Redberger[39] and Gemmell and Epstein[40]. This discrepancy was thought to be largely due to meniscus effects occurring in the small diameter experiments, and not considered in the theoretical treatments. For example, if the small diameter plastic pipe used for the experiments were preferentially oil–wet, the meniscus at the pipe wall would curve downward somewhat, causing a higher pressure gradient. The authors' approach was to minimize this effect by conducting their study using rectangular conduits of various aspect ratios. Despite these design precautions, their experimental pressure gradient reduction factor data still fell about 10% below their theoretical values. This difference was attributed partly to observed small flow disturbances caused by roughnesses in the meniscus at the interface between the phases. The same authors[42] described a method for the use of stereophotogrammetry to measure the amplitudes and wavelengths of wave patterns generated at the interface between two liquid layers flowing co–currently in a closed rectangular conduit. Stereophotogrammetry is familiar to many as the method used to interpret structural relief from aerial photographs; it has the advantage over other methods of wave measurement in flow experiments in that no probes of any kind interfere with the flowing liquids.

Charles and Lilleleht[41,43] recognized the usefulness of the Lockhart–Martinelli parameters for correlating stratified, immiscible liquid–liquid two–phase flows in horizontal pipes. This correlation technique was shown by the authors to represent well the data from several previous investigations, involving various oil and water Reynolds numbers. In this way the data from experiments of varying geometries, with fluids of various superficial velocities, viscosities and densities, etc., and even different flow regimes, may be brought together with little deviation from a best–fit curve.

Mechanistic approaches have been used to predict turbulent stratified flow parameters in horizontal flow. Govier and Aziz[29] and Agrawal *et al.*[44] calculated the frictional pressure drop in horizontal pipes as in single–phase flow using a geometrical model for the flow cross–section.

Taitel and Dukler[45,46] proposed a model for predicting flow regime transition incorporating a two–fluid model for two–phase stratified gas–liquid flow in circular pipes. The complex geometry of stratified flow in a pipe prevents an exact analysis. This difficulty was resolved by using an approach similar to that of Agrawal *et al.*[44], in which an equivalent diameter for the gas and liquid phases is determined. The gas is treated as a flow in a closed channel bounded by the pipe walls and the gas–liquid interface; the liquid as a flow in an open channel bounded only by the pipe walls. This is essentially a one–dimensional approach, since both phases are treated as bulk flow, and the detailed velocity profile structure and the shear stresses are calculated via empirical correlations based on the average velocity.

The next important model of two–phase gas–liquid pipe flow behaviour was developed by Shoham and Taitel[47]. The model predicts the liquid velocity field, holdup and pressure drop given the gas and liquid flow rates, physical properties, pipe size and angle of inclination. The two–dimensional momentum equation for fully developed (turbulent) flow of the liquid phase was solved using a finite–difference scheme combined with a novel gridding technique. A bipolar co-ordinate frame was utilized via conformal mapping, enabling the computing mesh to be fitted to the wall of the pipe and to the rectilinear gas–liquid interface simultaneously. The height of the liquid surface was not known in advance; hence, the solution had to be iterative, with the mesh being adjusted at each iteration to conform to the position of the interface. The effects of turbulence within the liquid were simulated using the eddy viscosity model, in which a mixing length scale characterizes the turbulent shear stresses. This is problematic in pipe flow problems, as the mixing length is difficult to quantify. The gas phase was treated as a bulk flow, with the wall and interface shear stresses being calculated from friction factors determined by the

average gas velocity. Since details of the gas phase flow behaviour were omitted from consideration, empirical correlations could not be entirely avoided.

These concerns were addressed by Issa[48], who developed a numerical model similarly based upon a bipolar grid across the pipe cross section, but which also adapted the use of a two–phase, low Reynolds number k–epsilon model for turbulence. The turbulence model used was first presented by Akai *et al.*[49], for use with their work on air–mercury planar flows in open channels. Issa numerically solved for the axial velocity, the turbulence energy, and the turbulence dissipation rate, for both phases in purely stratified pipe flow. The pressure drop across the pipe length and the height of the interface was also computed. The applicability of this type of turbulence modeling (which embodies an effective viscosity assumption) to two–phase flows is questionable. More sophisticated approaches to multiphase turbulence modeling, including those that solve for the Reynolds stresses directly, are awaited.

Hall and Hewitt[50] applied both the Taitel and Dukler model, and a numerical model similar to that of Issa, to the generation of Martinelli holdup parameter data for two–phase liquid–liquid stratified laminar flows in pipes and between flat plates. It was shown that while the Taitel and Dukler model predicts dependence of the holdup on the Martinelli parameter only, the more exact numerical solution demonstrates an additional dependence on the viscosity ratio of the two liquids. This conclusion is not surprising, as the variability of the viscosity ratio is really only a large factor in liquid–liquid flows (the ratio can vary from less than 1 to very large values, whereas in gas–liquid flows the ratio rarely exceeds 0.1).

As a result of carefully compiling and amending the models of several workers, including much of his own work, Barnea[51] was able to present a unified general model for steady–state two–phase gas–liquid flow in pipes for any inclination or size. The basis of the unified model is the incorporation and description of the mechanisms of flow boundary transitions. Largely based on this work and the work that preceded it are two comprehensive mechanistic models for two–phase flow; one for flow in horizontal and near horizontal pipelines developed by Xiao *et al.*[52], and the other for upwards flow in wellbores, presented by Ansari *et al.*[53]. Both models were found to provide superior pressure drop and liquid holdup predictions compared with the available correlations over a large database of cases. These results were independently supported for the case of the Ansari wellbore model in a case study presented by Pucknell *et al.*[54], in which the model was again compared with the available correlations using 246 data sets collected from eight producing oil and gas fields.

Cengel *et al.*[55] performed scaled pipe flow experiments using dispersions containing various volume fractions of a petroleum solvent dispersed in water. A dispersion is an unstable emulsion, defined as an emulsion which can separate into the original immiscible phases within a reasonable period of time while at rest. Dispersions can exhibit Newtonian or non–Newtonian rheological behaviour, depending on each specific oil–water system. Dispersion behaviour is further complicated by phase inversions, in which the dispersed phase switches to the continuous phase. Arirachakaran *et al.*[56] performed a large number of experiments with oil–water dispersions flowing in horizontal pipes. A correlation was proposed by the authors for the prediction of the inversion point of the oil–water dispersion. Pressure drop along the pipe was found to increase abruptly at the inversion point where the external (continuous) phase changes from water to oil. Two pressure drop prediction methods were presented, one each for stratified and homogeneously dispersed oil–water flows. Also, an experimental oil–water flow pattern map was presented. The assumption of homogeneous flow implies that there is no slip between the phases, and therefore no holdup. Volume–averaged values of the mixture density, superficial velocity and viscosity were calculated, in order to use them within a single–phase–type pressure drop equation to determine an approximation of the two–phase pressure drop. This is also the approach taken by the Brill and Beggs[6] pipe flow correlation. The equations used for dispersed oil–water flows are as follows. The volume fraction of the liquid A supplied to the system (i.e., the input volume fraction) is

$$C_A = \frac{q_A}{q_A + q_B} \tag{3–6}$$

where the q's refer to the input volumetric flow rates of liquids A and B (water and oil, for example). The in situ volume fraction of the fluid A may be measured in different ways, but it is given by

$$E_A = \frac{V_A}{V_A + V_B} = \frac{A_A}{A_A + A_B} \tag{3–7}$$

where the V's refer to the in situ volumes, and the (non-subscript) A's refer to the in situ cross sectional areas of each phase, respectively. For the case of no slip between the phases, the input and in situ volume fractions are identical. Thus,

$$C_A = E_A \tag{3–8}$$

The averaged density and viscosity of the flow are given by

$$\rho_m = C_A \rho_A + (1 - C_A)\rho_B \tag{3–9}$$

and

$$\mu_m = C_A \mu_A + (1 - C_A)\mu_B \tag{3–10}$$

where ρ and μ refer to the density and viscosity, respectively, and the m subscript indicates the averaged value. The averaged superficial velocity is given by

$$u_S = \frac{q_A + q_B}{A} \tag{3–11}$$

The two–phase pressure gradient is then

$$\left(\frac{\Delta P}{L}\right)_{tp} = \frac{f_m \rho_m u_S^2}{2D} \tag{3–12}$$

The friction factor f may be determined by known correlations or the Moody chart for single–phase flow, using the averaged quantities for density and viscosity (further description of the friction factor is given in Chapter 5).

The preceding equations are valid for dispersed oil–water flows, where the oil is dispersed as droplets in the continuous water phase. Beyond a limiting value of the in situ volume fraction of the oil phase inversion must be considered, which causes an upward kick in the pressure gradient. This kick is not modeled in the preceding pressure drop equation. The limiting in situ volume fraction of oil is given by[57]

$$E_{B\lim} = 0.5 + 0.1108 \log(1000 \times \mu_B) \tag{3–13}$$

For stratified flow, the following equations are used by Arirachakaran *et al.*[56] and Brill and Beggs[6] to determine the two–phase pressure gradient. Again it is assumed that no relative velocity exists between the fluid phases, and a smooth interface is also assumed. For this case, the pressure loss is given by the sum of the wall shear stresses for the tube wall wetted by the water and the oil. The average wall shear stress is

$$\tau_m = \tau_A \frac{S_A}{S} + \tau_B \frac{S_B}{S} \tag{3–14}$$

In this equation S is the perimeter of the tube, the subscripts indicate the perimeter wetted with each fluid phase. It is assumed that the wall shear stresses τ_A and τ_B can be evaluated using single–phase flow laws; i.e., they are calculated assuming the volume flow rate in the pipe to be entirely the A or B fluid phase, respectively. The frictional pressure loss of the two–phase flow is

$$\left(\frac{\Delta P}{L}\right)_{tp} = \frac{S_A}{S}\left(\frac{\Delta P}{L}\right)_A + \frac{S_B}{S}\left(\frac{\Delta P}{L}\right)_B \tag{3–15}$$

where the single–phase pressure drops are calculated as follows:

$$\left(\frac{\Delta P}{L}\right)_A = \frac{f_A \rho_A u_S^2}{2D}, \text{ and } \left(\frac{\Delta P}{L}\right)_B = \frac{f_B \rho_B u_S^2}{2D} \tag{3–16}$$

Stapelberg and Mewes[57] performed a series of oil–water pipe flow experiments as part of a three–phase flow study. Their oil–water data were found to differ quite markedly from values computed using the method of Arirachakaran *et al.*[56] and Brill and Beggs[6] just described, especially in the regions of stratified flow and dispersed oil drops in water. Stapelberg and Mewes[57] proposed the use of a correlation using Lockhart–Martinelli two–phase pressure loss parameters.

$$\phi_B^2 = \frac{X^{1.5589} + X^{0.5589} + a}{X^{1.5589} + aX} \tag{3–17}$$

where a is a constant dependent on the diameter of the tube. The authors used values of 1.10 and 0.46 for their experiments with pipe diameters of 23.8 mm and 59.0 mm, respectively.

4. EXPERIMENTAL PROCEDURE

4.1 Objectives and Strategy of the Experimental Program

The purpose of pursuing an experimental approach was to make physical measurements of pressure drop and holdup behaviour while allowing for observation of the flow regime and the flow disturbance caused by the influx stream for various flow rates.

Project budget and physical laboratory space limitations were limiting factors in the model design. The model length is approximately 12.2 metres, including the hose connection to the separation tank. It was decided to examine the influx behaviour of a single perforation only, in order to allow the most complete analysis possible, and keeping in mind more complex inflow patterns could be added later.

The model length was close to being as long as was possible within the laboratory space provided. The model tubing is approximately 1-in. ID (0.0254 m). This diameter was thought to be a good compromise. An ideal diameter for both highly turbulent flow and for the best scaling considerations would be significantly smaller, given the limited model length and considering the lengths of typical horizontal wells. However, going with a smaller diameter pipe would have made visual observations much more difficult.

A key point of discussion with respect to the original design considerations was the nature of the flow regime expected for two–phase liquid–liquid flow within a horizontal wellbore. Will the oil and water form an emulsion, either within the reservoir or once mixed in the wellbore? Or will the two fluids segregate under the influence of gravity, and flow in a somewhat stratified manner within the wellbore? These are difficult matters to consider, and it is likely that the answers would be case–dependent. Parameters such as each fluid viscosity and density, etc., reservoir porosity, permeability, pressure and temperature, the well and completion geometry, and the nature of the flow into the wellbore would all affect the resultant flow regime.

Consider that the oil and water zones are typically separated physically in the reservoir. This is a factor that would make emulsion formation less likely. Conversely, it is known that water tends to finger through oil banks in the reservoir under water drive, thereby promoting a high degree of contact between the phases and thus a greater likelihood of emulsion formation. Also, the turbulent mixing effects of both rapid axial two–phase flow and the confluent influx over various intervals of the horizontal wellbore would tend to promote greater contact.

Physical experiments involving both emulsions and separate fluid flows have been reported (see 3. Literature Review). The cases where the emulsion flows were studied demonstrated, however, the difficulty of maintaining the emulsion intact for any length of time once the mixing has ceased. Especially for the case of very light, low–viscosity oils, once the emulsion is flowing horizontally beyond the mixing tank, the constituent fluids rapidly separate because of gravity segregation and the mutual immiscibility of the fluids. Published field studies of production logs of horizontal wells also typically support a separate flow model. The difficulty of acquiring satisfactory production log data for multiphase flow in horizontal wells has been widely reported[63,64]. The inability of current production logging equipment to handle horizontally stratified flows is one of the chief difficulties. If a given flow were behaving homogeneously (e.g., as an emulsion), the production logging tools would not be nearly so handicapped. It was finally decided that the physical model for this project would be used to study primarily stratified, or at least initially separate flows, instead of emulsions. This approach required the use of two pumps and variable speed drives, one each for each fluid. There is no reason why future studies could not involve emulsion flow, if desired.

Preliminary Reynolds number calculations were performed in order to gauge the capacity requirements of the pumps used, and the associated power requirements of the pump drives. A suitable arrangement was specified which would allow for a wide range of volumetric flow rates, with ultimate capacities more than capable of sustained rates sufficient for fully turbulent flow in the model for each of the main pumps alone. The pumps themselves and the drive ratios are modifiable to alter their capacities for future experiments if so needed.

4.2 Model Design

A schematic of the model apparatus is provided in Figures 4 and 5. Table 1 lists the model dimensions. The model was comprised of four sections of 0.0254 m (1-in.) ID clear polyvinyl chloride (PVC). Three sections were approximately 3.05 m in length (10-ft.), and the fourth section, that used for the holdup measurement, was 2.13 m long (7-ft.). This holdup section was located third in order, from the inlet of the model. The first and second sections were connected using a short section of rubber hose and hose clamps. The other connections were made using threaded PVC bore-through true union ball-valves. These valves were located at either end of the third (holdup) section. The holdup section could be removed from the rest of the model by unscrewing the valves at either end of the section. The valve mechanisms were connected so that they may be opened or closed

simultaneously by the operator. A single long section of the pipe was initially considered for the design in order to minimize flow disturbances. This idea was rejected for several reasons, chiefly the difficulty of obtaining and then working with something so awkward, and also the inability of obtaining a holdup measurement. The inlet end of the first PVC section was connected to a Y–pipe constructed from PVC and rubber hose. This Y–pipe was specially designed to minimize the flow disturbance of the two confluent fluid streams.

Table 1: Dimensions of Model Apparatus

MODEL DIMENSIONS USED FOR EXPERIMENTS		
Lengths (m)	Overall Model Length	11.36
	Length Between Pressure Taps	9.514
	Entrance Length	1.372
	Exit Length	0.606
	Holdup Section Length	2.146
Diameters (m)	Model Diameter	0.0261
	Perforation Line Diameter	0.00208

At the other end of the model, the end of the last clear PVC section was connected to a large hose running into a separation tank. A large section of the top of the hose was cut away to prevent back pressure from forming at the end of the model. The separation tank received the flow of both oil and water together via the hose. The hose reached well down into the tank in order to baffle the output flow streams, especially the oil, from the input oil and water mixture. The separation tank was quite large, approximately 650 litres. It received the mixed fluid stream, and the oil and water phases rapidly separated due to their density difference. Outlets were located on the side of the tank for the oil (high) and the water (low). The outlets were connected to 3/4-in. (0.019 m) ID rubber hose.

Each hose was connected to its own Moineau progressing cavity (PC) pump. These spiral gear positive displacement pumps are very simple in design, using only a steel rotor rotating within a stator made out of an elastomer. The elastomer material used depends on the application, allowing for varying resistance to hydrocarbon aromatics, gas contaminants such as H_2S, high temperatures, etc. The PC pumps were selected for these experiments mainly because of the steady flow rate they produce compared with other similar capacity pumps such as diaphragm or piston–type pumps which typically generate an undesirable sinusoidal or pulsing flow condition. On the other hand, syringe type pumps offer still steadier flow, but are limited by their volumetric capacity. The PC pumps are widely used in Canada as submersibles for artificial lift, especially in heavy oil

applications. Their applicability under various conditions has been summarized by Mills (1994)[58]. Each PC pump was driven by a separate variable speed drive (VSD). The VSD's are electric motors with variac controls for motor speed. The VSD output shaft speed was thus completely variable below its maximum output. Ultimate pump capacity was adjustable by the pulley diameter ratio between the VSD output shaft and the PC pump drive shaft. The pumps and drives were specially mounted on a mobile steel frame for convenience. The pumps outlets were connected again to 3/4-in. rubber hoses which carried the fluids back to the Y–pipe inlet, thus completing the flow loop.

Manometer lines were positioned 9.514 m apart for pressure measurement, with the first (or left) manometer line 1.372 m (4.5-ft.) from the entrance and the second (right) manometer 0.606 m from the end of the clear PVC tubing. Sufficient entrance and exit lengths were determined using the guidelines provided by Govier and Aziz (1972)[29]. As design criteria in the area of turbulent flow are poorly understood, the conservative estimate of fifty times the diameter (50*D*) was used for the entrance length. The manometers were initially intended only to be used to calibrate electronic pressure transducers to be used for the pressure measurements. The experimental procedure allowed for relatively infrequent pressure recordings, however, and the superior accuracy and sensitivity of the manometers made their permanent use logical. The manometers used were simple straight glass capillary tubes, and they are connected to the model using lengths of 0.082-in. (2.083 mm) ID nylon tubing. The manometers were mounted in a box on a stand that is adjustable for both height and angle with respect to the floor of the laboratory. By varying the stand angle and height an ideal position could be obtained for each series of experiments.

Several holes were drilled in the pipe sections of the model, which could be used for alternate manometer line locations or for "perforations", i.e., points of controlled fluid influx. The holes were plugged with blanked hose when not in use. The influx location used for the current series of experiments was 4.649 m downstream from the left manometer, or a little less than half-way between the pressure measurements. The influx line is 0.082-in. (2.083 mm) ID nylon tubing where it was press–fitted into a 0.125-in. (3.175 mm) diameter hole drilled in the pipe tubing of the model. The influx line was connected via 0.125-in. Tygon flexible flow line to a third PC pump, which was in turn driven by the gearbox of a modified Ruska syringe pump. This setup allowed for a wide range of predetermined influx flow rates, and all three PC pumps could be set for rate independently.

4.3 Preparation and Calibration of Equipment

Initially, problems were encountered with respect to the pumps and drives. Their volumetric capacity was found to be far less than the specification. The model numbers were verified and the pumps disassembled and examined. Although little looked wrong with the pumps, it was determined that the elastomer of the stators (and in one case the steel rotor) were worn out. These were replaced and the capacities then measured up. It is recommended that the volumetric capacities of PC pumps be checked prior to their use in a series of experiments as the performance can be drastically affected by slight wear of the rotor and stator, and this wear can easily occur with incorrect use.

Another problem was encountered with the model tubing. Initially, a different material was used for the model tubing. This material was thought to be resistant to hydrocarbons, as it had not failed in the past. However, the oil used for the experiments is a refinery stream product similar to kerosene or jet fuel, and thus quite high in aromatic content. Over a period of a few weeks the oil attacked the model tubing to such an extent that the model cracked throughout and simply collapsed under its own weight. These sections were then replaced with sections of clear PVC tubing, which proved to be resistant under experimental conditions.

The first Y–pipe used at the inlet was also found to be inadequate. It was soldered together using short sections of metal pipe, the diameters of which were poorly matched. The sudden expansion of the fluids upon exiting the Y–pipe and entering the PVC tubing created a flow disturbance and bubbling. A new Y–pipe was designed and built using two rubber hoses glued within a plastic pipe. This Y–pipe provided a very smooth transition for flow within the hoses from the pumps to stratified two–phase flow within the model tubing. A third design was drawn up which was not used. It was to be machined from a single large block of Plexiglass and was to employ a butterfly valve in order to provide a nearly perfectly smooth transition into the model tubing. This design was rejected as expensive and unnecessary.

The two variable speed drives used to drive the main PC pumps were calibrated using a Micromotion mass flow meter (model B50 AF) and a Strobotac strobe (s/n 2781). The flow meter used provided a very accurate and unobtrusive measurement of the mass flow rate. The pumps were run at approximately twenty different speeds. The pump shaft speed was measured using the strobe while the mass flow rate was output by the flow meter. The strobe calibration was checked against a computer–controlled, high precision engine lathe in the Technical Services department. It was found to be accurate within 1 rpm

full-scale, which is less than 0.1 % error for the purposes of these experiments. The linearity of the pump calibrations was excellent. These calibrations are reproduced in Figures 2 and 3. The third (influx) pump was not calibrated per se, but flow rates were measured for the pump speeds used. The influx pump speed was controlled by the planetary transmission of a Ruska constant displacement pump. Since the speed was not variable beyond the given gear ratios, a calibration was not deemed necessary.

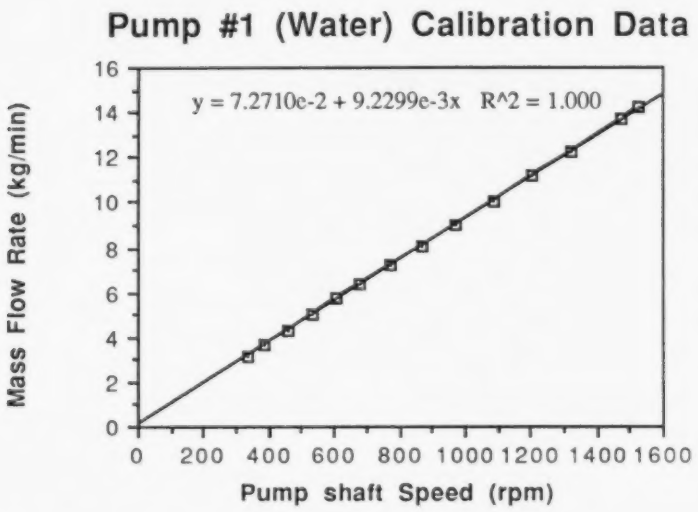

Figure 2: Calibration Data for Progressing Cavity Pump #1

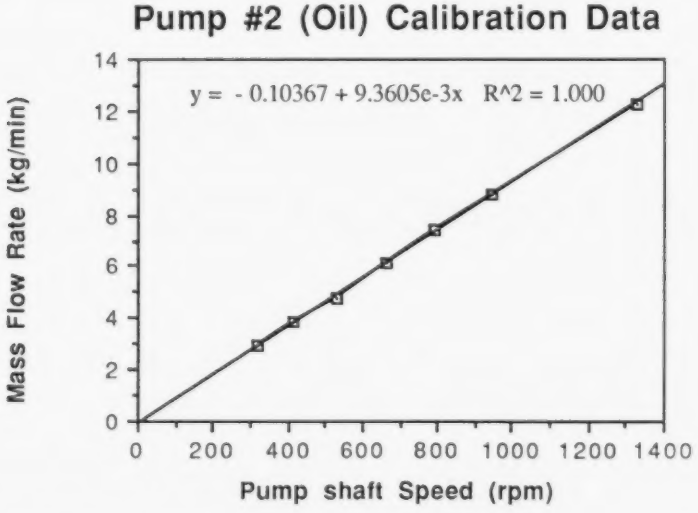

Figure 3: Calibration Data for Progressing Cavity Pump #2

As was mentioned above, the oil used in the experiments was a refinery stream product similar to kerosene, donated by a local refinery. The oil is perfectly clear, and has a density of 845.1 kg/m^3 and a viscosity of 2.4 mPa.s at room temperature (~20 ° C). A light oil was desired in order to generate easily turbulent flow in the oil phase. Since the Reynolds number is inversely proportional to viscosity, a high Reynolds number requires a low fluid viscosity, other parameters being equal.

$$\mathrm{Re} = \frac{\rho u D}{\mu} \qquad (4\text{-}1)$$

The water used was tap water, with a density of 998 kg/m3 and a viscosity of 1 mPa.s at 20 ° C.

Prior to initiation of the experiments the manometer box position with respect to the floor of the lab was measured. The height of the model tubing axis was also measured with respect to the lab floor, and the angle the manometer box made with the horizontal was recorded. These measurements allowed accurate calculation of the absolute pressures at each measurement location in addition to the pressure drop across the model. The model tubing was leveled prior to the first experiment and then repeatedly throughout the duration of the experimental runs. This was necessary because of the necessity of dis-assembling and re-assembling the model after each run in order to take a holdup measurement. A procedure was worked out to take this measurement with as little bother and delay as possible. The holdup section was calibrated by filling it with a known volume of fluid.

A photographic and videotape record of the experiments was desired. Dry runs were performed using different lighting arrangements, camera setups, etc. The optimum set–up for photography was then used during the experimental runs. This set–up included the following: Nikon F2 35mm SLR camera with internal light meter, 50 mm macro lens; camera mounted on a tripod about six inches from model tubing; back–lighting provided by two fluorescent lamps positioned about 18 inches directly behind model tubing; two flood lamps positioned 45 degrees to either side of point of interest, about 4 feet away; Kodak Ektachrome 200 ASA colour slide film; 1/125 or 1/250 shutter speeds used; f-stop set between 3 and 4.5; 80 A filter on macro lens; room lights out for photography. In addition, a very small amount of fuel dye was added to the oil to bring it into sharp contrast with the water.

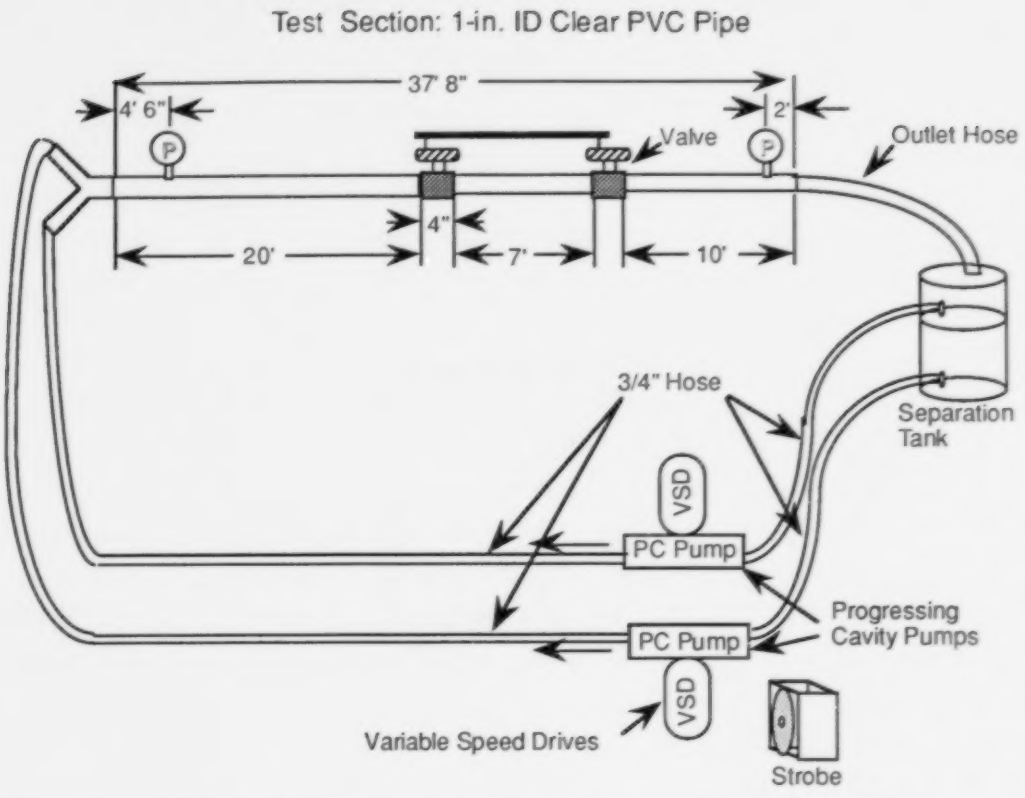

Figure 4: Layout of Physical Apparatus Used for Experiments

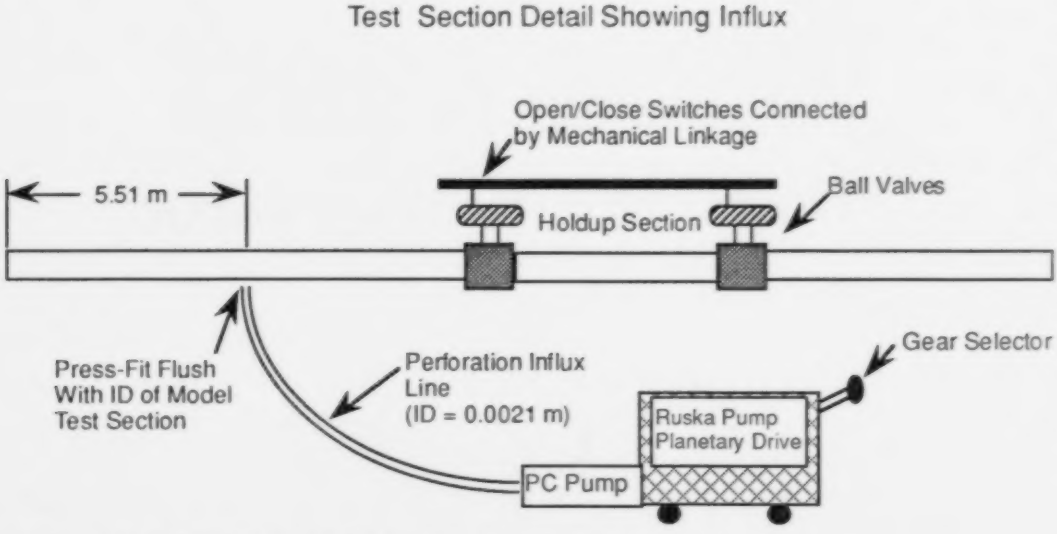
Test Section Detail Showing Influx
Open/Close Switches Connected by Mechanical Linkage
5.51 m
Ball Valves
Holdup Section
Gear Selector
Press-Fit Flush With ID of Model Test Section
Perforation Influx Line (ID = 0.0021 m)
Ruska Pump Planetary Drive
PC Pump

Figure 5: Test Section Detail of Model Apparatus

Due to time limitations created by delays and problems in construction of the model, the experimental program for this study was limited to 35 runs—5 single–phase water, 5 single–phase oil, 25 oil–water without perforation flow, and 75 oil–water with perforation flow—producing 110 data points. The parameters that were varied were: each of the main pump rates, five different volumetric rates for each pump; and the influx pump rate, four different rates (including zero) for the influx.

4.4 Experimental Procedure

Prior to each run, the manometer lines were purged using water from the influx pump. The influx line was then reconnected to the model. The model was leveled prior to each run, and after re-assembly. The model was filled with water and then capped and allowed to reach pressure equilibrium in order to check the manometers for zero pressure drop across the model.

Once the zero condition was satisfied, the model was reopened and both main pumps were started. Each main pump was set to provide the specified volumetric rate for any given run using the strobe to measure the pump shaft speed. This speed could then be used to calculate the volumetric rate using the pump calibrations. Each pump shaft speed was checked continuously throughout each experiment. For early runs especially, the pressures were measured frequently to become familiar with the transient response within the model. Research into the behaviour of the transient response was beyond the intended scope of this study; however, familiarity with the pressure response aided in accurate determination of the time to steady–state flow. Typically the meniscus level of each manometer tube became perfectly steady after five to ten minutes of run time. Once satisfied that a steady–state flow had been achieved, a section of the model was photographed and videotaped. The interface height was then measured, and visual observations of the flow were recorded. A laser–label "story board" was positioned on the model stand to record the pump speeds and manometer positions for each photograph and video segment, to ensure that there was no confusion later. The manometers and pump shaft speeds were again checked prior to switching on the influx pump at its first predetermined flow rate. Physical observations, photographs and videotape were again recorded, as were frequent pressure recordings. The manometer readings were again allowed to reach static equilibrium, which rarely required more than five minutes (this was verified for much longer periods in early experiments). The influx pump was then switched off, and a period of time was allowed to pass allowing the pressure drop to stabilize at its pre–influx value. This process was repeated for two more influx rates. Once

all the measurements had been recorded for all the influx rates, the pressure drop was once more allowed to stabilize to its initial steady–state reading. At this point all that remained for a given run was the holdup measurement. Both main pumps were shut off while simultaneously the ball valve open/close switch was thrown, closing both valves at either end of the holdup section. Pressure relief was provided by the manometer lines, preventing damage to the model, lines and pumps. With the holdup section effectively and instantaneously sealed during the run, a good measure of the in situ volume ratio of the constituent fluids was provided. The holdup section was removed from the model by unscrewing the true–union–threaded ball valves. The section was then stood on its end causing the fluids to separate. An hour or more of standing upright with steady vibration encouraged complete segregation of the fluids due to the density difference. The interface level was then recorded, and accurate knowledge of the in situ volume ratio as well as the input volume ratio allowed calculation of the holdup ratio for this series of experiments.

Ten experiments were run without either holdup measurements or influx. These were the single phase baseline experiments, performed in order to measure the single–phase oil and water pressure drops in the model. This data was important in demonstrating the validity of the two–phase pressure drop measurements, and for comparison with existing correlations and previous experiments. Problems were encountered with the single–phase oil experiments. The manometers used were of course in direct communication with the model tubing. The manometer lines contact the tubing at the bottom of the pipe in order to keep the oil out of the manometer lines and tubes, i.e., to keep the lines filled only with water. With the single–phase oil measurements it was impossible to keep the manometer lines completely free of oil, and this was found to affect the pressure measurement. For this reason, the single–phase oil experiments were repeated with the manometer tubes and lines completely saturated with the oil. This provided a more stable measurement, but these measurements still do not match very well with accepted correlations, while the single–phase water measurements match extremely well. This matter is discussed in greater detail in Chapter 5.

5. DISCUSSION OF EXPERIMENTAL RESULTS

5.1 Pressure Gradient Data

5.1.1 Theory

The discussion of pipe flow, as with any type of mass flow, necessarily begins with the principle of conservation of mass. For a given control volume such as a segment of a pipe, the mass in minus the mass out must equal the mass accumulated. For any constant area duct, (see Figure 6) the conservation of mass may be represented as:

$$\frac{\partial(\rho u)}{\partial L} + \frac{\partial \rho}{\partial t} = 0 \qquad (5\text{–}1)$$

where

ρ = the fluid density
u = the one–dimensional (axial) fluid velocity
L = the length of the control volume
t = time

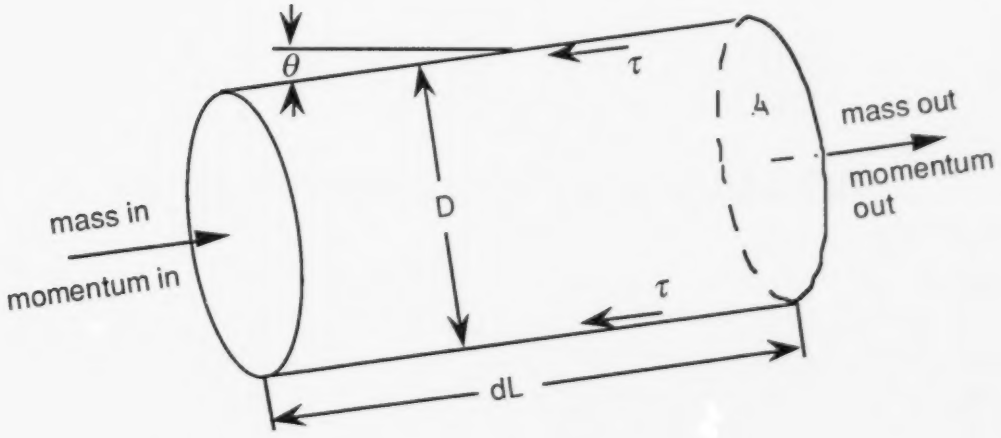

Figure 6: Control Volume for Pipe Flow

For the case of steady–state flow, no accumulation occurs, and Equation (5–1) reduces to

$$\frac{\partial(\rho u)}{\partial L} = 0 \tag{5–2}$$

Now considering the conservation of momentum for a similar control volume, the rate of momentum out minus the rate of momentum in plus the rate of momentum accumulation in the control volume must equal the sum of all the forces acting on the fluids. This relationship may be expressed as

$$\frac{\partial(\rho u^2)}{\partial L} + \frac{\partial(\rho u)}{\partial t} = -\frac{\partial P}{\partial L} - \tau\frac{\pi D}{A} - \rho g \sin\theta \tag{5–3}$$

where

τ	=	the shear stress acting on the inner wall of the control volume
D	=	the height of the control volume (diameter in the case of pipe flow)
A	=	the cross–sectional area of the control volume
g	=	the acceleration due to gravity, and
θ	=	the angle the control volume makes with the horizontal

The first term represents the momentum out minus the momentum in, or the rate of momentum eflux. It may be expanded as follows:

$$\frac{\partial(\rho u^2)}{\partial L} = u\frac{d(\rho u)}{dL} + \rho u\frac{du}{dL} \tag{5–4}$$

Combining Equations (5–2), (5–3), and (5–4) and assuming a steady–state flow condition (no accumulation of mass or linear momentum) gives

$$\rho u\frac{du}{dL} = -\frac{\partial P}{\partial L} - \tau\frac{\pi D}{A} - \rho g \sin\theta \tag{5–5}$$

Rearranging to solve for the pressure gradient gives

$$\frac{\partial P}{\partial L} = -\tau\frac{\pi D}{A} - \rho g \sin\theta - \rho u\frac{du}{dL} \tag{5–6}$$

This is the steady state pressure gradient equation, which has been derived by applying only the principles of conservation of mass and momentum. This equation is also known as the mechanical energy balance equation.[6]

For upward flow, pressure drops in the direction of the flow. The common sign convention calls for the pressure drop to be positive in the direction of flow, such that

$$\frac{\partial P}{\partial L} = \tau \frac{\pi D}{A} + \rho g \sin\theta + \rho u \frac{du}{dL} \tag{5–7}$$

This equation singles out the three components of the pressure gradient. The first term represents the frictional pressure gradient arising from the shear stress at the pipe wall. It is the most important component of the pressure gradient under most conditions of horizontal and near horizontal pipe flow. The second component is the elevation component. The final term is the change in velocity or accelerational pressure gradient component. It is insignificant and may be neglected for liquid flows. If only horizontal flow is considered, the focus becomes the frictional component of the pressure gradient.

$$\frac{\partial P}{\partial L} = \tau \frac{\pi D}{A} \tag{5–8}$$

Considering a finite length pipe with steady–state incompressible flow, the equation may be rearranged to obtain an expression for the shear stress at the pipe wall:

$$\tau = \frac{\Delta P}{L} \frac{D}{4} \tag{5–9}$$

The appropriate dimensionless parameters for the analysis of horizontal pipe flow may be obtained through application of the Buckingham Pi theorem to the problem (Olson[59]). The dimensional analysis yields the following variables:

$$\mathrm{Re} = \frac{\rho u D}{\mu} \tag{4–1}$$

$$\text{relative roughness} = \frac{\varepsilon}{D} \tag{5–10}$$

and

$$f = \frac{\Delta P}{L}\frac{2D}{\rho u^2} \tag{5–11}$$

where ε is the effective height of the roughness elements of the pipe, and f is called the friction factor, which is a function of the Reynolds number and the relative roughness of the pipe. The wall shear stress is related to the friction factor by comparing Equations (5–9) and (5–11).

$$\tau = f\frac{\rho u^2}{8} \tag{5–12}$$

For laminar flow conditions (Re < ~2000), the relationship between the shear stress and the velocity gradient across the cross section of the pipe is known. Further analysis yields an analytical expression for the friction factor in terms of the Reynolds number only:

$$f = \frac{64}{\mathrm{Re}} \tag{5–13}$$

For transition and turbulent flow conditions (Re > ~2000), the shear stress (and thus the fricition factor) are not obtainable analytically due to the complex relationship between the velocity gradient and the Reynolds number. A very widely used empirical correlation was proposed by Blasius (as cited in Dikken[3], and Olson[59]):

$$f = \frac{0.316}{\mathrm{Re}^{0.25}} \tag{5–14}$$

The turbulent friction factor may be determined using the Blasius or similar correlation, or by use of a Moody's chart. Rearrangement of Equation (5–11) leads to

$$\frac{\Delta P}{L} = \frac{f\rho u^2}{2D} \tag{5–15}$$

which may be used to obtain the pressure gradient.

5.1.2 Single–Phase Flow Data

Figure 7 is a plot of the pressure gradient across the pipe model vs. the water phase volumetric flow rate, with the oil phase volumetric flow rate as a cross parameter. The single–phase water baseline data is shown as the bottom–most curve on the plot. This data set plots linearly on the log–log scale used, indicating a power law or Blasius–type relationship between the pressure gradient and the flow rate. This is expected for turbulent single–phase flow, and it serves as a demonstration of the validity of the pressure gradient data for these experiments.

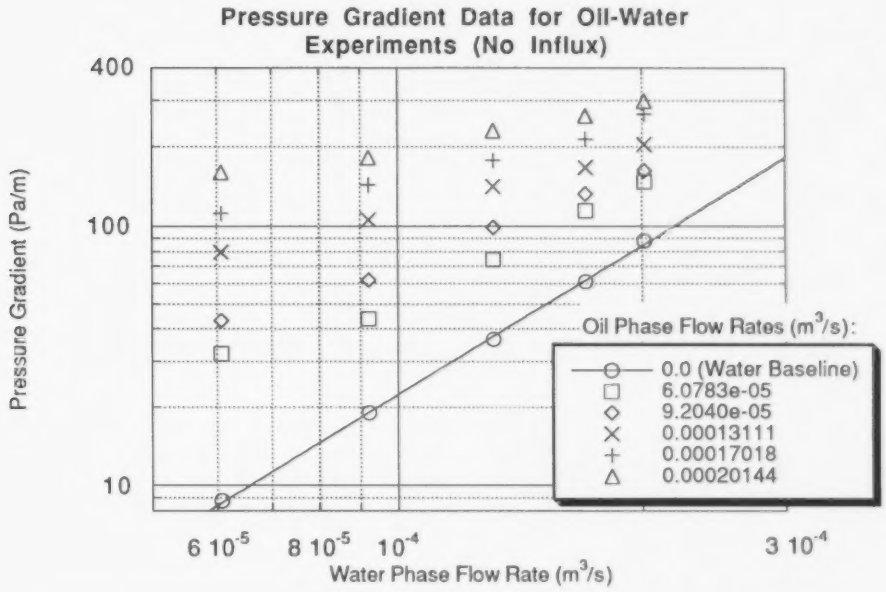

Figure 7: Oil–Water Pressure Gradient Data from Pipe Flow Experiments

In Table 2 compares the pressure gradients calculated using this simple method as compared with the measured gradients from the single–phase experiments. The agreement between the measured and calculated single–phase water pressure gradients is very good, the error being 8% on the average. The agreement gets better with increasing flow rate, as the flow regime moves further away from the transitional region.

The Blasius formulation is for use with Reynolds numbers under 100,000 and has otherwise been shown to be a simplified approach to the problem. Nikuradse[6,29,59]

Table 2: Single–Phase Water Pressure Gradients

Water Volumetric Flow Rate (m^3/s)	Reynolds Number	Blasius' Friction Factor	Calculated Pressure Gradient (Pa/m)	Measured Pressure Gradient (Pa/m)
2.01E–04	9.80E+03	3.18E–02	8.57E+01	8.79E+01
1.70E–04	8.28E+03	3.31E–02	6.38E+01	6.11E+01
1.31E–04	6.38E+03	3.54E–02	4.04E+01	3.66E+01
9.20E–05	4.48E+03	3.86E–02	2.18E+01	1.90E+01
6.08E–05	2.96E+03	4.29E–02	1.05E+01	8.79E+00

performed turbulent pipe flow experiments and was able to determine that the velocity profile in the pipe assumes a logarithmic form at higher Reynolds numbers. He also extended the friction factor calculations to pipes with finite surface roughness. Colebrook and White[6,29,59] developed a widely accepted equation for the single–phase turbulent friction factor which incorporates the findings of Nikuradse and others, and encompasses all flow regimes. This equation is

$$\frac{1}{\sqrt{f}} = 1.74 - 2\log\left(\frac{2\varepsilon}{D} + \frac{18.7}{\mathrm{Re}\sqrt{f}}\right) \tag{5–16}$$

where ε is the dimensional height of the surface roughness of the pipe. Due to the implicit nature of this equation, an iterative approach such as Newton–Raphson or another numerical method must be used to solve for the friction factor. A simple C program was written for this purpose, the listing of which is provided in Appendix C. In Table 3 compares the measured pressure gradients are compared with those calculated with the Blasius and Colebrook and White methods. For proper comparison with the Blasius method, the roughness is set at 1.5e–6 m.

The Colebrook and White equation agrees well with both the Blasius equation and the measured data for these experiments. The average error is about 7.5% for the Colebrook and White equation with respect to the measured pressure gradients. Again, the agreement between the calculated and measured pressure gradients worsens as the Reynolds number decreases because the flow regime approaches the transitional region.

It is concluded from this comparison that the measured single–phase water pressure gradient data is reasonably accurate. It may also be concluded that the two friction factor

equations presented agree reasonably well over the range of flow rates considered in this study.

Table 3: Comparison of Correlations with Measured Values for Single–phase Experiments

Water Volumetric Flow Rate (m^3/s)	Blasius Friction Factor	Colebrook & White Frict. Factor	(Blasius) Turbulent Pres. Grad. (Pa/m)	(C&W) Turbulent Pres. Grad. (Pa/m)	Measured Pres. Grad. (Pa/m)
2.01E–04	3.18E–02	3.12E–02	8.57E+01	8.41E+01	8.79E+01
1.70E–04	3.31E–02	3.26E–02	6.38E+01	6.28E+01	6.11E+01
1.31E–04	3.54E–02	3.50E–02	4.04E+01	4.00E+01	3.66E+01
9.20E–05	3.86E–02	3.87E–02	2.18E+01	2.18E+01	1.90E+01
6.08E–05	4.29E–02	4.38E–02	1.05E+01	1.08E+01	8.79E+00

5.1.3 Two–Phase Liquid–Liquid Flow

In Table 4 the two–phase oil–water experimental data without influx is listed

. Figure 7 shows the measured pressure gradient data for the oil–water experiments plotted against the water volumetric flow rate. It may be noted that while the single–phase water runs data (the lowermost curve) is well approximated by power law behaviour, i.e., it may be modeled by a function of the form

$$y = ax^b \tag{5–17}$$

where a and b are positive constants, the two–phase data does not follow this form. This is obvious because this data does not plot as a straight line on the log–log graph. This is an indication of the difficulty of correlating the pressure gradient behaviour of two–liquid flows. The liquid–liquid flow cannot be treated effectively as a homogeneous mixture with averaged density and viscosity, especially in the horizontal case due to the stratified nature of the flow created. The same data is plotted in Figure 8, but with the water phase volumetric flow rate as the cross parameter.

Although particular attention was paid to the problem of liquid–liquid flows in the 1960s, no adequate empirical correlation of the pressure gradient or the holdup was ever developed. The ultimate purpose of most of the early experimental work was to determine

a method of reducing the power requirements of heavy oil pipelines by adding water to the flow stream. Over a range of viscosity ratios and flow rates, the pressure gradient required for a given oil flow rate may be reduced somewhat by the addition of water to the flow

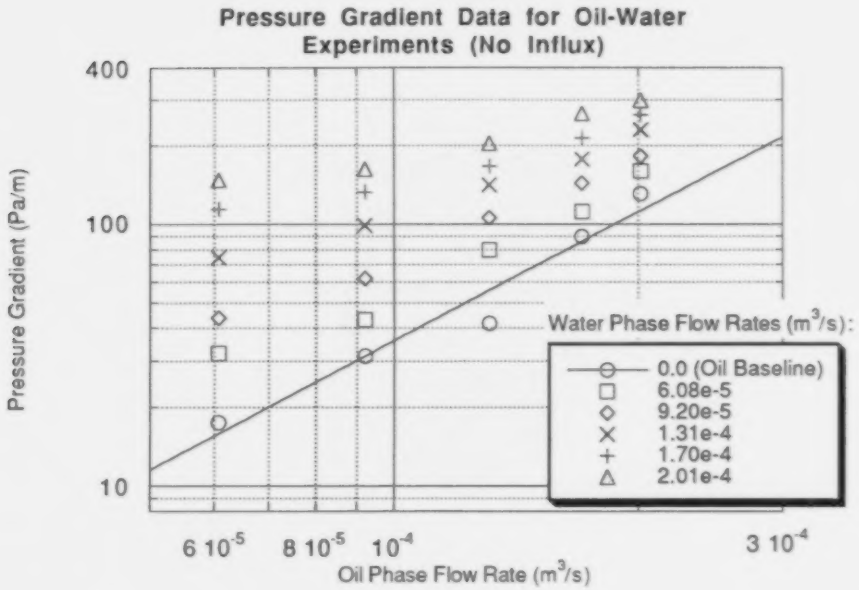

Figure 8: Oil–Water Pressure Gradient Data With Water Rate As Cross Parameter

stream, especially if the water can be made to flow in a continuous annular regime surrounding the oil. Under the conditions of the current experiments the pressure gradient was observed to increase smoothly from the single–phase oil baseline with increasing water phase flow rates.

Table 4: Oil–Water Pipe Flow Experimental Data

Exp.	Volumetric Flow Rates:		Superficial Velocities:		Inlet Press.	Press. Gradient	In situ H20 Vol. Frac.	Reynolds Numbers:	
	Water	Oil	Water	Oil				Water	Oil
	(m^3/s)	(m^3/s)	(m/s)	(m/s)	(Pa)	(Pa/m)			
1	6.08E-05	6.08E-05	0.11	0.11	942.81	32.07	0.48	3641.18	2061.22
2	9.20E-05	6.08E-05	0.17	0.11	1095.08	43.73	0.59	5204.45	2294.28
3	1.31E-04	6.08E-05	0.24	0.11	1406.54	74.34	0.66	7167.87	2496.54
4	1.70E-04	6.08E-05	0.32	0.11	1794.13	114.43	0.71	9101.47	2677.12
5	2.01E-04	6.08E-05	0.38	0.11	2122.90	147.23	0.74	10642.4	2803.84
6	6.08E-05	9.20E-05	0.11	0.17	1025.87	43.00	0.43	3789.26	2947.75
7	9.20E-05	9.20E-05	0.17	0.17	1198.90	61.95	0.52	5422.16	3208.23
8	1.31E-04	9.20E-05	0.24	0.17	1583.03	98.76	0.59	7405.35	3482.81
9	1.70E-04	9.20E-05	0.32	0.17	1918.72	132.65	0.64	9402.45	3672.96
10	2.01E-04	9.20E-05	0.38	0.17	2212.87	162.90	0.68	10933.4	3861.89
11	6.08E-05	1.31E-04	0.11	0.24	1413.46	79.44	0.33	4101.12	3841.47
12	9.20E-05	1.31E-04	0.17	0.24	1669.55	105.68	0.42	5778.53	4160.97
13	1.31E-04	1.31E-04	0.24	0.24	2029.46	141.40	0.52	7723.89	4570.13
14	1.70E-04	1.31E-04	0.32	0.24	2375.52	166.91	0.57	9723.88	4840.18
15	2.01E-04	1.31E-04	0.38	0.24	2638.53	204.81	0.61	11260.3	5081.13
16	6.08E-05	1.70E-04	0.11	0.32	1731.84	112.24	0.27	4364.62	4719.63
17	9.20E-05	1.70E-04	0.17	0.32	2036.38	143.58	0.35	6084.80	5089.57
18	1.31E-04	1.70E-04	0.24	0.32	2375.52	177.47	0.45	8067.00	5547.62
19	1.70E-04	1.70E-04	0.32	0.32	2749.28	214.28	0.51	10112.4	5846.75
20	2.01E-04	1.70E-04	0.38	0.32	3254.53	267.12	0.54	11698.0	6086.20
21	6.08E-05	2.01E-04	0.11	0.38	2205.95	160.35	0.24	4568.20	5397.81
22	9.20E-05	2.01E-04	0.17	0.38	2430.89	182.21	0.30	6391.24	5746.59
23	1.31E-04	2.01E-04	0.24	0.38	2915.39	231.04	0.39	8392.31	6243.59
24	1.70E-04	2.01E-04	0.32	0.38	3219.93	262.38	0.46	10360.7	6666.04
25	2.01E-04	2.01E-04	0.38	0.38	3579.83	298.83	0.50	11977.8	6912.93

5.1.3.1 Numerical Predictive Approach

The goal of reducing pipeline power requirements was shared by an early numerical attempt at solving this problem in a paper written by Gemmell and Epstein (1962)[40]. Their study considered the steady–state, stratified laminar flow of two immiscible, incompressible, Newtonian fluids. A pipe cross–section is overlain by a Cartesian grid of nodes (see Figure 9), and the relevant form of the Navier–Stokes equation is discretized for each phase. The boundary conditions to be satisfied include no slip at the pipe wall or the interface between the phases, and the requirement of equal and opposite shear stresses at and with respect to the interface. The equations are written in dimensionless form so as to apply to any pressure gradient, pipe diameter or viscosity ratio of the two phases.

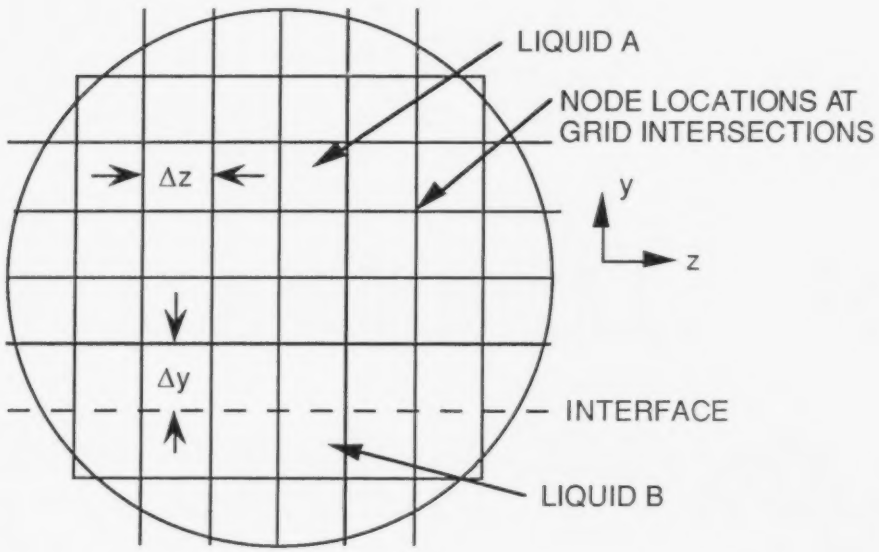

Figure 9: Discretization of Pipe Cross Section

A simplified form of the two–dimensional Navier–Stokes equation is:

$$\frac{dP}{dx} = \mu\left(\frac{\partial^2 u}{\partial y^2} + \frac{\partial^2 u}{\partial z^2}\right) \qquad (5\text{–}18)$$

This equation applies for each liquid, each with its own viscosity. The boundary conditions are given by:

(1) $u = 0$ for each liquid at the pipe wall (5–19)

(2) $u_A = u_B$, and (5–20)

(3) $\mu_A \frac{\partial u_A}{\partial y} = \mu_B \frac{\partial u_B}{\partial y}$ at the interface between the liquids. (5–21)

The equations are non–dimensionalized as follows,

$$\tilde{y} = \frac{y}{R} \qquad \tilde{z} = \frac{z}{R} \tag{5–22}$$

where R is the pipe radius.

$$\tilde{u} = \frac{u}{U_A} \tag{5–23}$$

where U_A is the average velocity in the pipe when it is full of liquid A under the same pressure gradient as in two–phase flow, and which is defined by the Poiseuille Equation

$$U_A = \frac{R^2}{8\mu_A}\left(-\frac{dP}{dx}\right) \tag{5–24}$$

The resulting form of the Navier–Stokes equation is

$$\frac{\partial^2 \tilde{u}}{\partial \tilde{y}^2} + \frac{\partial^2 \tilde{u}}{\partial \tilde{z}^2} = -8\frac{\mu_A}{\mu} \tag{5–25}$$

and the third boundary condition, Equation (5–21) becomes

$$\tilde{\mu}\frac{\partial \tilde{u}_A}{\partial \tilde{y}} = \frac{\partial \tilde{u}_B}{\partial \tilde{y}} \tag{5–26}$$

where $\tilde{\mu}$ is the non–dimensionalized viscosity ratio, μ_A/μ_B .
The finite difference approximation of Equation (5–25) is expressed as

$$\frac{\tilde{u}_{i,j+1} - 2\tilde{u}_{i,j} + \tilde{u}_{i,j-1}}{(\Delta\tilde{y})^2} + \frac{\tilde{u}_{i+1,j} - 2\tilde{u}_{i,j} + \tilde{u}_{i-1,j}}{(\Delta\tilde{z})^2} = -8\frac{\mu_A}{\mu} \qquad (5\text{–}27)$$

By letting $\Delta\tilde{y} = \Delta\tilde{z}$ and substituting subscripts 0, 1, 2, 3 and 4 for (i,j), $(i,j-1)$, $(i+1,j)$, $(i,j+1)$, and $(i-1,j)$, respectively, Equation (5–27) simplifies to (see Figure 10)

$$\tilde{u}_1 + \tilde{u}_2 + \tilde{u}_3 + \tilde{u}_4 - 4\tilde{u}_0 + 8\frac{\mu_A}{\mu}(\Delta\tilde{y})^2 = 0 \qquad (5\text{–}28)$$

Equation (5–28) must be satisfied for every nodal point in the grid network for each liquid.

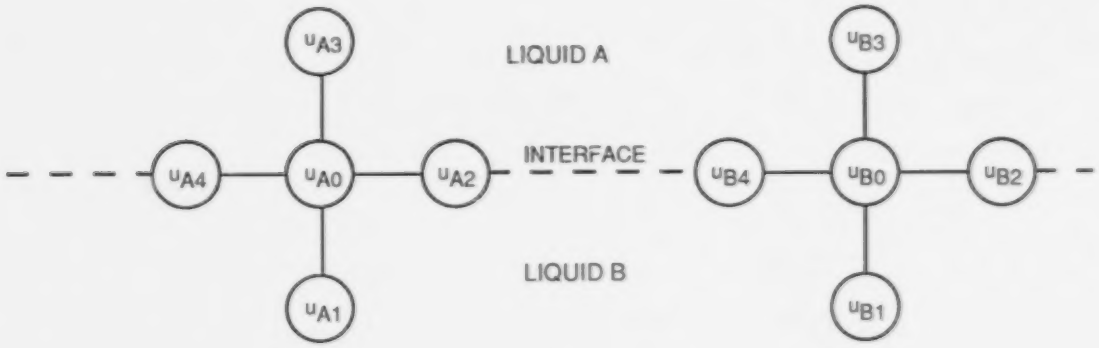

Figure 10: Nodal Representation of Pipe Cross Section

The finite difference equation used to approximate the third boundary condition (Equation 5–26) is

$$\tilde{\mu}\left(\tilde{u}_{A_3} - \tilde{u}_{A_1}\right) = \tilde{u}_{B_3} - \tilde{u}_{B_1} \qquad (5\text{–}29)$$

Now writing the finite difference approximation of the Navier–Stokes Equation (Equation 5–27) for each liquid phase, for liquid *A* (the oil)

$$\tilde{u}_{A_2} + 2\tilde{u}_{A_3} + \tilde{u}_{A_4} - 4\tilde{u}_{A_0} + 8(\Delta\tilde{y})^2 = 0 \qquad (5\text{–}30)$$

and for liquid *B* (the water),

$$\tilde{u}_{B_1} + \tilde{u}_{B_2} + \tilde{u}_{B_3} + \tilde{u}_{B_4} - 4\tilde{u}_{B_0} + 8\tilde{\mu}(\Delta\tilde{y})^2 = 0 \qquad (5\text{–}31)$$

These equations are solved for each node in the main body of each liquid respectively. Multiplying Equation (5–30) for liquid A by $\tilde{\mu}$ and adding Equation (5–29) to the result gives

$$\tilde{\mu}\left[\tilde{u}_{A_2} + 2\tilde{u}_{A_3} + \tilde{u}_{A_4} - 4\tilde{u}_{A_0} + 8(\Delta\tilde{y})^2\right] = \tilde{u}_{B_3} - \tilde{u}_{B_1} \qquad (5\text{–}32)$$

Adding this equation to Equation (5–31) for liquid *B*, and then substituting the *B* liquid interface velocities with their identical *A* liquid counterparts, gives

$$\frac{2}{\tilde{\mu}+1}\tilde{u}_{B_1} + \tilde{u}_{A_2} + \frac{2\tilde{\mu}}{\tilde{\mu}+1}\tilde{u}_{A_3} + \tilde{u}_{A_4} - 4\tilde{u}_{A_0} + \frac{16\tilde{\mu}}{\tilde{\mu}+1}(\Delta\tilde{y})^2 = 0 \qquad (5\text{–}33)$$

This equation relaxes interface nodes in two dimensions and is solved for all node points falling on the interface. This completes the set of equations necessary to solve for the node velocities.

The main weakness of this numerical approach is the Cartesian grid, which does not lend itself well to the circular pipe cross–section combined with the horizontal interface between the phases. The interface height may be located at any height with respect to the pipe diameter. The irregular regions left over by the grid at the pipe wall make calculation of the node velocities near the wall difficult. The associated error is minimized by selecting the densest grid possible. The velocities near the wall are determined by interpolation between nodal velocities and boundary values.

The volumetric flow rate was calculated by first multiplying each node velocity by its surrounding grid area, i.e., by $(\Delta\tilde{y})^2$. The summation of the individual dimensionless flow rates in the various squares is for liquid *A* and *B*, respectively,

$$\Sigma\tilde{u}_A(\Delta\tilde{y})^2 \qquad (5\text{–}34)$$

$$\Sigma\tilde{u}_B(\Delta\tilde{y})^2 \qquad (5\text{–}35)$$

The ratio of these two quantities represents the input volume ratio. The ratio of the two flow cross–sectional areas for each fluid is the in situ volume ratio, and is defined only by

the location of the interface, which for the purposes of this program is specified by the user. The holdup ratio, then is given by

$$\frac{\sum \tilde{u}_A (\Delta\tilde{y})^2}{\sum \tilde{u}_B (\Delta\tilde{y})^2} \Big/ \frac{\text{flow area of liquid A}}{\text{flow area of liquid B}} \tag{5–36}$$

Gemmell and Epstein[40] defined the volumetric flow rate factor, *vfrf* as

$$vfrf = \frac{q_A}{q_{A_{full}}} = \frac{\sum u_A (\Delta y)^2}{U_A \pi R^2} = \sum \tilde{u}_A (\Delta\tilde{y})^2 \tag{5–37}$$

where q_A is the dimensional volumetric flow rate of liquid *A* under the two–liquid flow, and $q_{A_{full}}$ is the corresponding flow rate for the pipe flowing full of liquid *A*, under the same pressure gradient as for two–phase flow. Volumetric flow rate factors greater than one indicate that, at the same pressure gradient, more liquid *A* can be transported by two–phase flow than by single–phase flow, while factors less than unity signify the opposite effect. The *vfrf* term is thus suitable for comparison of two–phase flow with single–phase flow at equivalent pressure gradients. This is based on the direct proportionality between the pressure gradient and the volumetric flow rate given by the Poiseuille relation for strictly laminar flow. Thus,

$$\frac{q_A}{q_{A_{full}}} \text{ for constant } \left(-\frac{dP}{dx}\right) = \frac{\sum \tilde{u}_A (\Delta\tilde{y})^2}{\pi} = \frac{(-dP/dx)_{full}}{(-dP/dx)} \text{ for constant } q_A \tag{5–38}$$

The factor, by which the volumetric flow rate of liquid *A* at a fixed pressure gradient is increased by the addition of liquid *B*, is equal to the factor by which the pressure gradient due to a fixed volumetric flow of liquid *A* is reduced by the addition of the same proportion of liquid *B*. This is the historical perspective in attempting to reduce the pressure gradient and thus the power requirements necessary in heavy oil pipelines and in other applications. From the perspective of the current study, the *vfrf* term may be used to determine the additional pressure gradient associated with a given flow rate of liquid *A* flowing together with another liquid, over the case of the same volumetric rate of liquid *A* flowing alone in the pipe. In other words, the calculated *vfrf* term may be used to determine the two–phase pressure gradient if the single–phase pressure gradient and the input volume ratio are known, as they are in the case of these experiments.

The limitation in applying this model to the current series of experiments is that the model is limited to strictly stratified and laminar flow of the two fluids in the pipe. All of the experiments conducted were turbulent–turbulent, by definition from the Reynolds number calculations. Despite this limitation, a program was written for comparison purposes (listed in Appendix C) to solve for the *vfrf* term for any location of the interface input by the user. The program runs were limited to a maximum grid density of 60x60, because this corresponds to the program solving by Gaussian elimination of a 1440x1440 matrix, and this represented the limit of the computer system used. The *vfrf* term was computed for the whole range of interface heights within the pipe. The program accuracy was checked by comparison with Gemmell and Epstein's[40] results and by confirming that *vfrf* equaled unity for the case of the interface being located at the bottom of the pipe (i.e., single–phase oil flow).

Each interface height corresponds to an in situ volume ratio, using the following method (as outlined in Agrawal and Gregory[44], and Govier and Aziz[29]). Please refer to Figure 11.

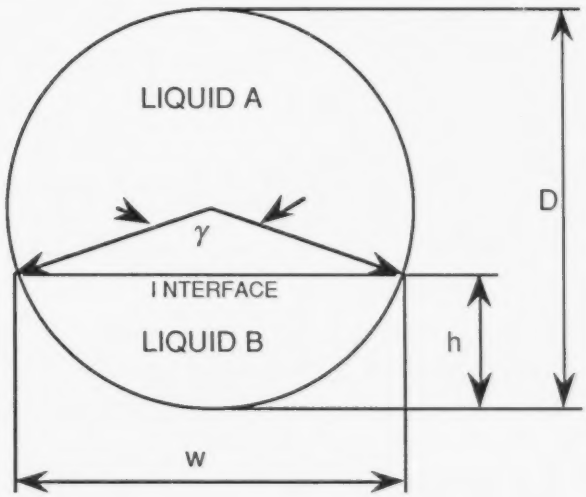

Figure 11: Critical Parameters Defining Relationship Between Interface and Pipe Wall

For the purposes of the program, the interface height is assumed to be known and is input by the user as a fraction of the pipe radius; (for the actual experiments conducted, the exact location of the interface is difficult to measure directly. Although the height of the interface was not directly measured during the experiments conducted, a good approximation was obtained using the holdup measurement.) Computer runs are performed for the whole

range of interface heights, and the output *vfrf* values are entered into a spreadsheet program. The angle γ is found from the geometrical relationship

$$\gamma = 2\cos^{-1}\left(1 - 2\frac{h}{D}\right) \tag{5–39}$$

This angle is used to calculate the in situ volume ratio, which is equivalent to the ratio of the in situ respective cross–sectional areas of the two fluids.

$$\text{in situ volume ratio} = \left(1 - \frac{\gamma - \sin\gamma}{2\pi}\right) \Big/ \left(\frac{\gamma - \sin\gamma}{2\pi}\right) \tag{5–40}$$

For each interface height, the output *vfrf* was multiplied by the measured single–phase oil pressure gradient to determine the corresponding two–phase pressure gradient for that in situ volume ratio. The in situ volume ratio calculated from the interface height was used to determine the associated in situ volumetric flow rate of the water phase from the (known and specified) input oil–phase flow rate. The holdup ratio acquired from each experiment is applied to the corresponding water flow rate. Recall that the holdup ratio, H, is given by

$$H = \frac{\text{input volume ratio}}{\text{in situ volume ratio}} = \frac{q_A/q_B}{A_A/A_B} \tag{5–41}$$

where A_A and A_B refer to the cross–sectional areas of fluid A (oil) and fluid B (water), respectively. Thus, for any given interface height and input oil flow rate,

$$q_B = \frac{q_A}{\left(H \times \left(A_A/A_B\right)\right)} \tag{5–42}$$

This method is used to calculate the water volumetric flow rate for each arbitrary interface height and for each oil volumetric flow rate. The desired two–phase pressure gradients for the oil and water volumetric flow rates are then found from linear interpolation between the closest interface height locations. The two–phase pressure gradients calculated by this method are presented in Figures 12 through 16, each for a different oil phase flow rate. The predicted pressure gradients do not match the measured values well except at the lowest fluid rates, where the flow regimes are laminar or transitional (the Reynolds numbers for each phase of each experiment, calculated using the method outlined by Agrawal and Gregory[44], are listed in Table 4 above.) The inaccuracy is also a result of

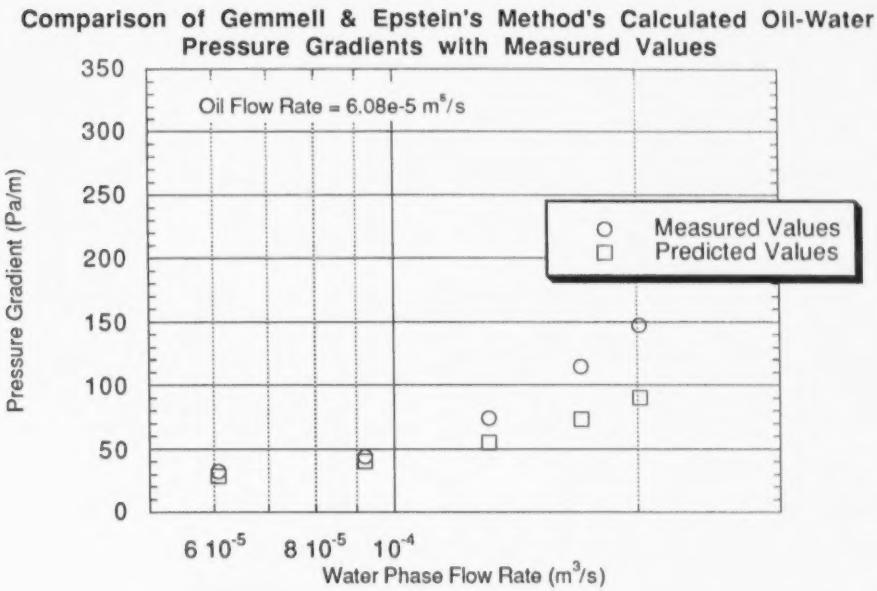

Figure 12: Measured and Predicted Oil–Water Pipe Flows, Oil Flow Rate = 6.08e–5 m^3/s

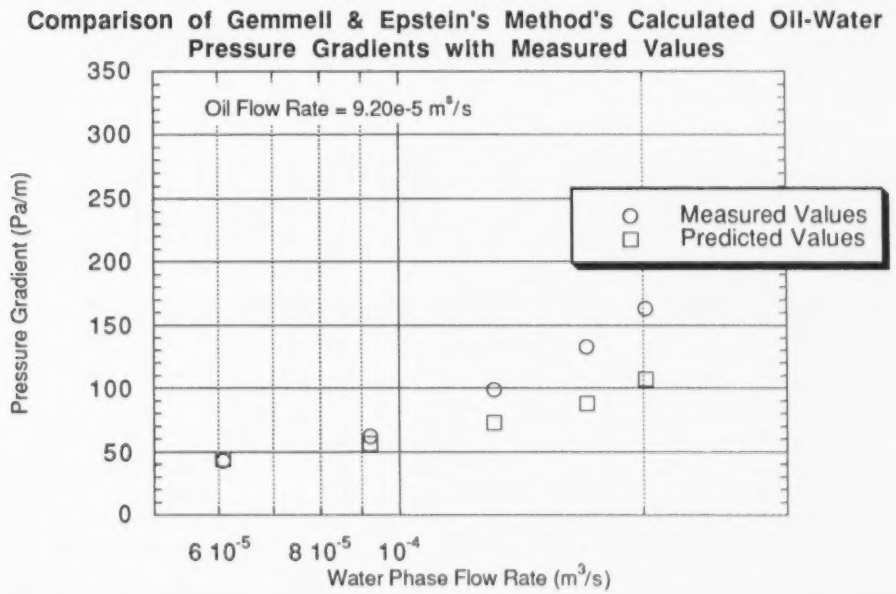

Figure 13: Measured and Predicted Oil–Water Pipe Flows, Oil Flow Rate = 9.20e–5 m^3/s

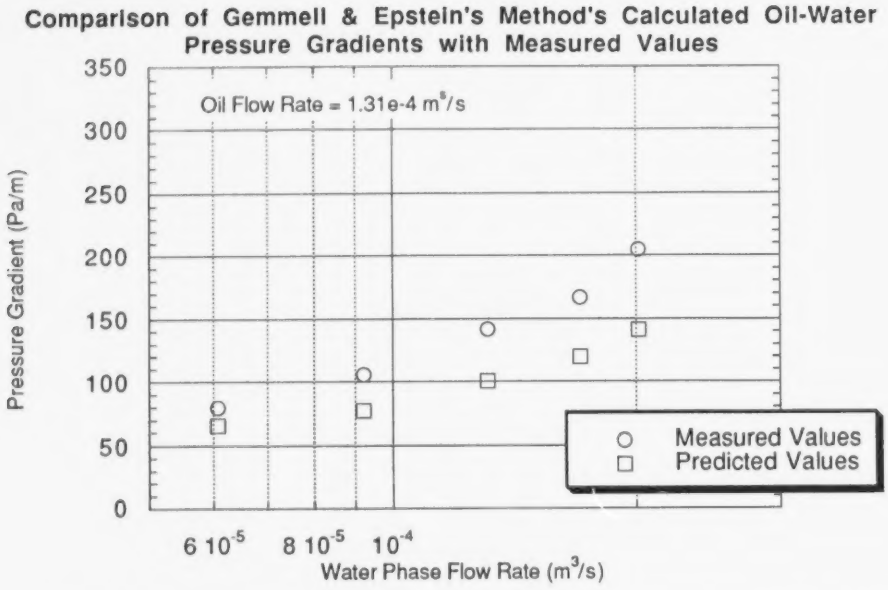

Figure 14: Measured and Predicted Oil–Water Pipe Flows, Oil Flow Rate = 1.31e–4 m^3/s

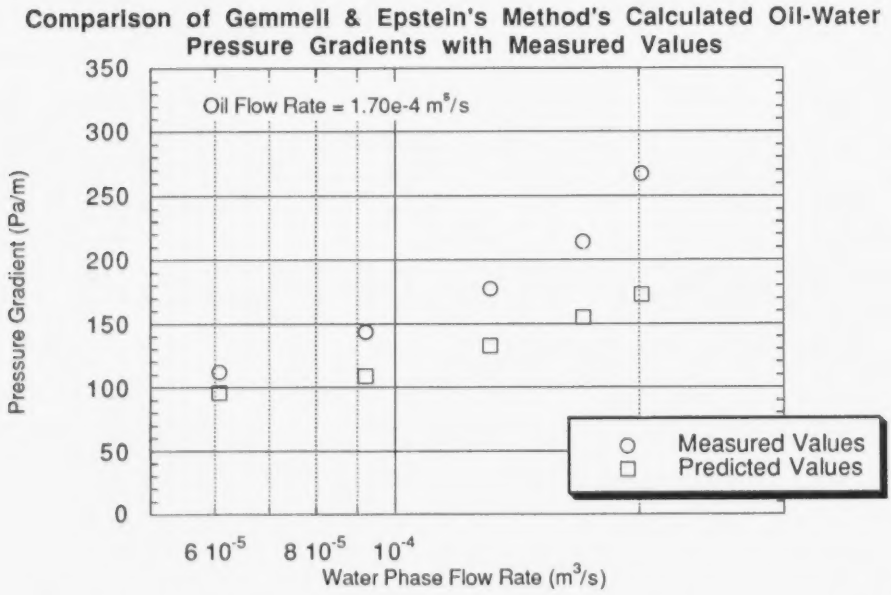

Figure 15: Measured and Predicted Oil–Water Pipe Flows, Oil Flow Rate = 1.70e–4 m^3/s

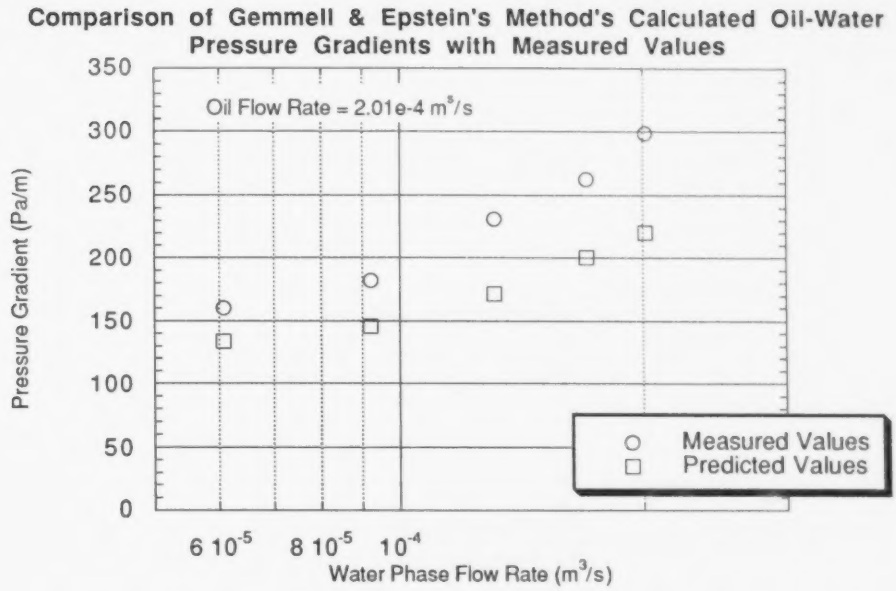

Figure 16: Measured and Predicted Oil–Water Pipe Flows, Oil Flow Rate = 2.01e–4 m^3/s

decreasing stratification of the liquid phases at higher flow rates. Recall that the Gemmell and Epstein[40] numerical model assumes perfectly stratified laminar flow of each phase.

The figures clearly demonstrate the limitation of Gemmell and Epstein's[40] numerical model with respect to turbulence and mixing. In the literature, more sophisticated attempts have been made to model two–phase gas–liquid flows using various mathematical models for turbulence (Issa[48]; Akai *et al.*[49]). No liquid–liquid model has been published incorporating a mechanistic turbulence model at this time. The complex interactions between the liquid phases at the interface makes numerical modeling difficult in the turbulent regime.

5.1.3.2 Hall and Hewitt's Correlation Method

Lockhart and Martinelli[34] were the first to present a general pressure drop correlation for two–phase flow in horizontal pipes. This correlation does not follow the friction factor analogy used thus far. It presents the two–phase pressure gradient in terms of a single–phase pressure gradient multiplied by a correction factor. The correlation has some limited theoretical basis, though it was developed empirically. The correlation is based upon the assumption that the pressure drop must be the same for each phase, and it

ignores the accelerational pressure drop component. Lockhart and Martinelli[34] defined liquid and gas two–phase parameters as follows:

$$\phi_L = \sqrt{\frac{\left(\Delta P/L\right)_{tp}}{\left(\Delta P/L\right)_{L_s}}} \tag{3–5}$$

$$\phi_G = \sqrt{\frac{\left(\Delta P/L\right)_{tp}}{\left(\Delta P/L\right)_{G_s}}} \tag{5–43}$$

where $\left(\Delta P/L\right)_{tp}$ is the two–phase pressure gradient, identical for each phase.

For an oil–water flow system, the L and G subscripts may be replaced by W (water) and O (oil), respectively.

The correlation was not provided by the authors in the form of an equation, but as a set of type curves, with ϕ plotted against X, and X separately plotted against the in situ volume fraction of the liquid. Recall that for oil–water flows the Martinelli parameter X is defined as:

$$\mathrm{X} = \sqrt{\frac{\left(\Delta P/L\right)_{W_s}}{\left(\Delta P/L\right)_{O_s}}} \tag{5–44}$$

Many attempts to develop and improve correlations of this type have been made, especially for liquid–gas flows. Figure 17 is a plot of the dimensionless interface heights from the current oil–water flow experiments against the measured ϕ_W values. It can be observed that the data plots in a fairly smooth and consistent trend, resulting in a good match by the best fit curve. The equation of the best fit curve may be used to generate calculated ϕ_W values, and these values may be plotted against the X values found via Hall and Hewitt's[50] numerical method (described in 3. Literature Review, Appendix B and 5.3) in order to determine a correlation between the two Martinelli parameters for the oil–water experiments conducted. Figure 18 is the resulting plot.

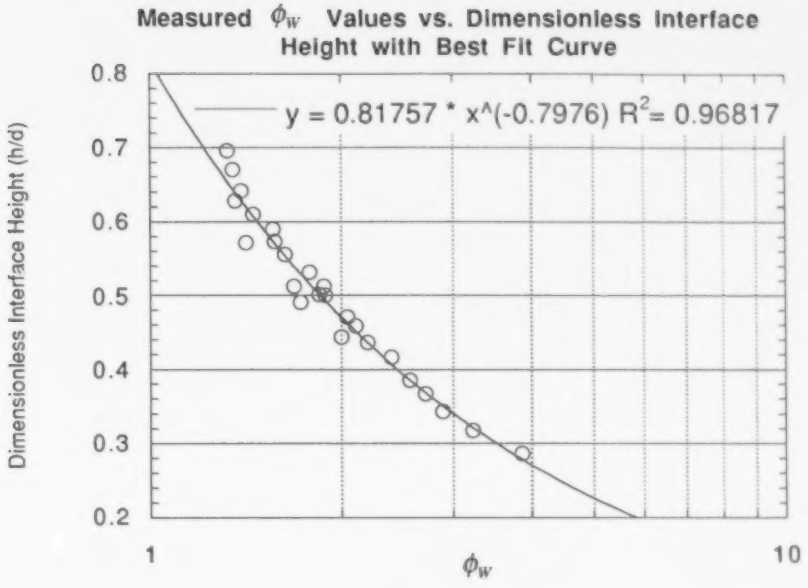

Figure 17: Best Fit Curve Drawn Through Measured Data for Oil–Water Experiments

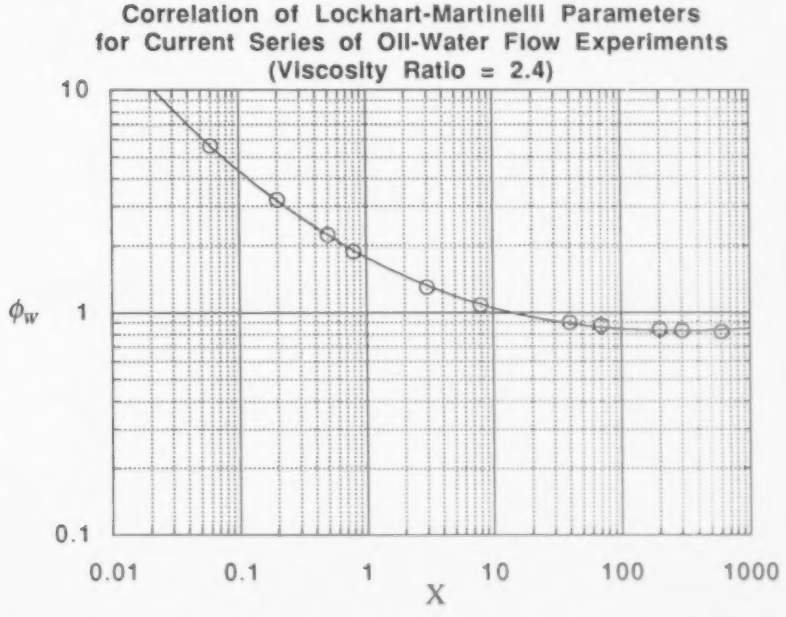

Figure 18: Correlation of Martinelli Parameters for Oil–Water Pipe Flow Experiments

The following equation was used to fit the data:

$$\log \phi_w = 0.250 - 0.303 \log X + 0.0802 (\log X)^2 - 0.00488 (\log X)^3 \qquad (5\text{–}45)$$

with the goodness of fit being 99.993%.

Although this equation is valid only for the viscosity ratio of 2.4 used in the current series of experiments, the form of the equation and this method may be used to correlate accurately pressure gradient data for oil–water pipe flows of any viscosity ratio.

5.1.3.3 Beggs and Brill Correlation Method

The Beggs and Brill[6] correlation method is widely known and well accepted for multiphase pipe flow calculations. Liquid–liquid flows are treated as homogeneous, with averaged parameters such as density and viscosity. The correlation was adapted for use in an Excel worksheet for this project from code developed for a programmable calculator by Hein[60,61]. The program was checked by matching Hein's results for seven different examples. Figure 19 contains a comparison of the measured values with the predicted values from the Beggs and Brill correlation method for the oil–water flow experiments.

The Beggs and Brill pressure gradient predictions are quite good for the oil–water pipe flows conducted (without flow through a perforation—this will be investigated in 5.2). The average absolute error for the oil–water flows is less than 7%. The largest errors are encountered for single–phase oil flow, located on the plot where the superficial water velocity (x axis) is zero. These larger errors are due to measurement error associated with the manometers used for the oil–only pipe flow experiments (see Chapter 4. Experimental Procedure).

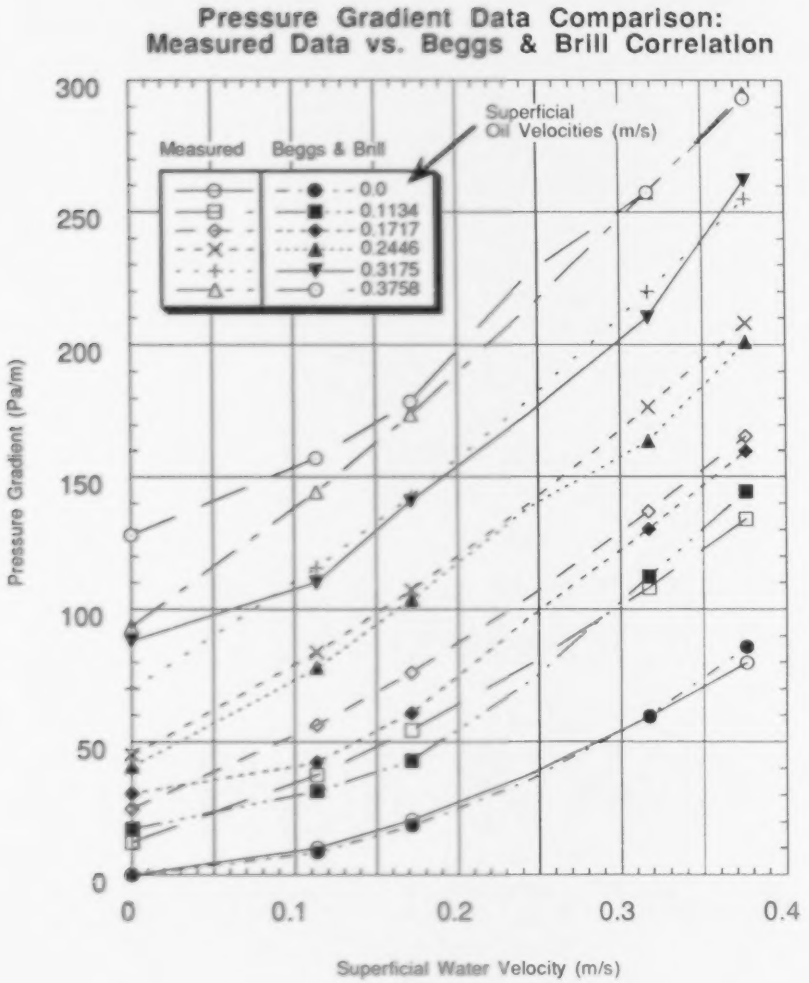

Figure 19: Comparison of Measured Pressure Gradient Data With Beggs and Brill[6] Correlation

5.2 Pipe Flow With Confluent Influx

The discussion and analysis thus far has centered on axial flow in a horizontal wellbore, which has been treated as a form of pipe flow. This is a logical starting point, since the well is shaped like a pipe, and the focus of multiphase flow has been on pipe flow for decades. Only recently have workers begun to examine in detail the more complex nature of the confluent influx into a horizontal well, whether via gun perforations, slotted liner or open–hole completions. There is a general disagreement among contemporary researchers as to the effect of the influx on the pressure gradient along the wellbore. This is somewhat due to confusion regarding the different types of pressure loss from various sources.

5.2.1 Single–Phase Pipe Flow With Flow Through A Single Perforation

Consider the simplest case of an axial single–phase flow within a circular pipe of diameter D, with a perpendicular flow intersecting the pipe via a duct of much smaller diameter, d. The fluid inflow through the perforation might be expected to affect the flow resistance in the pipe in three ways:

(1) By disrupting the thin boundary layer at the pipe wall, thus altering the wall friction forces. Even for the case of fully developed turbulent axial flow in the pipe, flow in a boundary layer of some finite thickness will likely be laminar. This effect may tend to increase or decrease the flow resistance.

(2) If the confluent influx momentum is sufficiently high with respect to the axial momentum, a more complex, three–dimensional flow disruption will be caused, which is likely to affect the entire axial flow cross section. This effect would be very difficult to analyze in detail, but the results may be examined in experiments.

(3) The confluent influx may be considered to enter the wellbore with zero axial velocity. Therefore energy must be consumed to accelerate the perforation flow in the axial direction. This effect is both the easiest to examine analytically, and likely to be the most important over a wide range of practical horizontal well conditions.

The last of these three mechanisms has been examined by Asheim *et al.*[62], via a momentum balance across a single perforation in a pipe. The method used is summarized as follows (see Figure 20).

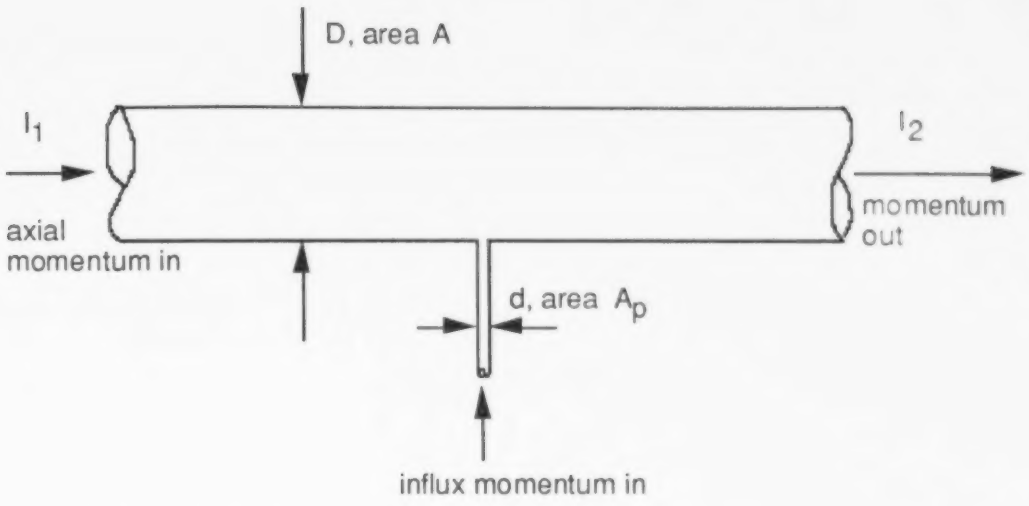

Figure 20: Pipe Flow With Influx Flow Through Single Perforation

Upstream of the perforation, the axial flowing momentum is defined as

$$I_1 = \dot{m}u = q\rho u = A\rho u^2 \tag{5–46}$$

where $\dot{m}$ is the mass flow rate in kg/s, and the other variables are as defined previously.

Downstream of the perforation the mass has increased by the addition of the perforation inflow:

$$I_2 = (q + \Delta q)\rho(u + \Delta u)$$

$$= \left(u + u_p \frac{A_p}{A}\right) A\rho \left(u + u_p \frac{A_p}{A}\right)$$

$$= \left(u + u_p \frac{A_p}{A}\right)^2 A\rho \tag{5–47}$$

where the subscript p and the Δ symbols refer to quantities associated with the perforation.

The force required to accelerate the confluent flow up to the axial flow velocity is equal to the momentum change across the perforation.

$$\text{momentum out} - \text{momentum in} = \text{accelerational force} \tag{5–48}$$

Writing this equation with the cross sectional areas replaced with the corresponding diameters gives

$$F_a = I_2 - I_1$$

$$= \left(u + u_p \frac{d^2}{D^2}\right)^2 \frac{\pi D^2}{4}\rho - \frac{\pi D^2}{4}\rho u^2$$

$$= \frac{\pi D^2}{4}\rho\left[\left(u + u_p \frac{d^2}{D^2}\right) - u^2\right]$$

$$= \frac{\pi D^2}{4}\rho\left[2uu_p\left(\frac{d}{D}\right)^2 + u_p^2\left(\frac{d}{D}\right)^4\right] \qquad (5\text{–}49)$$

The pressure which corresponds to the accelerational force is simply the force divided by the cross sectional area of the pipe. Thus

$$\Delta P_a = \frac{F_a}{A}$$

$$= \rho\left[2uu_p\left(\frac{d}{D}\right)^2 + u_p^2\left(\frac{d}{D}\right)^4\right]$$

$$= \rho u^2\left[2\frac{u_p}{u}\left(\frac{d}{D}\right)^2 + \left(\frac{u_p}{u}\right)^2\left(\frac{d}{D}\right)^4\right] \qquad (5\text{–}50)$$

The single perforation case may be extended to the more practical one of n perforations per unit length of wellbore quite easily[62]. The pressure gradient becomes

$$\frac{\Delta P_a}{L} = n\frac{F_a}{A}$$

$$= n\rho u^2\left[2\frac{u_p}{u}\left(\frac{d}{D}\right)^2 + \left(\frac{u_p}{u}\right)^2\left(\frac{d}{D}\right)^4\right]$$

$$= \rho u^2 \left[2\frac{q_p}{q} + \frac{1}{n}\left(\frac{q_p}{q}\right)^2 \right] \tag{5–51}$$

where $q_p = nu_pA_p$ is the inflow rate per unit length, and q is the pipe (axial) volumetric flow. Asheim *et al.*[62] adapted this accelerational pressure gradient for use as an equivalent accelerational friction factor component. By definition, for single–phase pipe flow

$$\frac{\Delta P}{L} = \frac{f\rho u^2}{2D} \tag{5–15}$$

This equation may be rearranged in order to define an accelerational friction factor component.[62]

$$f_a = \frac{2D\left(\Delta P/L\right)}{\rho u^2} = 2D\left[2\frac{q_p}{q} + \frac{1}{n}\left(\frac{q_p}{q}\right)^2 \right] \tag{5–52}$$

where the total friction factor may be defined as,

$$f = f_w + f_a \tag{5–53}$$

with *w* and *a* referring to the wall and accelerational terms, respectively.

5.2.2 Open–Hole Completion

The Asheim *et al.*[62] analysis only examined perforated wellbores. The model may be expanded easily to include the case of open–hole completions. Consider a section of a horizontal wellbore, with a thin interval Δx open to flow from the surrounding reservoir, as in Figure 21. The axial flowing momentum upstream and downstream, respectively, of the open interval are, as before:

$$I_1 = \dot{m}u = q\rho u = A\rho u^2 \tag{5–54}$$

$$I_2 = (q + \Delta q)\rho(u + \Delta u) \tag{5–55}$$

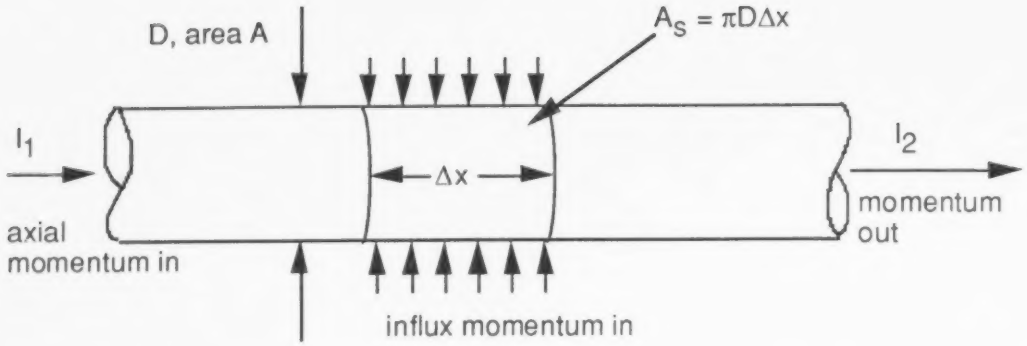

Figure 21: Pipe Section With Segment of Continuous Influx

Now using the subscript s to indicate the influx parameters, the momentum values may be expanded as follows:

$$I_1 = \frac{\pi D^2}{4}\rho u^2 \tag{5–56}$$

$$I_2 = \left[u + u_s \frac{\pi D\Delta x}{\left(\pi D^2/4\right)}\right]^2 \frac{\pi D^2}{4}\rho$$

$$= \left(u + u_s \frac{4\Delta x}{D}\right)^2 \frac{\pi D^2}{4}\rho \tag{5–57}$$

Then the accelerational force is

$$F_a = I_2 - I_1$$

$$= \frac{\pi D^2}{4}\rho\left[\left(u + u_s \frac{4\Delta x}{D}\right)^2 - u^2\right]$$

$$= \frac{\pi D^2}{4}\rho u^2\left[2\frac{4u_s}{uD}\Delta x + \left(\frac{4u_s}{uD}\Delta x\right)^2\right] \tag{5–58}$$

Recalling that pressure is simply force divided by cross–sectional area, the accelerational pressure drop across the open interval is defined as:

$$\Delta P_a = \rho u^2 \left[2\left(\frac{4u_s}{uD}\Delta x\right) + \left(\frac{4u_s}{uD}\Delta x\right)^2 \right] \tag{5–59}$$

Since

$$\frac{q_s}{q} = \frac{u_s \pi D}{\left(u\pi D^2/4\right)} = \frac{4u_s}{uD} \tag{5–60}$$

where q_s is the influx flow rate per unit length, the pressure drop becomes:

$$\Delta P_a = \rho u^2 \left[2\frac{q_s}{q}\Delta x + \left(\frac{q_s}{q}\Delta x\right)^2 \right] \tag{5–61}$$

or, in terms of a friction factor:

$$f_a = \frac{2D}{\Delta x}\left[2\frac{q_s}{q}\Delta x + \left(\frac{q_s}{q}\Delta x\right)^2 \right] \tag{5–62}$$

5.2.3 Liquid–Liquid Pipe Flow With Flow Through A Single Perforation

The preceding Asheim *et al.*[62] analysis may also be extended to a general (perforated) two–phase case as follows. The flowing momentum upstream of the perforation is now defined as

$$I_1 = q_O \rho_O u_O + q_W \rho_W u_W = A_O \rho_O u_O^2 + A_W \rho_W u_W^2 \tag{5–63}$$

in which the O and W subscripts refer to the oil and water phases, respectively (this analysis applies equally well to other two–phase cases, neglecting compressibility). Downstream of the perforation the flow momentum is,

$$I_2 = (q_o + \Delta q_o)\rho_o(u_o + \Delta u_o) + (q_w + \Delta q_w)\rho_w(u_o + \Delta u_o)$$

$$= \left(u_O + u_{po} \frac{A_{po}}{A_O} \right) A_O \rho_O \left(u_O + u_{po} \frac{A_{po}}{A_O} \right)$$

$$+ \left(u_W + u_{pw} \frac{A_{pw}}{A_W} \right) A_W \rho_W \left(u_W + u_{pw} \frac{A_{pw}}{A_W} \right)$$

$$= \left(u_O + u_{po} \frac{A_{po}}{A_O} \right)^2 A_O \rho_O + \left(u_W + u_{pw} \frac{A_{pw}}{A_W} \right)^2 A_W \rho_W \qquad (5\text{–}64)$$

The accelerational force is again determined by subtracting the upstream momentum from the downstream momentum:

$$F_a = I_2 - I_1$$

$$= \left(u_O + u_{po} \frac{A_{po}}{A_O} \right)^2 A_O \rho_O + \left(u_W + u_{pw} \frac{A_{pw}}{A_W} \right)^2 A_W \rho_W - A_W \rho_W u_W^2 + A_W \rho_W u_W^2$$

$$= A_O \rho_O \left[2 u_O u_{po} \frac{A_{po}}{A_O} + \left(u_{po} \frac{A_{po}}{A_O} \right)^2 \right] + A_W \rho_W \left[2 u_W u_{pw} \frac{A_{pw}}{A_W} + \left(u_{pw} \frac{A_{pw}}{A_w} \right)^2 \right]$$

$$= A_O \rho_O u_O^2 \left[2 \frac{u_{po}}{u_O} \frac{A_{po}}{A_O} + \left(\frac{u_{po}}{u_O} \frac{A_{po}}{A_O} \right)^2 \right]$$

$$+ A_W \rho_W u_W^2 \left[2 \frac{u_{pw}}{u_W} \frac{A_{pw}}{A_W} + \left(\frac{u_{pw}}{u_W} \frac{A_{pw}}{A_W} \right)^2 \right] \qquad (5\text{–}65)$$

and the associated pressure drop across the perforation is again simply

$$\Delta P_a = \frac{F_a}{A} \qquad (5\text{–}66)$$

The equations may be simplified for the case of the experiments presently considered in which only one phase (the water) is flowing through the perforation. The pressure drop across the perforation becomes:

$$\Delta P_a = \frac{A_W \rho_W u_W^2}{A}\left[2\frac{u_{pw}}{u_W}\frac{A_{pw}}{A_W} + \left(\frac{u_{pw}}{u_W}\frac{A_{pw}}{A_W}\right)^2\right] \tag{5–67}$$

Now considering the case of a well with a continuous perforation density of n perforations per unit length:

$$\frac{\Delta P_a}{L} = \frac{nF_a}{A} = \frac{nA_W \rho_W u_W^2}{A}\left[2\frac{u_{pw}}{u_W}\frac{A_{pw}}{A_W} + \left(\frac{u_{pw}}{u_W}\frac{A_{pw}}{A_W}\right)^2\right]$$

$$= \frac{A_W \rho_W u_W^2}{A}\left[2\frac{q_p}{q_W} + \frac{1}{n}\left(\frac{q_p}{q_W}\right)^2\right] \tag{5–68}$$

in which the perforation flow rate per unit length is now defined as

$$q_p = n u_p A_p \tag{5–69}$$

Recalling the equation for the friction factor in pipe flow,

$$\frac{\Delta P}{L} = \frac{f\rho u^2}{2D} \tag{5–15}$$

and letting the effective diameter of the pipe flowing water be defined as

$$D_W = 2\sqrt{\frac{A_W}{\pi}} \tag{5–70}$$

then the accelerational friction factor component for two–phase oil–water flow with water flowing through n perforations per unit length may be defined as:

$$f_a = \frac{4\sqrt{\frac{A_W}{\pi}}\frac{\Delta P_a}{L}}{\rho_W u_W^2} = \frac{2D_W^2}{D}\left[2\frac{q_p}{q_W} + \frac{1}{n}\left(\frac{q_p}{q_W}\right)^2\right] \tag{5–71}$$

It is important to note that in practice all quantities are in situ. In the case of steady–state two–phase flow in a long pipe the in situ flow rates will not necessarily be equivalent to the corresponding rates at the pipe entrance, due to the holdup effect. One of the phases, typically the more dense one, will tend to collect in the pipe since the other phase will flow preferentially such that there is a net slip velocity between the phases. The holdup ratio may be defined as

$$H = \frac{\text{in situ volume fraction of water to oil}}{\text{input volume fraction of water to oil}}$$

$$= \frac{\left(q_W / q_O\right)_{in\ situ}}{\left(q_W / q_O\right)_{input}}$$

$$= \frac{\left(u_W A_W / u_O A_O\right)_{in\ situ}}{\left(u_W A_W / u_O A_O\right)_{input}} \qquad (5\text{–}72)$$

The method used to obtain the holdup ratio for the present series of experiments was described in the section on experimental procedure. The input volumetric flow rates are known, and the static volume ratio of a section of the model is measured by simultaneously isolating the test section and stopping the pumps. This is an inexpensive and reasonably accurate method of determining the in situ volume ratio of the constituent fluids, but unfortunately it does not provide a measure of the in situ flow velocities, u. Thus, to determine the pressure gradient or friction factor via the method outlined, either the slip velocity must be obtained in some manner, or an assumption will be necessary. The most reasonable assumption to make is that the total (oil plus water) in situ flow rate is identical to the total input flow rate. Since the input flow rates and the in situ volume ratios are known, the calculated holdup ratio may be applied to determine a fair estimate of the in situ superficial velocities. This may be expressed using the following equations. The first equation represents the assumption used:

$$\left(q_W + q_O\right)_{in\ situ} = \left(q_W + q_O\right)_{input} \qquad (5\text{–}73)$$

$$H\left(q_W / q_O\right)_{input} = \left(q_W / q_O\right)_{in\ situ} \qquad (5\text{–}74)$$

There are two equations with two unknowns, the in situ flow rates. Therefore, after rearrangement:

$$q_{w_{in\ situ}} = (q_W + q_O)_{input} - \frac{(q_W + q_O)_{input}}{H\left(q_W / q_O\right)_{input} + 1} \qquad (5\text{–}75)$$

This flow rate may then be used in Equation (5–71) to determine the oil–water accelerational pressure drop across a perforation flowing only water.

5.2.4 Experimental Data and Model Predictions

The method described in the preceding section was used to produce the following plots (Figures 22 through 26). Each graph plots the pressure gradient against the total water flow rate for a given oil flow rate for three sets of data: the values measured in the current series of experiments; predicted values generated using the Beggs and Brill[6] correlation for pipe flow; and predicted values again produced using the Beggs and Brill pipe flow correlation, now supplemented by the modified Asheim *et al.*[62] accelerational pressure drop as described in this section.

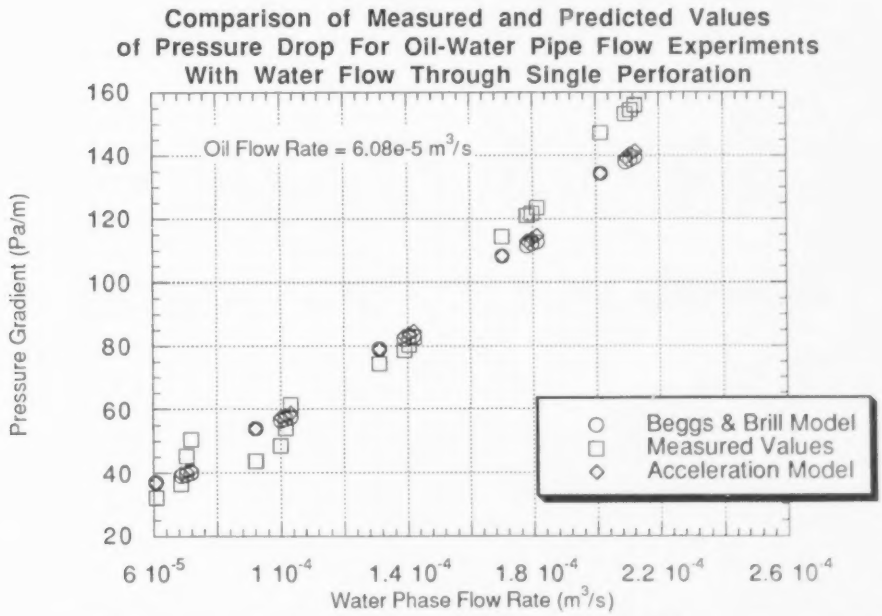

Figure 22: Measured and Predicted Pressure Gradients for Oil–Water Experiments With Flow Through A Single Perforation (Oil Rate = 6.08 e–5 m^3/s)

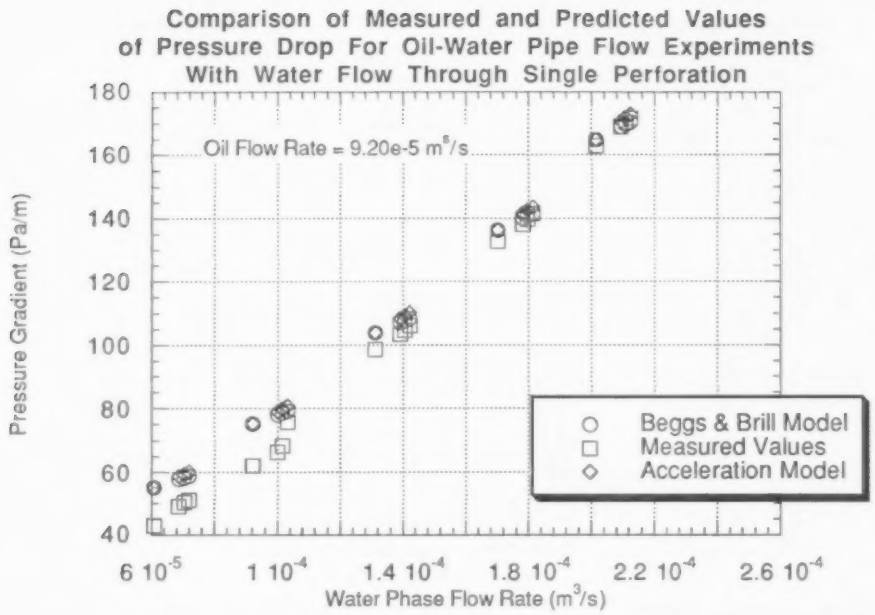

Figure 23: Measured and Predicted Pressure Gradients for Oil–Water Experiments With Flow Through A Single Perforation (Oil Rate = 9.20 e–5 m^3/s)

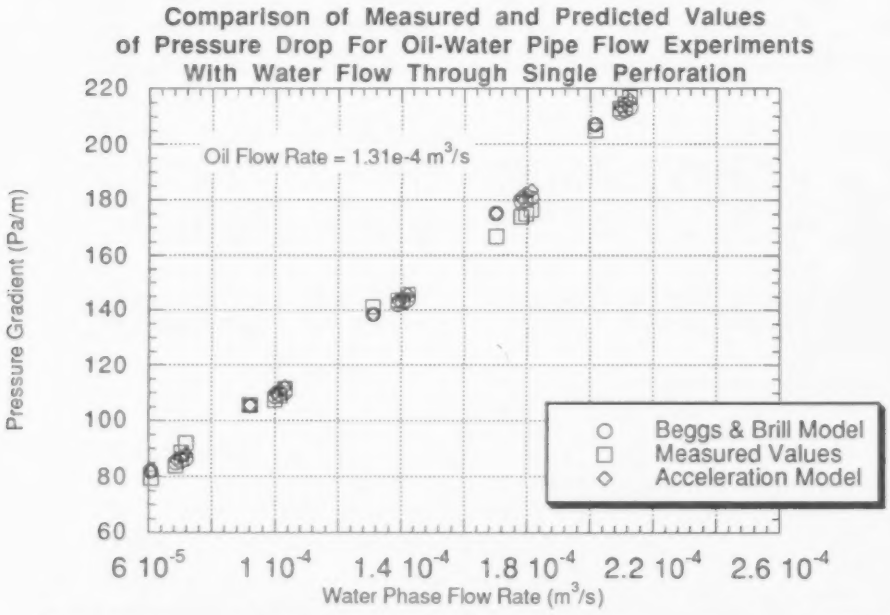

Figure 24: Measured and Predicted Pressure Gradients for Oil–Water Experiments With Flow Through A Single Perforation (Oil Rate = 1.31 e–4 m^3/s)

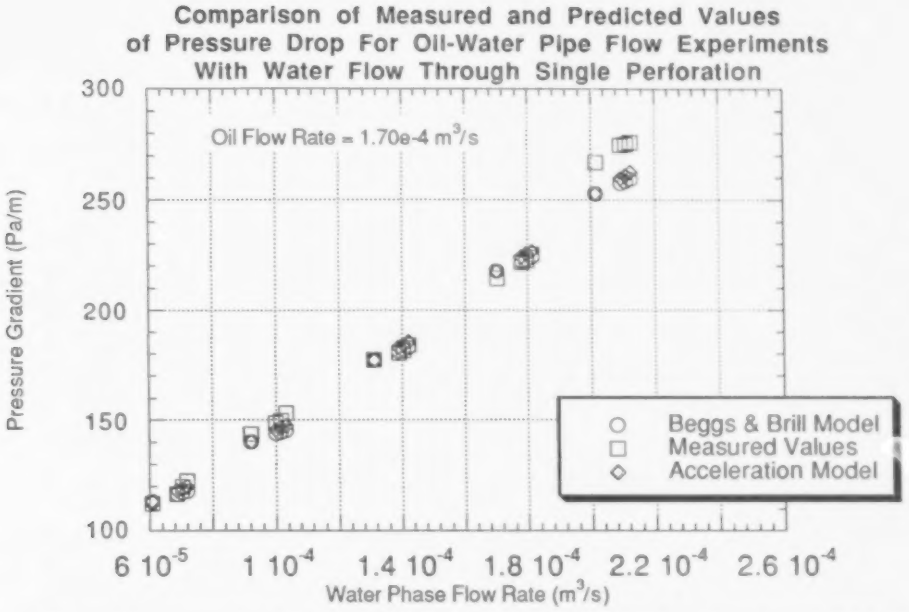

Figure 25: Measured and Predicted Pressure Gradients for Oil–Water Experiments With Flow Through A Single Perforation (Oil Rate = 1.70 e–4 m^3/s)

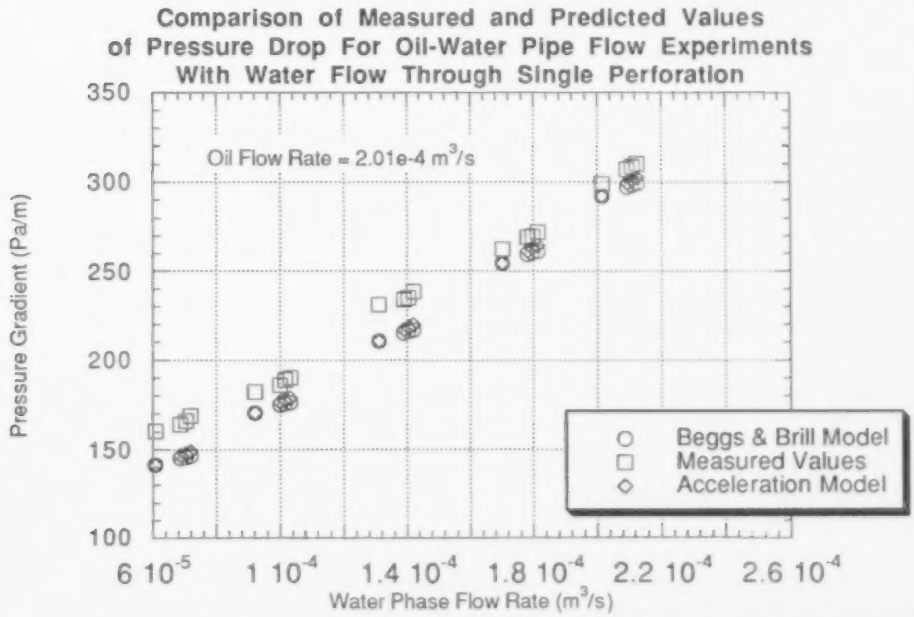

Figure 26: Measured and Predicted Pressure Gradients for Oil–Water Experiments With Flow Through A Single Perforation (Oil Rate = 2.01 e–4 m^3/s)

Each plot contains from left to right five groups of data, representing five different main pipe water flow rates: 6.08e–5, 9.20e–5, 1.31e–4, 1.70e–4, and 2.01e–4 m^3/s, respectively. The data points furthest to the left (with the lowest water flow rates) within each group represent experiments without water flowing through the single perforation. The data points bunched closely to the right were obtained during experiments run with water flowing through the perforation. Hence, the *x* axis represents the total (main pipe plus perforation) water flow rate in the model for any given experiment.

The plots show reasonable agreement between the Beggs and Brill[6] model and the measured values, and slightly better agreement with the accelerational model incorporated into the calculations. The level of error is generally observed to increase with the oil flow rate; the average error for both the Beggs and Brill and accelerational methods is about 5.7%. However, the pressure gradients reported have been averaged over the model length of 9.5 m, thus having a smoothing or masking effect on the pressure drop directly associated with the water flow through the perforation. The following plots (Figures 27–31) serve to further isolate this pressure drop for the same experiments. Each plot compares the observed pressure drop across the single perforation to a predicted value calculated using the modified Asheim *et al.*[62] method described above. Data points falling on the *x* axis correspond with experiments in which there was no flow through the

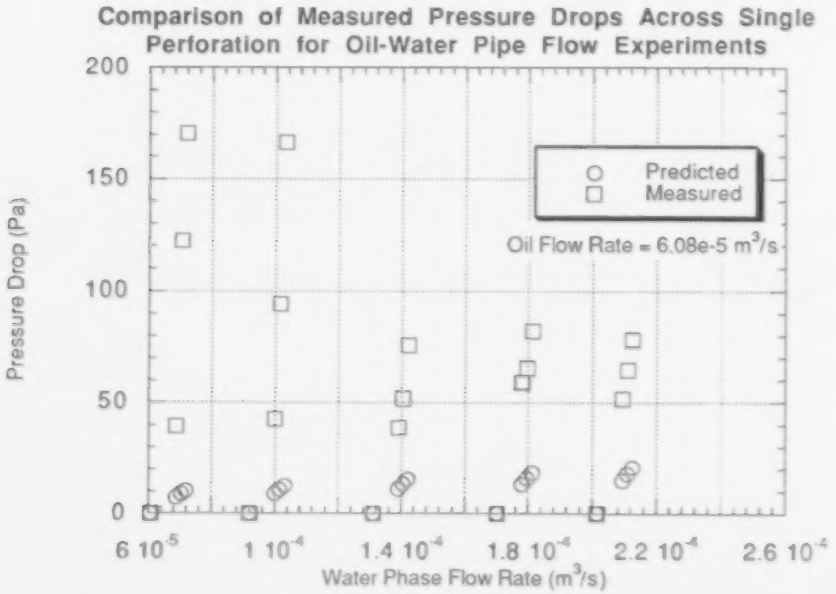

Figure 27: Measured and Predicted Pressure Drops Across A Single Perforation, Oil–Water Pipe Flow Experiments (Oil Flow Rate = 6.08 e–5 m^3/s)

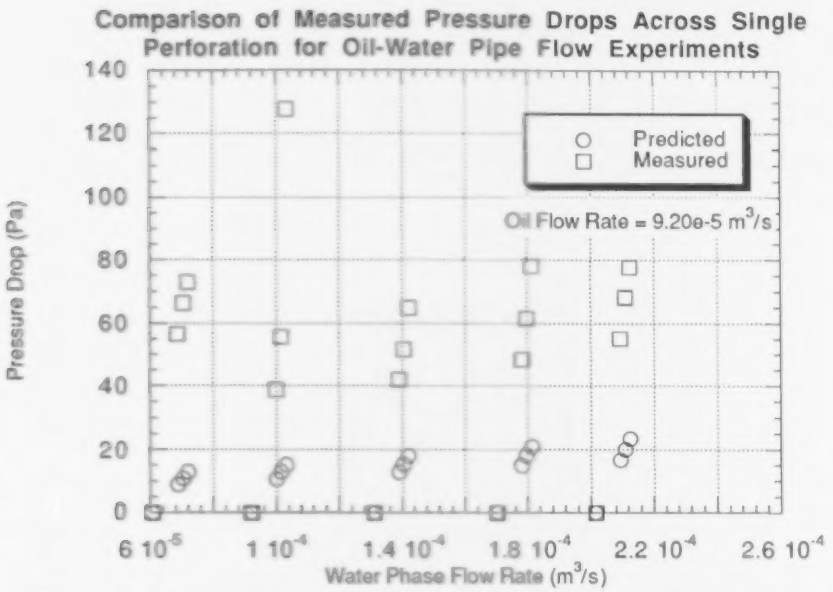

Figure 28: Measured and Predicted Pressure Drops Across A Single Perforation, Oil–Water Pipe Flow Experiments (Oil Flow Rate = 9.20 e–5 m^3/s)

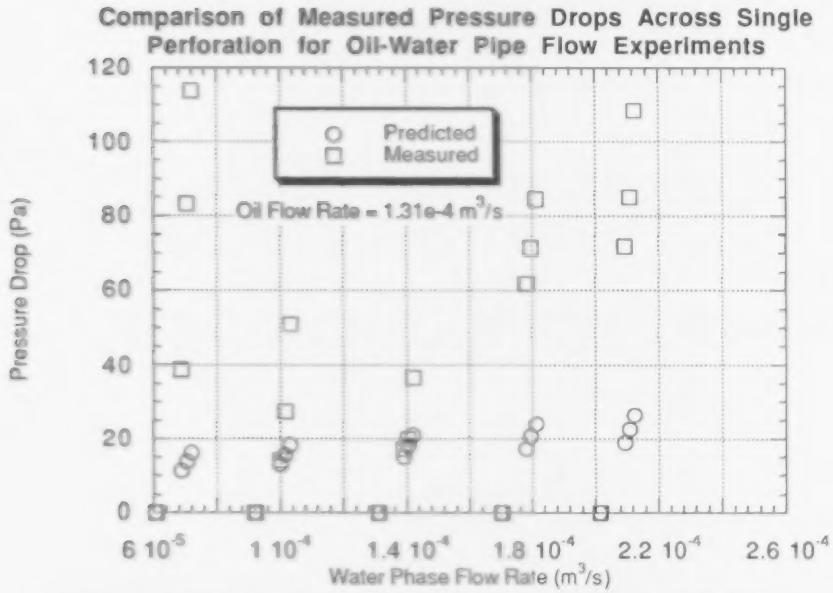

Figure 29: Measured and Predicted Pressure Drops Across A Single Perforation, Oil–Water Pipe Flow Experiments (Oil Flow Rate = 1.31 e–4 m^3/s)

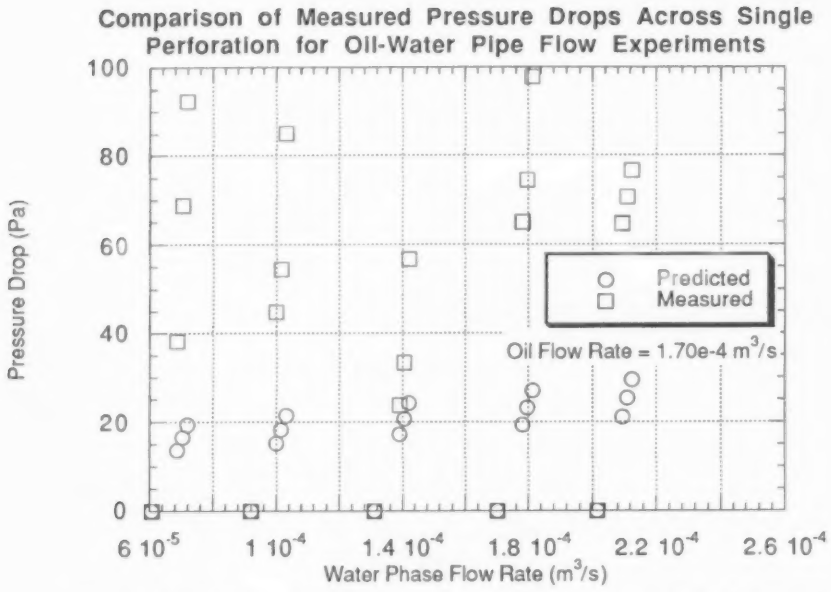

Figure 30: Measured and Predicted Pressure Drops Across A Single Perforation, Oil–Water Pipe Flow Experiments (Oil Flow Rate = 1.70 e–4 m^3/s)

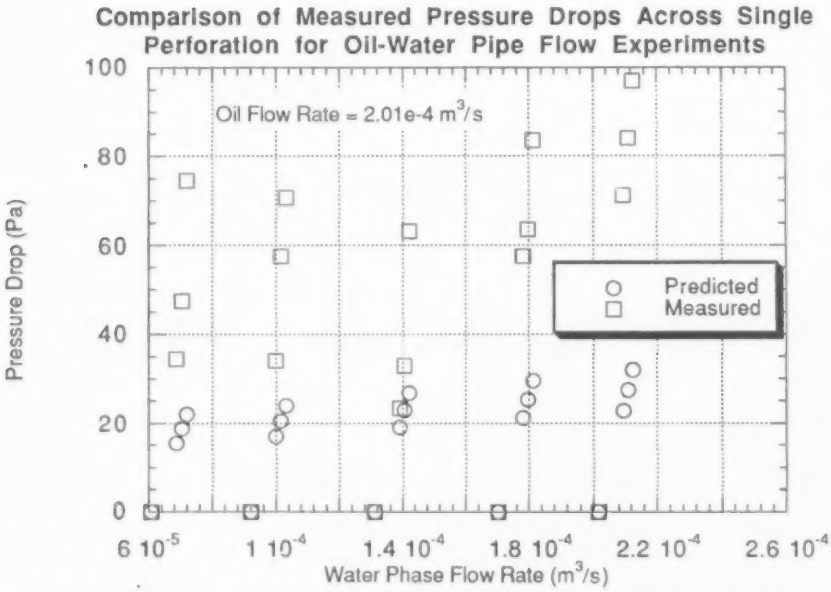

Figure 31: Measured and Predicted Pressure Drops Across A Single Perforation, Oil–Water Pipe Flow Experiments (Oil Flow Rate = 2.01 e–4 m^3/s)

perforation. The other data points (three measured and three predicted values) correspond with the three non–zero influx flow rates through the perforation.

Again, each plot contains five groups of data, identifiable in rough columns. The data points located on the x axis represent pipe flow without inflow through the single perforation. These plots demonstrate very clearly that the Asheim *et al.*[62] acceleration model, modified for two–phase oil–water flow, does not adequately predict the pressure drop across a single perforation for the conditions under which the current series of experiments were conducted. This is not entirely unexpected, since Asheim *et al.*[62] set a working range of validity for his model defined by:

$$u_p < 3u \tag{5–76}$$

which for the current experiments may be expressed as:

$$u_p < 3u_w \tag{5–77}$$

Unfortunately, all of the experiments carried out for this study fail to satisfy this condition (i.e., the perforation water velocity was greater than three times the main pipe water velocity for all of the experiments). The difference between the measured and predicted pressure drops across the single perforation is associated neither with accelerational nor pipe wall friction pressure drop. It must therefore be caused by an additional (third) flow disturbance. This disturbance may be described as a venturi or constriction effect. Flow through the perforation of sufficient velocity creates a partial barrier to flow in the main pipe. The main flow is thus constricted as it passes the perforation, before expanding again somewhat downstream of it. This effect is depicted in Figure 32.

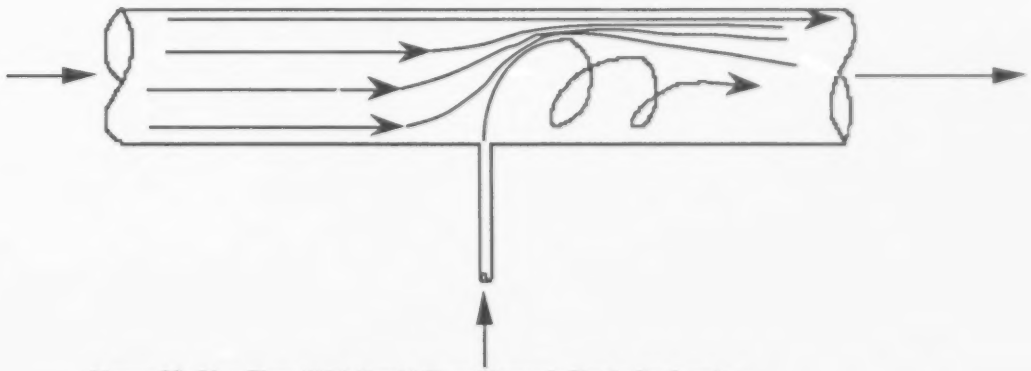

Figure 32: Pipe Flow With Rapid Flow Through Single Perforation

5.2.5 Field–Scale Prediction Methods

Asheim *et al.*[62] conducted single–phase liquid pipe flow experiments with flow through a single perforation, confirming the validity of their accelerational model within the working range of flow velocities given above. The authors argued that this range covers the expected range of flow velocity ratios in actual horizontal wells. In Section 5.1.3.3 of this thesis, the Beggs and Brill[6] correlation was shown to adequately predict the pressure gradient of horizontal (immiscible) liquid–liquid pipe flows without flow through a perforation, despite the simplified treatment in which density and viscosity parameters are averaged, and slip between the phases is neglected. For the purpose of field–scale predictions, the condition stated by Asheim *et al.*[62] in Equation (5–76), and the homogeneous flow assumptions used in the Beggs and Brill[6] correlation are therefore considered to be reasonable.

Landman and Goldthorpe[4] and Landman[8] developed a set of numerical models to analyze pressure drop for single–phase incompressible flow in horizontal wells. The methods used were adapted for this project to include the effect of laminar flow and accelerational pressure gradient for both cased and perforated, and open–hole completed horizontal wells. The procedures were written for the Mathematica programming language, and the listings are provided in Appendix C. A number of computer runs were performed in order to observe the effect of variation of various parameters.

5.2.5.1 Simple Constant Influx Open–Hole Model

The first series of runs was conducted to model conditions typical of heavy oil reservoirs in eastern Alberta and western Saskatchewan. The completion type typical in these fields is open–hole or slotted liner, and open–hole completion is used in the numerical model. Other well and production parameters are listed in Table 5.

Table 5: Well and Production Data Used In Figures 33 – 35

WELL AND PRODUCTION DATA			
Flow Rate (m^3/d)	100	Drawdown (MPa)	3.5
Well Length (m)	1000	Oil Density (kg/m^3)	950
Diameter (m)	0.125	Oil Viscosity (mPa.s)	1000

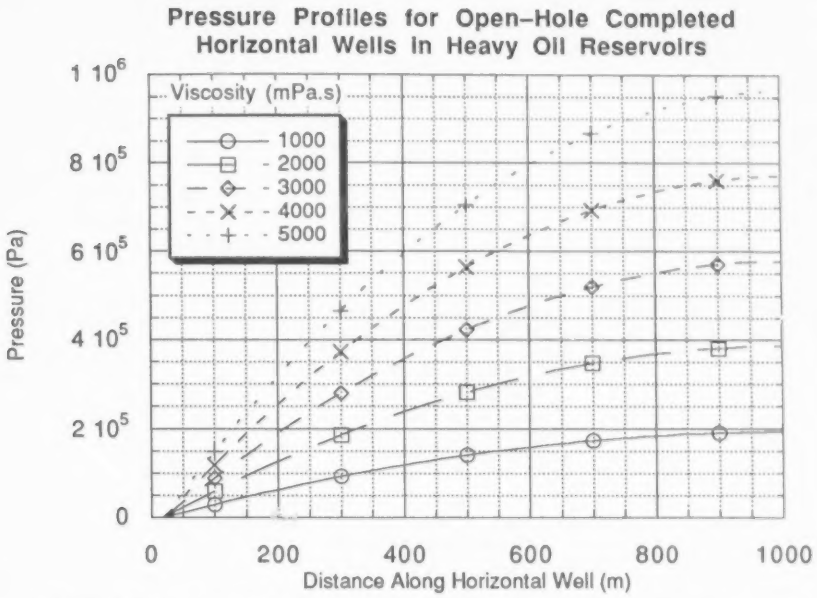

Figure 33: Predicted Field–Scale Pressure Profiles Assuming Constant Influx, With Fluid Viscosity As A Cross Parameter

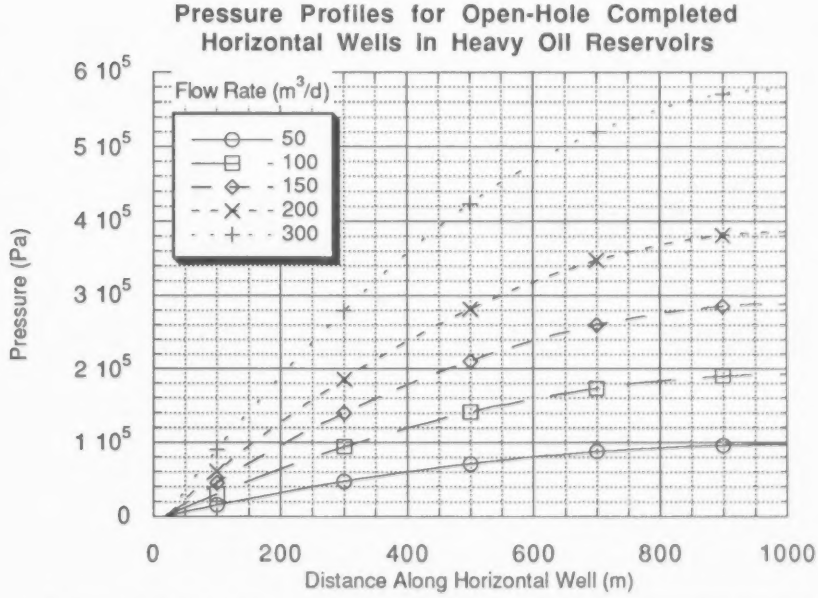

Figure 34: Predicted Field–Scale Pressure Profiles Assuming Constant Influx, With Fluid Flow Rate As A Cross Parameter

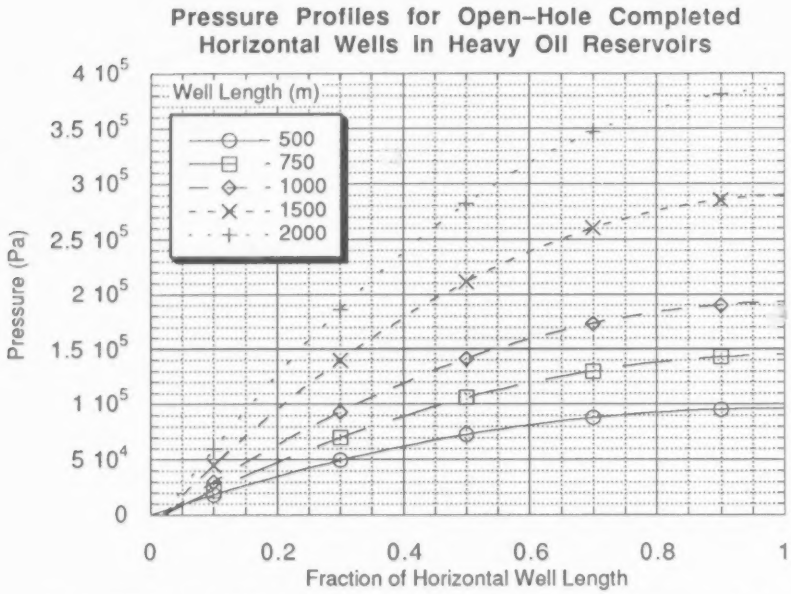

Figure 35: Predicted Field–Scale Pressure Profiles Assuming Constant Influx, With Well Length As A Cross Parameter

The model used to generate Figures 33 – 35 is not coupled to reservoir flow; thus, the calculations are not dependent on reservoir permeability or drawdown. The assumption of constant influx over the length of the open wellbore is employed (see Figure 1(a) in Section 3.1.1). For the high viscosities used, wellbore flow lies entirely within the laminar regime, such that wellbore roughness and pressure drop due to acceleration of the influx play no part in the calculation of the pressure profile.

5.2.5.2 Reservoir–Coupled Cased and Perforated Model

A second numerical model was used to obtain the data in the following plots. This version of Landman's[4] model is for cased and perforated horizontal wells. Well flow behaviour is coupled to reservoir flow via a simple Darcy relationship. Drawdown pressure is specified and equated with the well flowing pressure at the producing end. Perforation dimension and reservoir permeability parameters are also specified. The program used is numerically intensive; a coefficient matrix of size nxn must be inverted , where n is the number of perforations specified. For reasonable running times, runs were made with no more than 200 perforations specified. It follows that the well lengths used in the computer runs were similarly limited for realistic perforation densities.

Figure 36 is a comparison of well pressures calculated using variations of Landman's[4] numerical model for cased and perforated horizontal wells. The original Landman[4] model data is compared with data from the same model modified for this study to incorporate pressure calculations for both laminar flow conditions occurring at or near the toe end of the well, and the Asheim *et al.*[62] model for accelerational pressure drop across perforations.

Table 6: Well and Production Data Used in Figure 36

WELL AND PRODUCTION DATA			
Number of Perforations	200	Drawdown (kPa)	50
Well Length (m)	400	Oil Density (kg/m^3)	750
Diameter (m)	0.125	Oil Viscosity (mPa.s)	0.5
Well Roughness (m)	0.001	Perforation Radius (m)	0.01
Permeability (D)	1	Perforation Length (m)	0.35

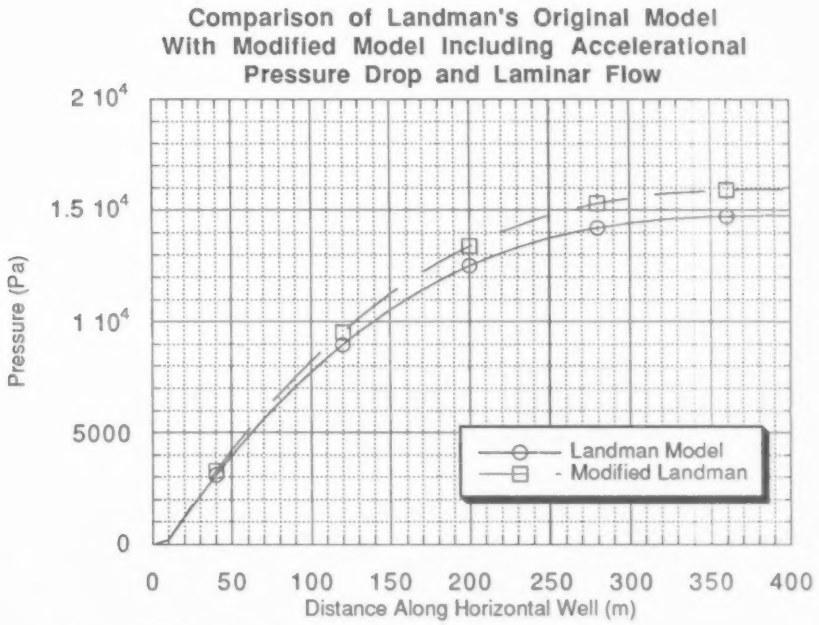

Figure 36: Field–Scale Prediction Model Comparison

From Figure 36 it is clear that the accelerational pressure drop makes up a small but significant fraction of the total pressure drop. The absolute difference in predicted pressures at the toe of the well is over 8%. This contradicts Landman's assertion that the pressure drop due to acceleration of the confluent influx is always insignificant for realistic

production conditions. The conditions used for this comparison are taken from Landman's paper[4] and are listed in Table 6.

The following figures show the effect of variation of well and reservoir parameters using the modified Landman[4] (cased and perforated) model incorporating Asheim *et al.*'s acceleration model[62] (well and production data used are listed in Table 7).

Table 7: Well and Production Data Used in Figures 37 – 40

WELL AND PRODUCTION DATA			
Number of Perforations	200	Drawdown (kPa)	1000
Well Length (m)	200	Oil Density (kg/m^3)	750
Diameter (m)	0.125	Oil Viscosity (mPa.s)	2
Well Roughness (m)	0.001	Perforation Radius (m)	0.01
Permeability (D)	1	Perforation Length (m)	0.35

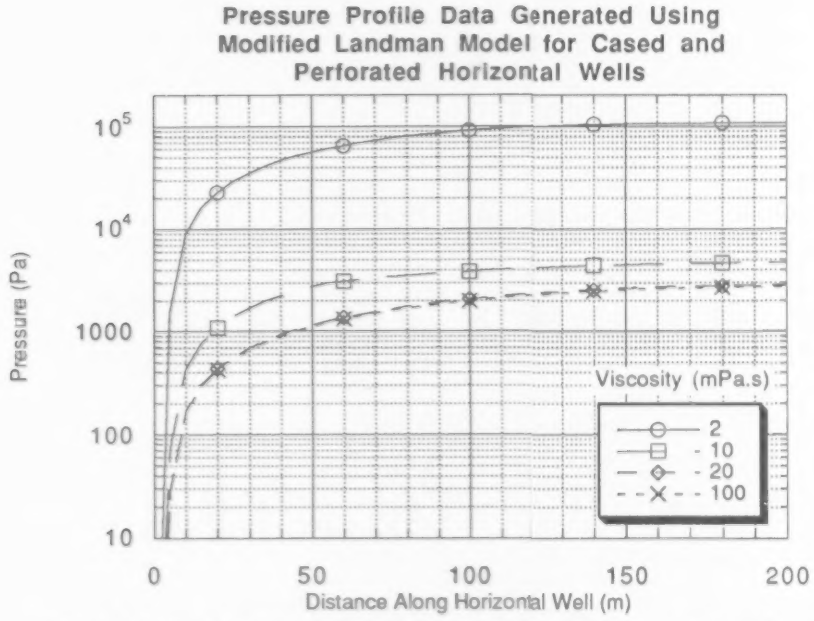

Figure 37: Field–Scale Pressure Profile Predictions for Cased and Perforated Horizontal Wells With Viscosity As A Cross Parameter

Figure 37 shows the effect of the variation of well fluid viscosity on the pressure profile of a horizontal well. Note the large variation in pressure drop between viscosities of 2 and 10 mPa.s, and that there is virtually no difference in the pressure profiles for viscosities of 20 and 100 mPa.s. The Reynolds number is inversely proportional to viscosity, and beyond a certain threshold, frictional pressure drop becomes practically independent of viscosity.

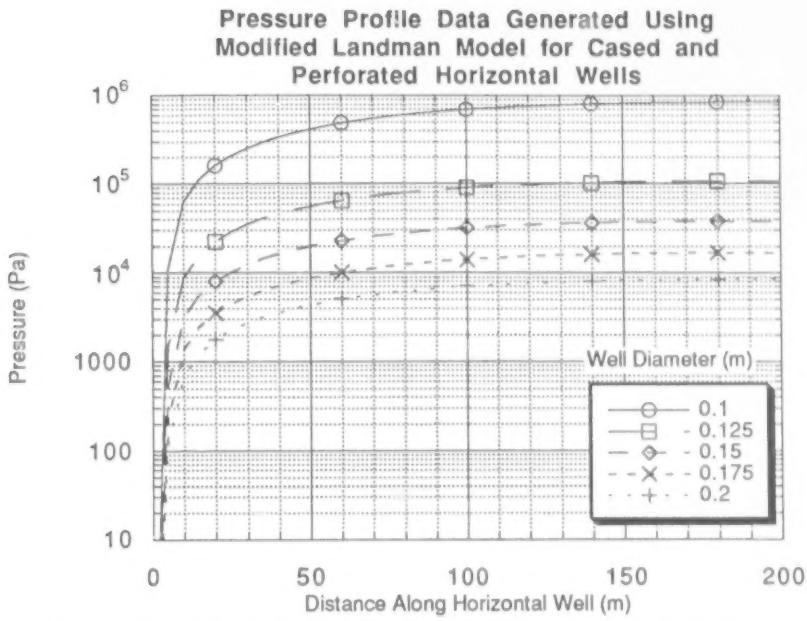

Figure 38: Field–Scale Pressure Profile Predictions for Cased and Perforated Horizontal Wells With Well Diameter As A Cross Parameter

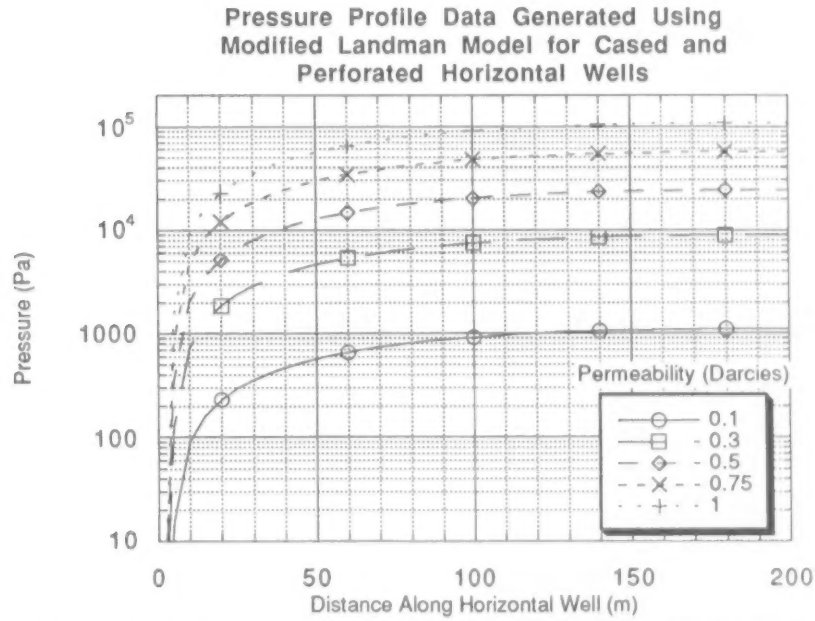

Figure 39: Field–Scale Pressure Profile Predictions for Cased and Perforated Horizontal Wells With Permeability As A Cross Parameter

The variation of the pressure drop profile with changing well diameter is illustrated in Figure 38. The pressure drop across the well increases rapidly with decreasing well diameter, especially below 0.125 m. Figure 39 shows the effect on the pressure drop of variation of the reservoir permeability. Increasing the reservoir permeability allows for higher flow rates into the well and resulting higher rates within the well, leading to a higher frictional pressure drop.

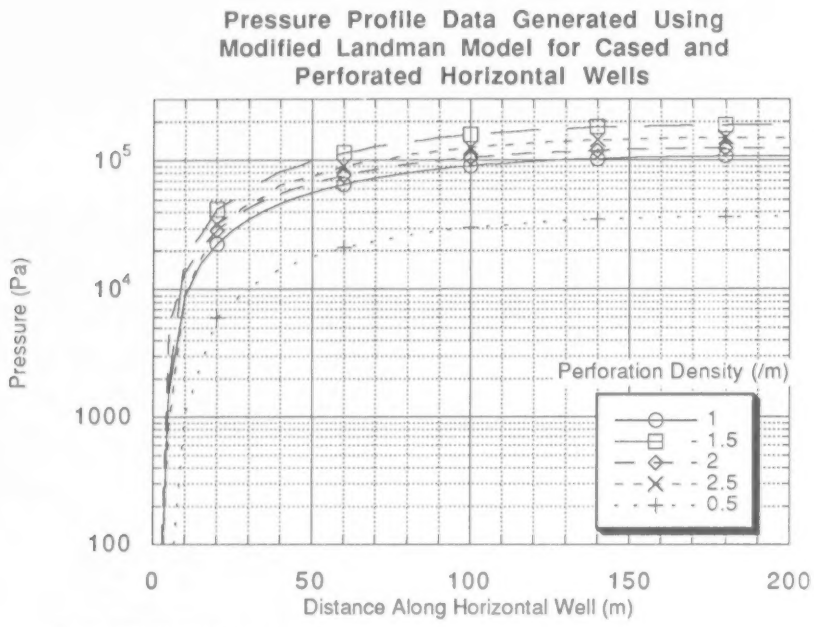

Figure 40: Field–Scale Pressure Profile Predictions for Cased and Perforated Horizontal Wells With The Perforation Density As A Cross Parameter

Figure 40 shows the effect on the pressure profile with variation of the perforation density. The pressure drop is seen to increase rapidly with increasing perforation density between 0.5 and 1 perforations per meter well length, and then to increase much more gradually above 1 perforation per metre (recall that the well length used for this series of runs is 200 m). Landman and Goldthorpe[4] performed a series of runs investigating the effects of varying the perforation density along the length of horizontal wells, and the interested reader is referred to this paper.

5.2.5.3 Reservoir–Coupled Open–Hole Model

Landman[8] developed another pressure drop prediction model based on Dikken's model[3] for open–hole completions. Instead of requiring numerical integration for solution

as in Dikken's model (see Appendix A), Landman's approach put the solution in the form of two non–linear simultaneous equations, one of which included the Gauss hypergeometric function, which may be evaluated rapidly using a rational approximation. Unlike the cased and perforated model which explicitly used roughness as an input parameter, the hypergeometric model employed a Blasius–type exponent, α to represent the well roughness, as had Dikken's model. The model is not nearly so numerically intensive as the cased and perforated model, but has the slight disadvantage that one of the pressure drawdown, the specific productivity index, or the total well flow rate must be specified beforehand. In the figures that follow, both the pressure drop and the specific inflow profile are plotted (well and production data used are listed in Table 8).

Table 8: Well and Production Data Used in Figures 41 – 46

WELL AND PRODUCTION DATA			
Permeability (D)	1	Flow Rate (m^3/d)	1000
Well Length (m)	1000	Oil Density (kg/m^3)	750
Alpha	0.23	Number of Segments	200
Diameter (m)	0.125	Oil Viscosity (mPa.s)	1

Figure 41 plots the pressure and specific inflow profiles along the length of a horizontal well, with well diameter as a cross parameter. Note that the pressure axis is logarithmic while the specific inflow axis is linear. The well diameter has a large effect on both the pressure drop across the horizontal well and the drawdown pressure. These effects are manifested in a large variation in the specific inflow profile with well diameter for the input values used. The specific inflow profile is very flat for a well diameter of 0.2m, but the inflow becomes highly skewed, favouring the producing end of the well with decreasing well diameter. In a field situation where suppresion of water or gas coning is a prime consideration, a flat specific inflow profile along the horizontal wellbore is beneficial.

Figure 42 has well length as the cross parameter. Note that for a given total flow rate (1000 m^3/d for the current series of runs) the specific inflow favours the near (producing) end of the well to the far end for all the cases tested, and to a slightly greater extent with increasing well length.

Reservoir permeability is the cross parameter in Figure 43. A large variation in the specific inflow profile is observed over the range of permeabilities tested. In reservoir–coupled models such as the Landman[8] hypergeometric model used for this series of runs, the reservoir permeability directly affects the production flow rate, on which the frictional pressure drop in the wellbore is dependent.

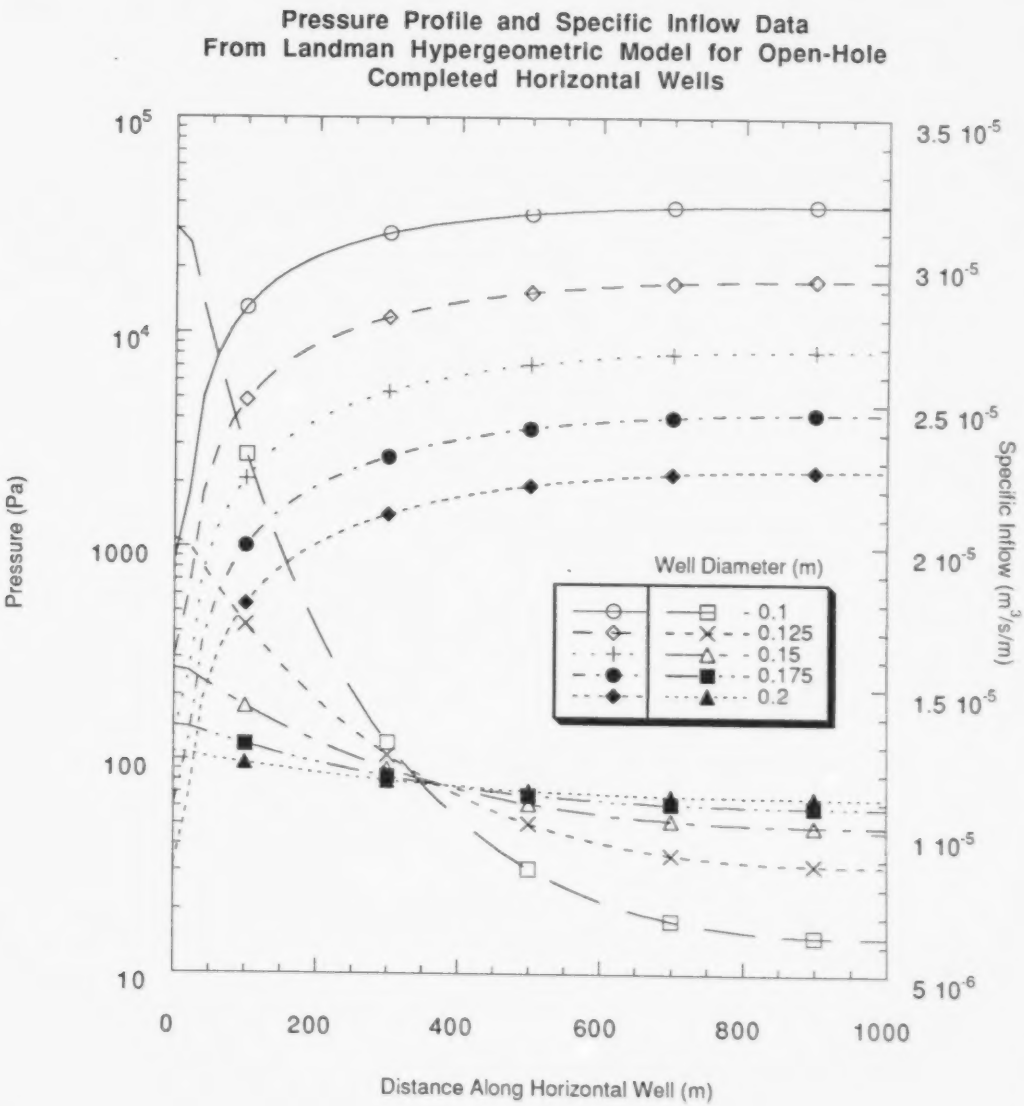

Figure 41: Field–Scale Pressure and Specific Inflow Profile Predictions for Open Hole Horizontal Wells With Well Diameter As A Cross Parameter

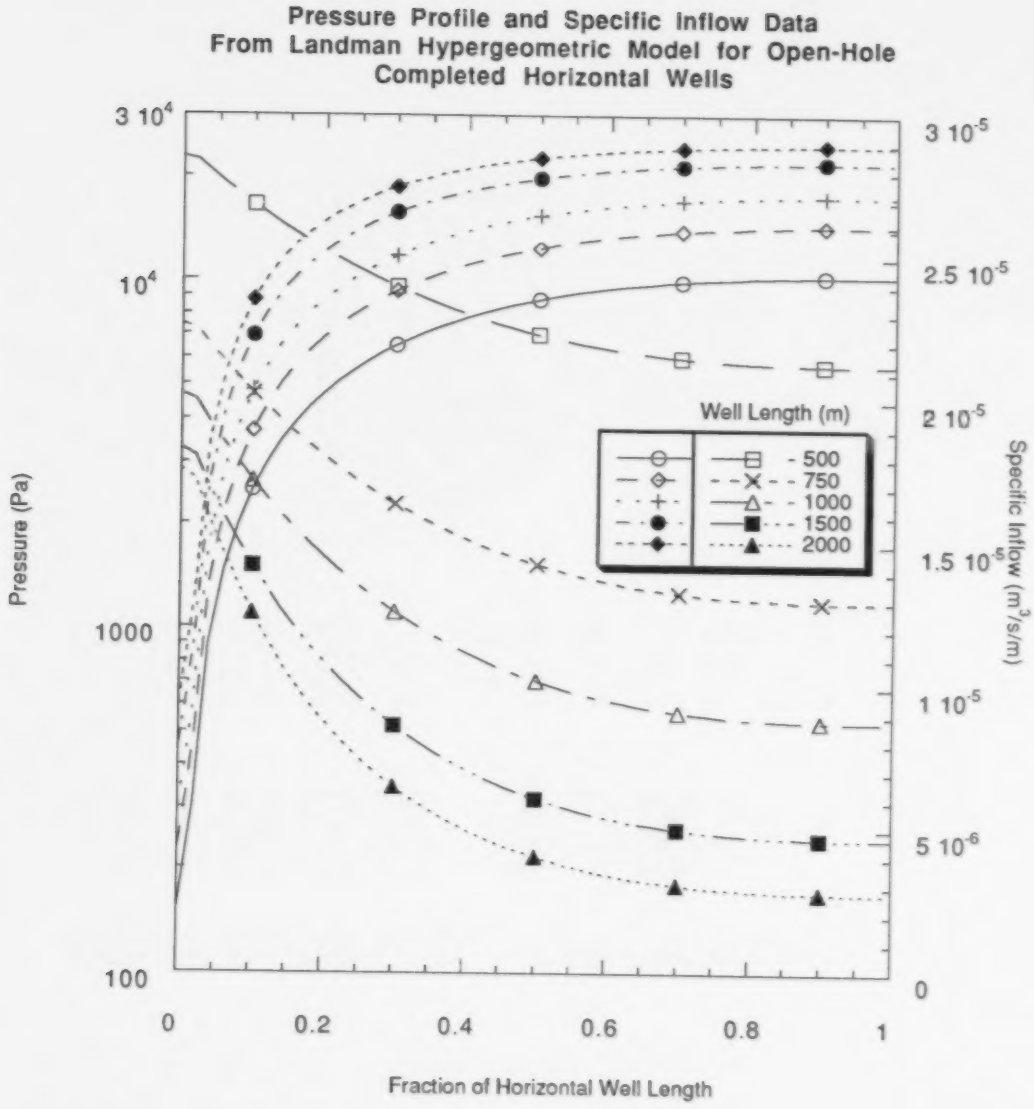

Figure 42: Field–Scale Pressure and Specific Inflow Profile Predictions for Open Hole Horizontal Wells With Well Length As A Cross Parameter

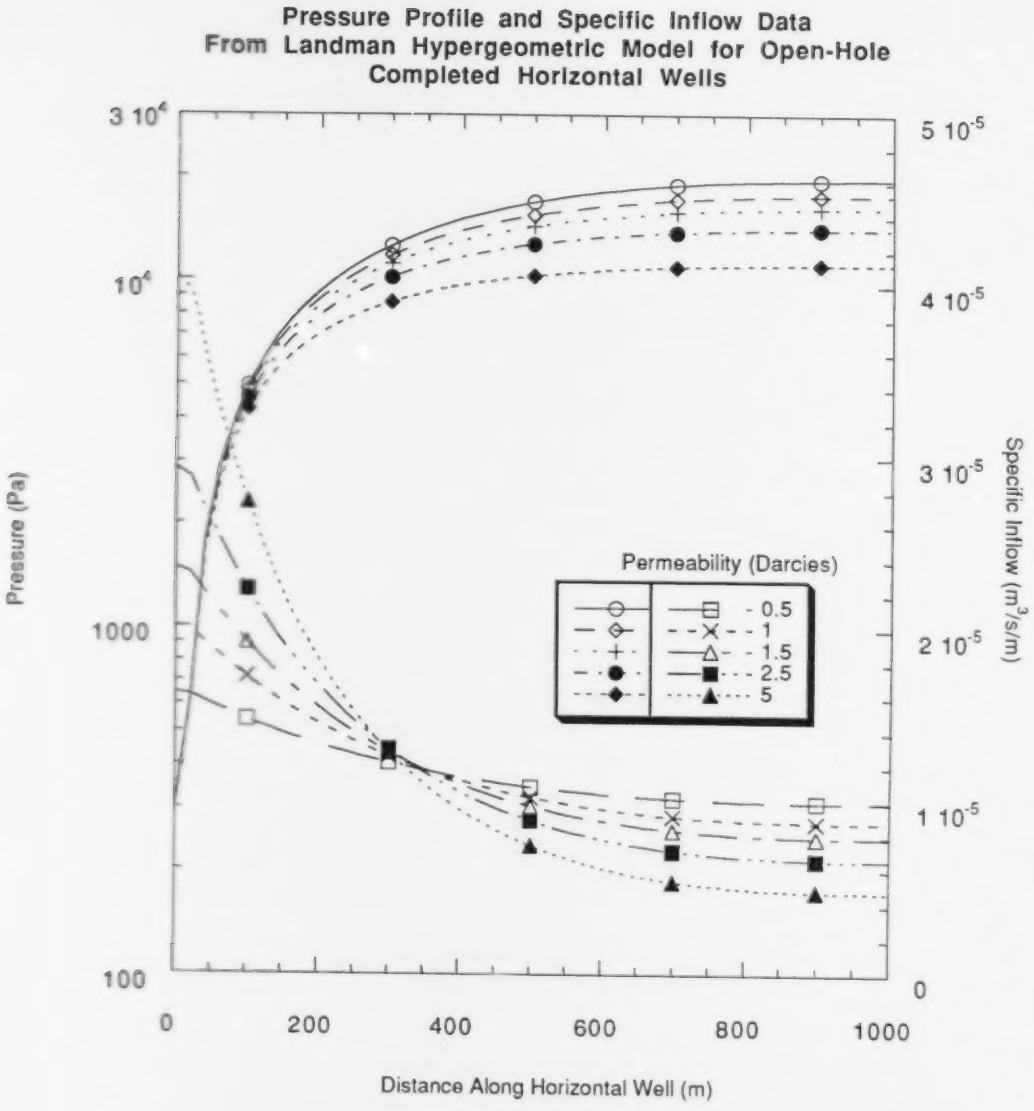

Figure 43: Field–Scale Pressure and Specific Inflow Profile Predictions for Open Hole Horizontal Wells With Permeability As A Cross Parameter

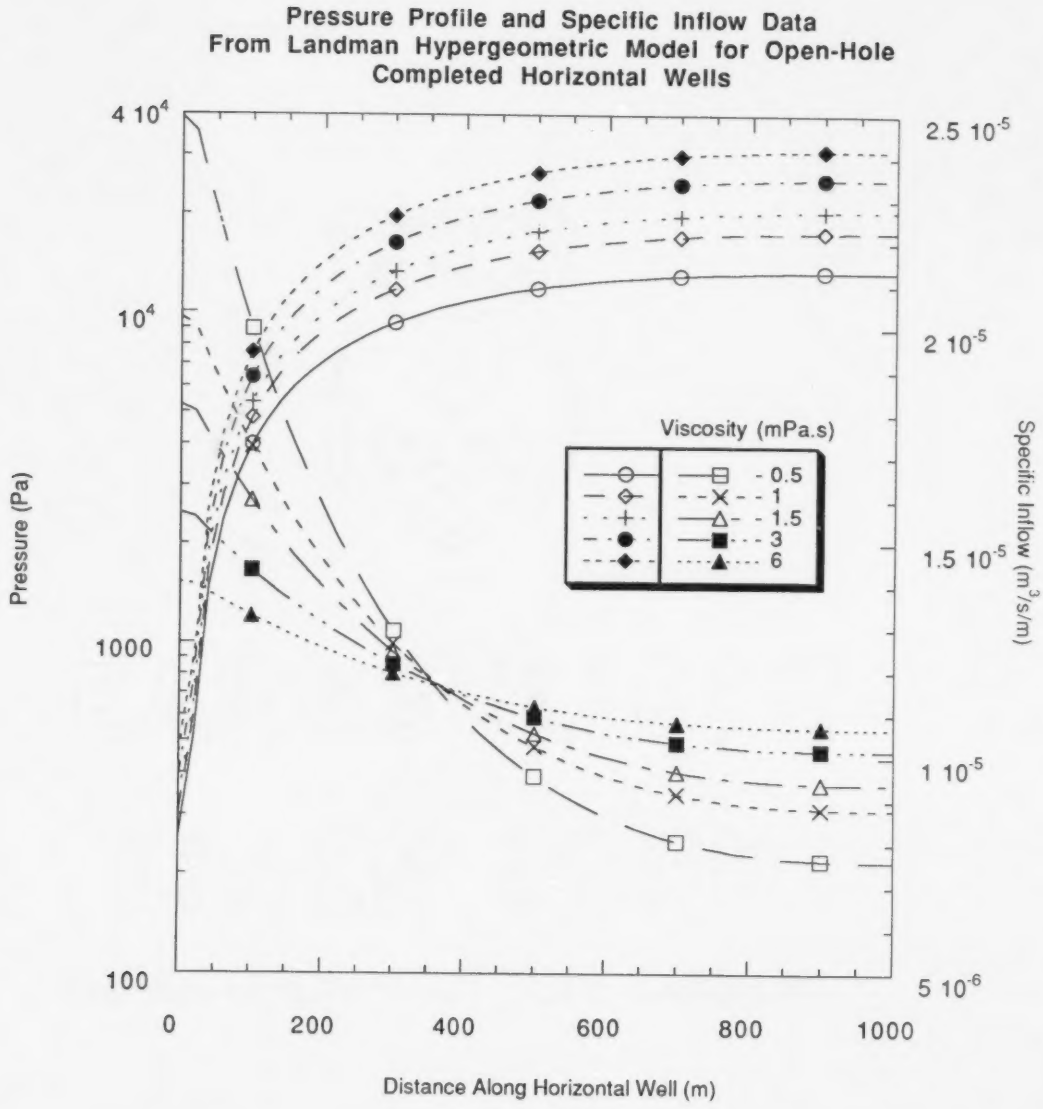

Figure 44: Field–Scale Pressure and Specific Inflow Profile Predictions for Open Hole Horizontal Wells With Viscosity As A Cross Parameter

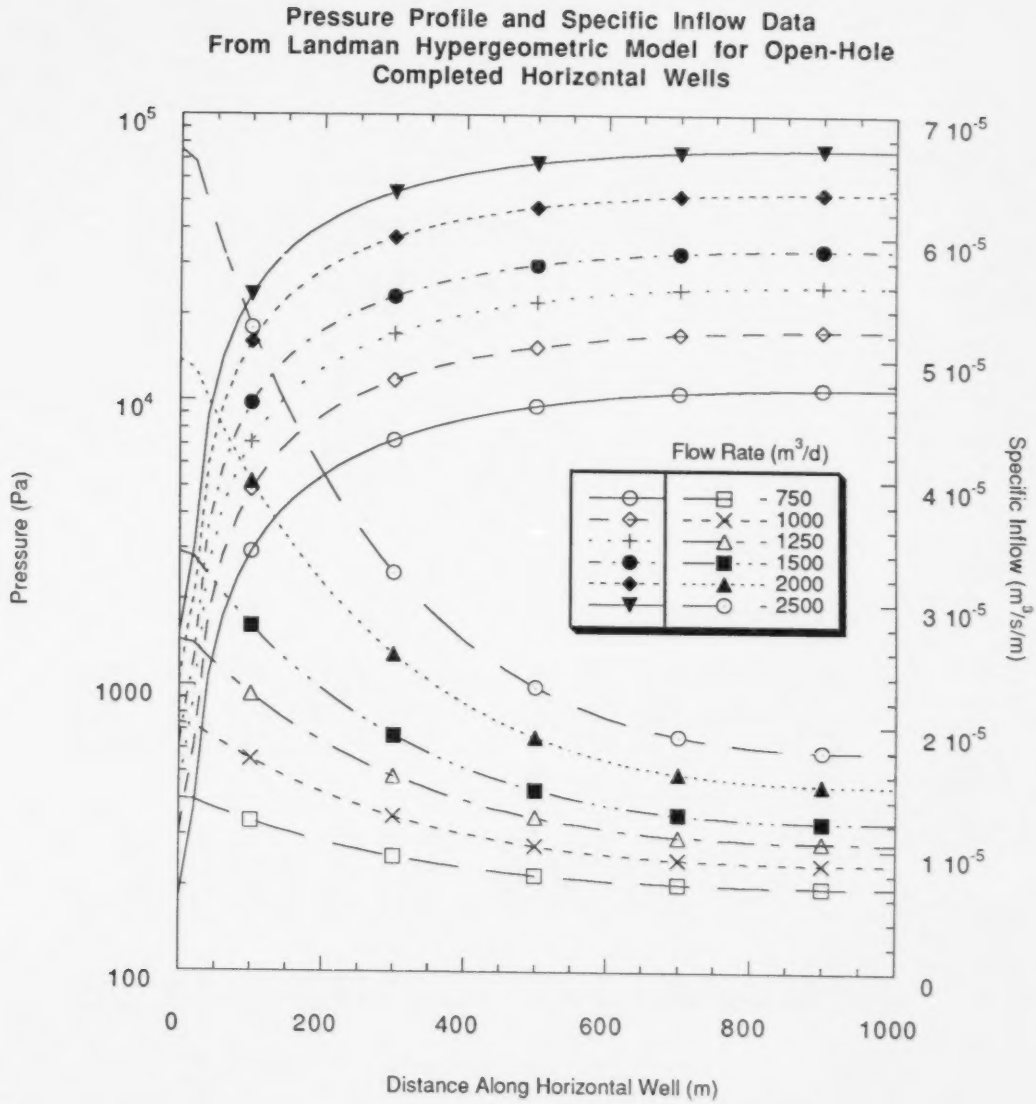

Figure 45: Field–Scale Pressure and Specific Inflow Profile Predictions for Open Hole Horizontal Wells With Flow Rate As A Cross Parameter

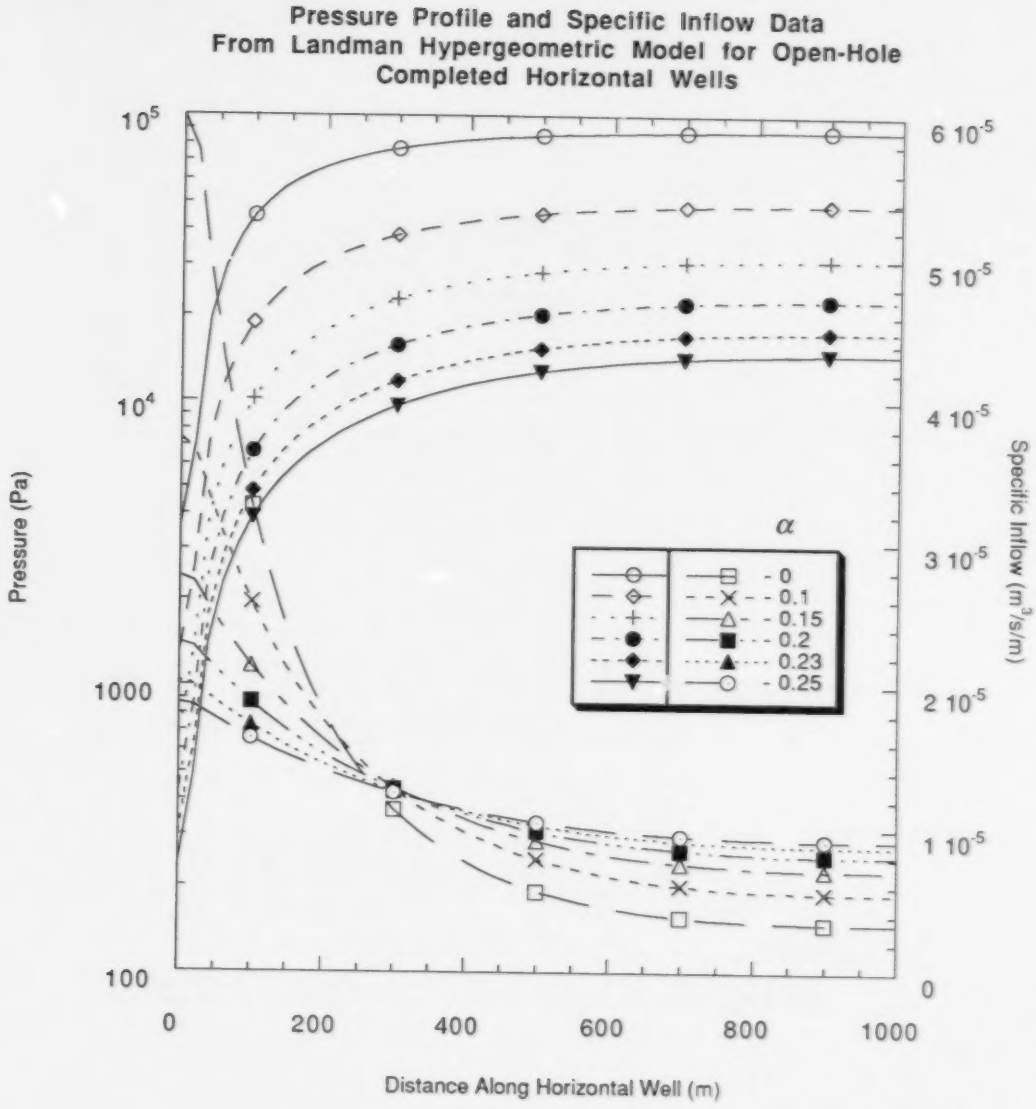

Figure 46: Field–Scale Pressure and Specific Inflow Profile Predictions for Open Hole Horizontal Wells With The Blasius Exponent α As A Cross Parameter

Figure 44 has the viscosity of the well fluid as the cross parameter. Note that while the well pressure drop is increasing with increasing viscosity, the specific inflow profile becomes more skewed with decreasing viscosity. Coning and cresting are far more likely to be a problem, therefore, when the produced fluid is low in viscosity, despite higher anticipated pressure drops across a horizontal well when producing higher viscosity fluids.

Variable flow rate (depicted in Figure 45) effects a large variation in both the pressure drop and the specific inflow profiles in a horizontal well. Pressure drop and coning are much more likely to be a problem in field situations with high production rates.

Figure 46 has as its cross parameter the Blasius exponent α. This variable is used within Dikken's[3] model and Landman's[8] hypergeometric model to represent the the roughness of the well. The range used for turbulent flow is given by $0 \le \alpha \le 0.25$, with 0.25 corresponding with a perfectly smooth pipe. This value decreases with increasing roughness of the wellbore, and increasing turbulence. Whether or not a value anywhere near 0 is possible is highly controversial, as was discussed in 3. Literature Review. Note in Figure 46 that the specific inflow profile becomes drastically skewed in favour of production occurring toward the near (producing) end of the well with decreasing α.

5.2.5.4 Modified Coupled Open Hole Model

The Landman[8] hypergeometric method was modified for this project in order to evaluate the effect of acceleration of the confluent influx on the pressure and specific inflow profiles. An approximation of the specific productivity index is calculated using an equation for partially penetrating horizontal wells, and this value is specified, as follows,

$$J_s(x) = \frac{4\pi k}{\mu}\left[\ln\left(\frac{L - x + \sqrt{(L-x)^2 + R^2}}{-x + \sqrt{x^2 + R^2}}\right)\right]^{-1} \tag{5–78}$$

$$J_s = \frac{1}{n}\sum_n J_s(x) \tag{5–79}$$

where J_S is the specific productivity index, R is the wellbore radius, and n is the number of segments used. The Reynolds number is calculated at each well position and its value determines whether a laminar or turbulent pressure calculation method is used. Additionally, the Asheim *et al.*[62] accelerational friction factor is calculated for each well position, and this friction factor is summed with the wall friction component before being

used to determine the well pressure. The following series of plots (Figures 47 through 50) compare the pressure profiles obtained using Landman's[8] hypergeometric method with the profiles obtained with the modified method (well and production data used are listed in Table 9). Other than laminar flow and accelerational pressure drop effects, the two methods produced identical results.

Table 9: Well and Production Data Used in Figures 47 – 50

WELL AND PRODUCTION DATA			
Permeability (D)	1	Flow Rate (m^3/d)	500
Well Length (m)	500	Oil Density (kg/m^3)	850
Alpha	0.23	Number of Segments	200
Diameter (m)	0.2	Oil Viscosity (mPa.s)	2

These figures show a small but non–negligible effect due to the acceleration of the confluent influx as it enters the wellbore. Thus Landman's hypergeometric numerical method[8], based on Dikken's work[3], has been improved slightly with no cost in terms of ease of use of the program. The program listings provided in Appendix C may be used to solve for the pressure and specific inflow profiles for cased and perforated, or open–hole completed horizontal wells.

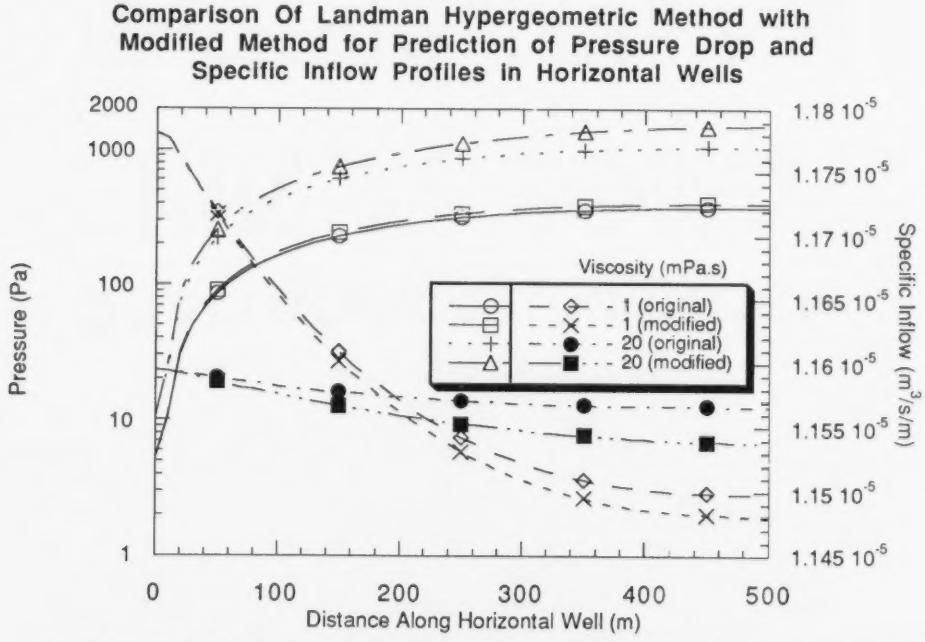

Figure 47: Comparison of Landman Hypergeometric and Modified Predictive Methods for Open Hole Completed Horizontal Wells With Viscosity As A Cross Parameter

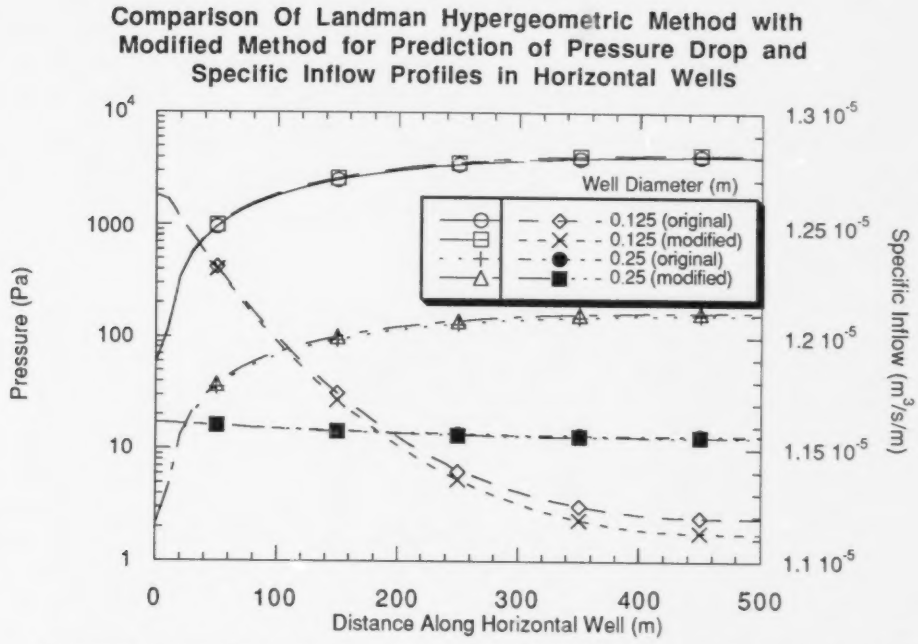
Comparison Of Landman Hypergeometric Method with Modified Method for Prediction of Pressure Drop and Specific Inflow Profiles in Horizontal Wells
Pressure (Pa)
Specific Inflow (m3/s/m)
Distance Along Horizontal Well (m)
Well Diameter (m)
0.125 (original)
0.125 (modified)
0.25 (original)
0.25 (modified)

Figure 48: Comparison of Landman Hypergeometric and Modified Predictive Methods for Open Hole Completed Horizontal Wells With Well Diameter As A Cross Parameter

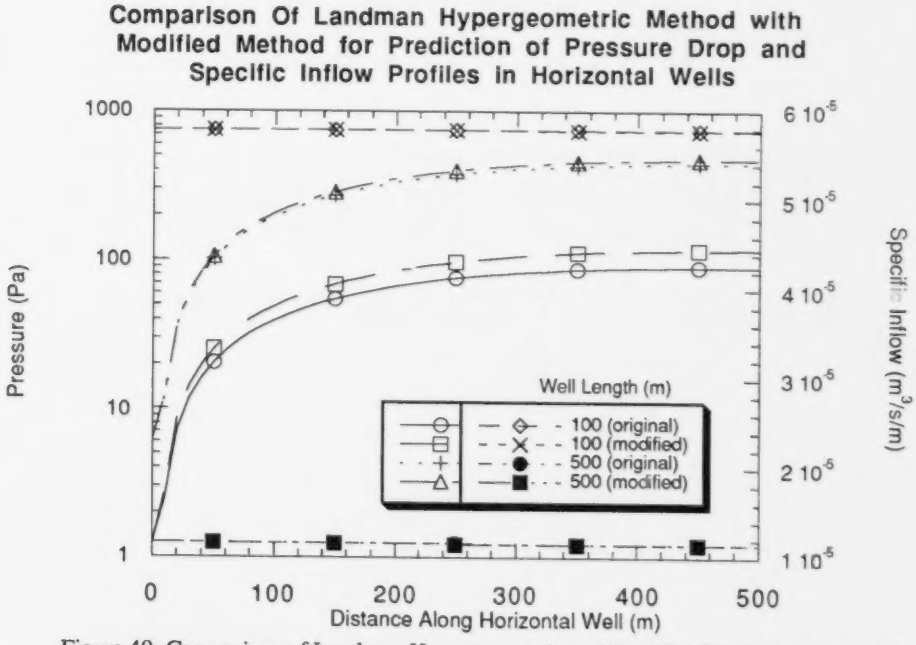
Comparison Of Landman Hypergeometric Method with Modified Method for Prediction of Pressure Drop and Specific Inflow Profiles in Horizontal Wells
Pressure (Pa)
Specific Inflow (m3/s/m)
Distance Along Horizontal Well (m)
Well Length (m)
100 (original)
100 (modified)
500 (original)
500 (modified)

Figure 49: Comparison of Landman Hypergeometric and Modified Predictive Methods for Open Hole Completed Horizontal Wells With Well Length As A Cross Parameter

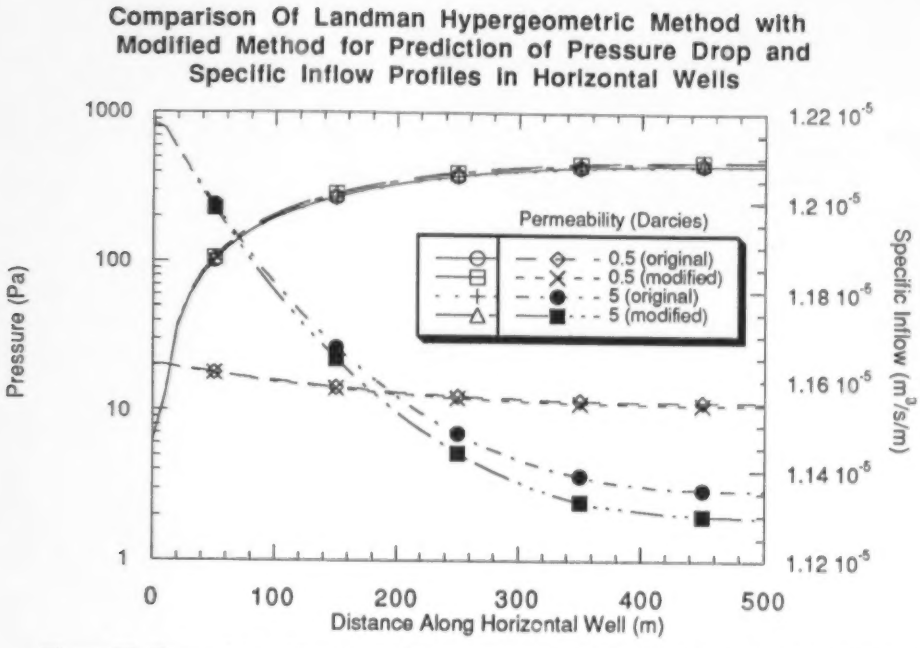

Figure 50: Comparison of Landman Hypergeometric and Modified Predictive Methods for Open Hole Completed Horizontal Wells With Permeability As A Cross Parameter

5.3 Holdup Data

Holdup in two–phase flow may be described as the phenomena in which one of the phases (typically the more dense phase) is "held up" in the pipe; i.e., the other phase flows preferentially leading to a higher in situ volume fraction of the held up phase. This concept is analogous to that of relative permeability in multiphase flow in porous media.

The method used to perform the holdup measurement in the experiments was described in Chapter 4. At the end of each experiment, with the fluids flowing in a steady–state condition, a section of the model length is suddenly isolated by simultaneously closing ball valves at either end of the section. The section is removed from the model and inverted in order to measure the level of the interface. The method used provides a reasonably accurate measure of the in situ volume fraction of the two liquids. The input volumetric flow rates of the two liquids are known beforehand; thus, the input volume fraction of the liquids is also known. The holdup ratio may then be calculated using the following formula:

$$H = \frac{\text{in situ volume fraction ratio, heavier to lighter phase}}{\text{input volume fraction ratio, heavier to lighter phase}}$$

$$= \frac{\left(E_W / E_O\right)_{in\ situ}}{\left(E_W / E_W\right)_{input}} \qquad (5\text{–}80)$$

where E is the volume fraction of the liquid phase (water or oil), which is also identical to the cross–sectional area fraction for unit volumes.

Figure 51 is a plot of the holdup ratios observed from the experiments vs. the superficial oil phase velocity, with the superficial water phase velocity as a cross parameter. The general trend of the holdup data is very similar to that of previous oil–water pipe flow experiments, such as those of Russell, Hodgson and Govier[36]. For each superficial water velocity, the holdup ratio increases until it passes through a maximum, and then decreases to a value at or below unity. The explanation for this behaviour is a phase inversion. With increasing oil phase flow rate, at some point the continuous phase changes from water to oil. Since the inversion point depends on the relative value of the flow rates, it would be reasonable to expect that the inversion point would occur at a lower oil phase flow rate for the lower water phase flow rates, and this is observed in the plot.

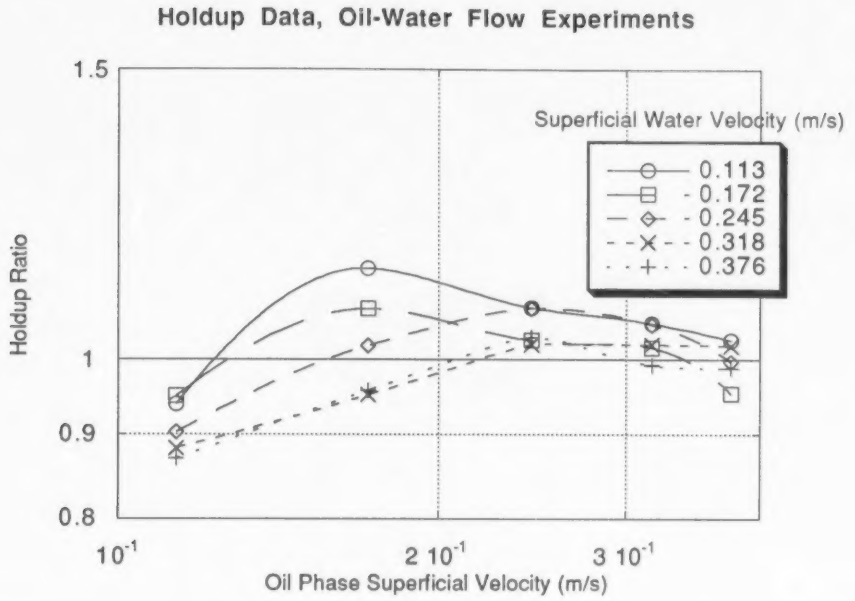

Figure 51: Measured Holdup Data For Oil–Water Pipe Flow Experiments

The holdup ratio is affected by the relative viscosities of the fluids as well as the relative densities. The oil used for the current series of experiments had a viscosity of 2.4 mPa.s and a specific gravity of 0.845 at room temperature, giving a viscosity ratio between the liquid phases of 2.4 and a density ratio of 0.847. The low viscosity and density ratios result in the generally small variance from unity for the holdup ratio, in comparison with other workers' measured data with more viscous oils.[36,38]

Although oil–water flow experiments were quite popular in the 1960's, no generalized correlations were developed for holdup predictions with liquid–liquid horizontal pipe flow until quite recently. Hall and Hewitt's[50] liquid–liquid holdup correlation work was an extension of a great deal of previous work that had focused on liquid–gas predictive models.

Lockhart and Martinelli[34] presented an empirical correlation for the average in situ volume fraction of the liquid phase as a function of the parameter X for two–phase gas–liquid flows.

$$X = \sqrt{\frac{\left(\Delta P/L\right)_{L_s}}{\left(\Delta P/L\right)_{G_s}}} \qquad (3\text{–}4)$$

where $\left(\Delta P/L\right)_{L_s}$ is the pressure gradient that would occur if the liquid were flowing alone at a velocity equal to its superficial velocity, and $\left(\Delta P/L\right)_{G_s}$ is the pressure gradient that would occur if the gas were flowing alone at a velocity equal to its superficial velocity. These single–phase pressure gradients may be determined by experiment for special cases, but are more commonly found by calculation:

$$\frac{\Delta P}{L} = \frac{f\rho u^2}{2D} \tag{5–15}$$

This equation applies fairly generally, but as was noted above, the difficulty often lies in accurately determining the friction factor for a given fluid. The holdup correlation was provided in the form of type curves, not as an equation.

Taitel and Dukler[45] presented a model that provided a theoretical mechanistic basis for the Lockhart–Martinelli parameters. Their work included an important analysis of flow regime boundaries for horizontal and near horizontal two–phase flow, based on transitions from the most common regime, stratified flow.

Hall and Hewitt[50] modified Taitel and Dukler's[45] theoretical definitions of X, for the case of stratified horizontal pipe flow of oil and water. The result is a useful set of equations from which holdup values may be obtained (see Figure 52):

$$\mathrm{X} = \sqrt{\frac{\left(\Delta P/L\right)_{W_s}}{\left(\Delta P/L\right)_{O_s}}} \tag{5–81}$$

$$\mathrm{X}^2\left[\left(\tilde{u}_W \tilde{D}_W\right)^{-n} \tilde{u}_W^2 \left(\frac{\tilde{S}_W}{\tilde{A}_W} + \frac{\tilde{S}_i}{\tilde{A}_W} + \frac{\tilde{S}_i}{\tilde{A}_O}\right)\right] - \left[\left(\tilde{u}_O \tilde{D}_O\right)^{-l} \tilde{u}_O^2 \frac{\tilde{S}_O}{\tilde{A}_O}\right] = 0 \tag{5–82}$$

$$\mathrm{X}^2 = \frac{\dfrac{4C_W}{D}\left(\dfrac{u_{W_s} D \rho_W}{\mu_W}\right)^{-n} \dfrac{\rho_W u_{W_s}^2}{2}}{\dfrac{4C_O}{D}\left(\dfrac{u_{O_s} D \rho_O}{\mu_O}\right)^{-l} \dfrac{\rho_O u_{O_s}^2}{2}} \tag{5–83}$$

where: u_{O_s}, u_{W_s} are the superficial velocities of each phase respectively

ρ_O, ρ_W are the respective densities

μ_O, μ_W	are the respective viscosities
D	is the pipe diameter
n, l, C	are flow regime–dependent constants
A_O, A_W	are the pipe cross–sectional areas occupied by each phase
S_O, S_W	are the portions of the pipe circumference wetted by each phase (the wetted perimeters)

and the "tilde", ~ above each symbol refers to a dimensionless quantity.

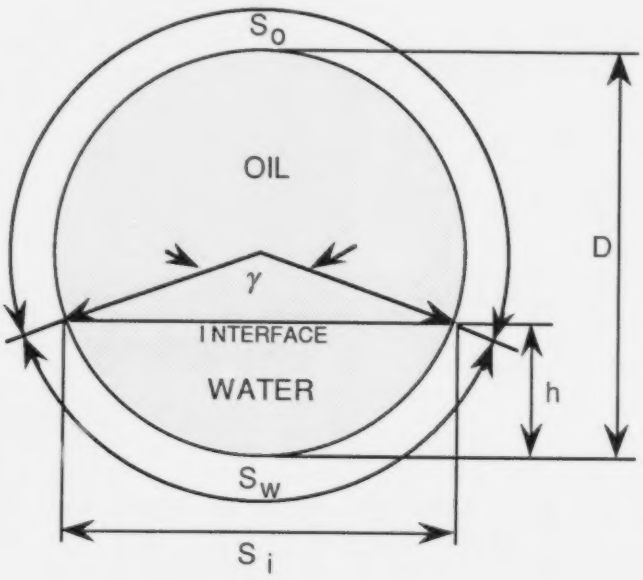

Figure 52: Pipe Geometry Parameters

The definitions of each dimensionless variable are as follows:

$$\tilde{A} = \frac{A}{D^2} \tag{5–84}$$

$$\tilde{h} = \frac{h}{D} \tag{5–85}$$

(h being the height of the stratified interface between phases)

$$\tilde{A}_W = 0.25\left[\pi - \cos^{-1}\left(2\tilde{h}-1\right) + \left(2\tilde{h}-1\right)\sqrt{1-\left(2\tilde{h}-1\right)^2}\right] \tag{5–86}$$

$$\tilde{A}_O = 0.25\left[\cos^{-1}\left(2\tilde{h}-1\right)-\left(2\tilde{h}-1\right)\sqrt{1-\left(2\tilde{h}-1\right)^2}\right] \tag{5–87}$$

$$\tilde{S}_W = \pi - \cos^{-1}\left(2\tilde{h}-1\right) \tag{5–88}$$

$$\tilde{S}_O = \cos^{-1}\left(2\tilde{h}-1\right) \tag{5–89}$$

$$\tilde{S}_i = \sqrt{1-\left(2\tilde{h}-1\right)^2} \tag{5–90}$$

$$\tilde{u}_W = \frac{\tilde{A}}{\tilde{A}_W} \tag{5–91}$$

$$\tilde{u}_O = \frac{\tilde{A}}{\tilde{A}_O} \tag{5–92}$$

The concept of hydraulic diameter for the purposes of two–phase stratified Reynolds number calculations was proposed by Agrawal, Gregory and Govier[44]. The hydraulic diameters for each phase are defined as follows:

$$D_W = \frac{4A_W}{\left(S_W + S_i\right)} \tag{5–93}$$

$$D_O = \frac{4A_O}{S_O} \tag{5–94}$$

and in dimensionless form:

$$\tilde{D}_W = \frac{4\tilde{A}_W}{\left(\tilde{S}_W + \tilde{S}_i\right)} \tag{5–95}$$

$$\tilde{D}_O = \frac{4\tilde{A}_O}{\tilde{P}_O} \tag{5–96}$$

Taitel and Dukler[45] noted that all the dimensionless variables depend only on $\tilde{h} = \frac{h}{D}$, such that the holdup parameter X may be found for varying dimensionless interface height from Equation (5–82). Hall and Hewitt[50] duplicated these calculations for the case of stratified oil–water flow. They also found X values using a more sophisticated numerical method, involving a discretization of the Navier–Stokes equation for each phase, transformed onto a bipolar coordinate grid (see Appendix B). The following are the Navier–Stokes equations for each phase:

$$\frac{\partial^2 u_w}{\partial x^2} + \frac{\partial^2 u_w}{\partial y^2} = \frac{1}{\mu_w}\frac{dP}{dx} \tag{5–97}$$

$$\frac{\partial^2 u_o}{\partial x^2} + \frac{\partial^2 u_o}{\partial y^2} = \frac{1}{\mu_o}\frac{dP}{dx} \tag{5–98}$$

Figure 53 presents oil–water holdup prediction results obtained using Hall and Hewitt's[50] modification of the Taitel and Dukler correlation, and those obtained using the numerical method described in Appendix B. The dimensionless interface height is plotted against the X parameter, with viscosity ratio as a cross parameter for the numerical results.

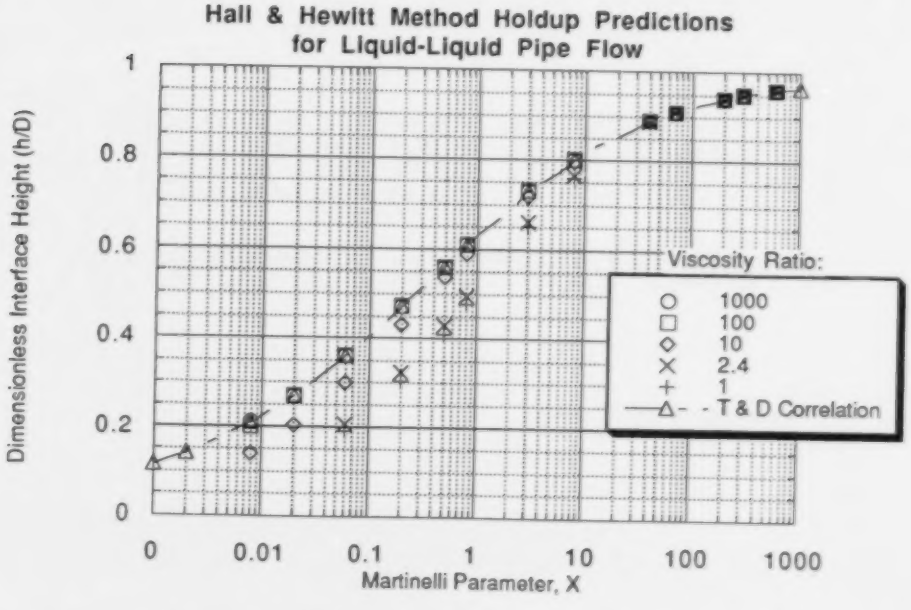

Figure 53: Correlation of Martinelli Holdup Parameter by Hall and Hewitt[50]

The modified Taitel and Dukler[45] correlation is not a function of viscosity ratio. But the numerical results demonstrate that for stratified laminar liquid–liquid horizontal pipe flow the Martinelli parameter X depends not only upon the interface position, $\tilde{h}$, but also upon the viscosity ratio of the two fluids.

Figure 54 is a plot of the modified Taitel and Dukler[45] correlation and the predicted (numerical) interface height for a viscosity ratio of 2.4 vs. the Martinelli parameter X, compared with the measured data for the current series of experiments.

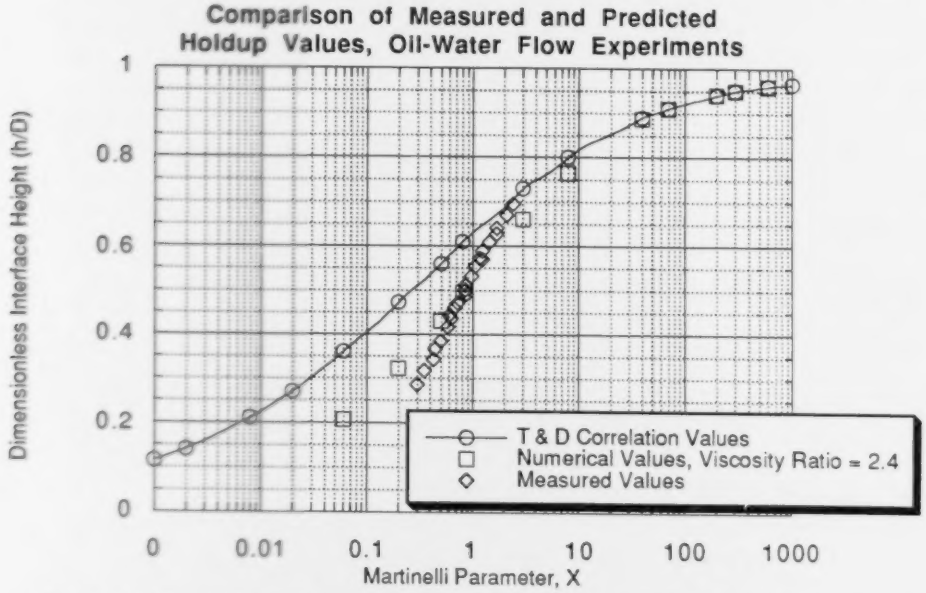

Figure 54: Comparison of Measured and Predicted Holdup Values in the Form of the Martinelli Parameter, X

The discrepancy between the measured and predicted values is likely mostly due to the turbulent experimental flow conditions for each phase. The numerical model does not consider turbulence. Also, the numerical model is based on the assumption of a perfectly stratified flow condition, and this condition was not present for most of the experiments.

The measured holdup ratios for the experiments conducted during this project are all very close to unity, due to the nature of the oil used. The usefulness and importance of the holdup measurements for the purpose of the current series of experiments is therefore mostly limited to being an aid in correlation methods for pressure gradient prediction. However, for liquid–liquid flow of heavier, more viscous oils and water, the held up phase

is likely to be the oil ($H < 1$), and water will flow preferentially, which in the field can lead to very high produced water–oil ratios (WOR), even though the contact area between the water zone in the reservoir and a horizontal well may be very small. Typically, the holdup effect is far more important in gas–liquid flows, because of the large density and viscosity difference between the gas and liquid phases, and making the consequences of gas breakthrough far more evident in the field.

6. FLOW REGIME OBSERVATIONS

Although the focus of this study is pressure drop in horizontal wells, during the physical experiments simple observations were made concerning flow pattern behaviour. A transparent polyvinyl chloride (PVC) pipe was chosen for the model to allow visual observations, photographs and videotape recordings to be taken. No special procedure was used in taking the photographs or making the visual observations, so the refractive distortion caused by the thickness of the pipe wall must be acknowledged.[42]

6.1 Oil–Water Pipe Flow

Figure 55 is a flow regime map developed from experiments performed by Russell, Hodgson and Govier (1959)[36] and reproduced from Govier and Aziz (1972)[29]. The experiments were performed using an 18 mPa.s, 0.834 specific gravity oil and water in a 0.806-in. (0.0205 m) ID pipe model.

Arirachakaran *et al.* (1989)[56] conducted a large series of experiments involving oil-water flows in horizontal pipes. A wide variety of oil viscosities was used (4.7 to 2116

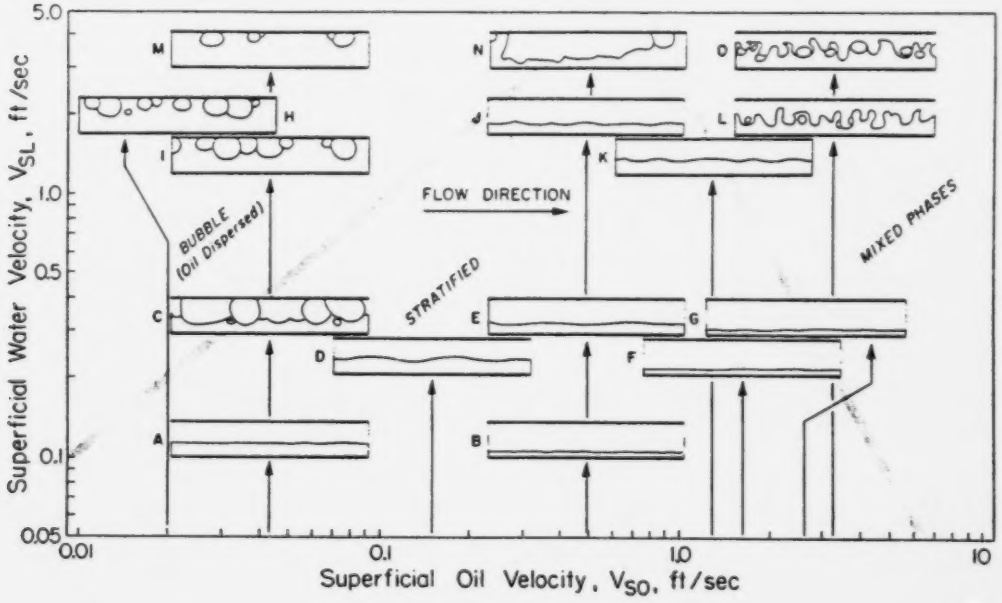

Figure 55: Experimental Oil–Water Flow Pattern Map Based on Observations of Russell, Hodgson and Govier[36] and Reproduced from Govier and Aziz[29].

Table 10: Flow Regime Data and Observations, Oil–Water Pipe Flow Experiments

FLOW REGIME DATA—OIL-WATER PIPE FLOW EXPERIMENTS

Experiment:	Superficial Velocities: Water (m/s)	Oil (m/s)	Mix. Velocity (m/s)	Input Water Volume Fraction	Flow Regime	Interface
1	0.113401	0.113401	0.226802	0.5	strat.	smooth
2	0.1717161	0.113401	0.2851171	0.6022652	strat.	wavy
3	0.24461	0.113401	0.358011	0.6832472	strat.	rough/bubbly
4	0.317504	0.113401	0.4309049	0.7368306	strat.	v. bubbly
5	0.3758191	0.113401	0.4892201	0.7682005	strat.	v. bubbly
6	0.113401	0.1717161	0.2851171	0.3977348	strat.	wavy
7	0.1717161	0.1717161	0.3434322	0.5	strat.	wavy
8	0.24461	0.1717161	0.4163262	0.5875442	strat.	rough/bubbly
9	0.317504	0.1717161	0.4892201	0.6490003	strat.	v. bubbly
10	0.3758191	0.1717161	0.5475352	0.6863834	strat.	v. bubbly
11	0.113401	0.24461	0.358011	0.3167528	strat./iw	rough/bubbly
12	0.1717161	0.24461	0.4163262	0.4124558	strat.	v. bubbly
13	0.24461	0.24461	0.4892201	0.5	strat.	v. bubbly
14	0.317504	0.24461	0.562114	0.5648391	strat./mw	v. bubbly
15	0.3758191	0.24461	0.6204291	0.6057406	mw	v. bubbly
16	0.113401	0.317504	0.4309049	0.2631694	iw/mw	v. bubbly
17	0.1717161	0.317504	0.4892201	0.3509997	strat./iw	v. bubbly
18	0.24461	0.317504	0.562114	0.4351609	strat.	v. bubbly
19	0.317504	0.317504	0.6350079	0.5	strat.	v. bubbly
20	0.3758191	0.317504	0.693323	0.5420548	strat./mw	v. bubbly
21	0.113401	0.3758191	0.4892201	0.2317995	mw/mo	v. bubbly
22	0.1717161	0.3758191	0.5475352	0.3136166	mw	v. bubbly
23	0.24461	0.3758191	0.6204291	0.3942594	strat./iw	v. bubbly
24	0.317504	0.3758191	0.693323	0.4579452	strat.	v. bubbly
25	0.3758191	0.3758191	0.7516382	0.5	strat./mw	v. bubbly

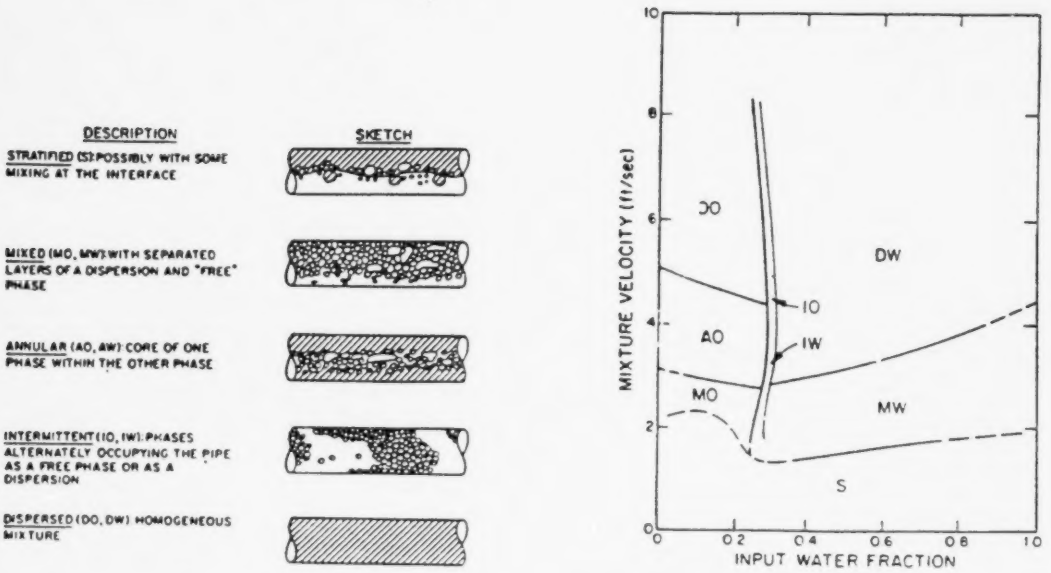

Figure 56: Oil–Water Experimental Flow Pattern Map Along With Classification and Description of Patterns; Reproduced from Arirachakaran *et al.* (1989)[56]

mPa.s) and flow pattern maps were generated for each oil. A typical flow pattern map with descriptions of the different regimes is reproduced in Figure 56; this particular map was generated for an oil with a viscosity of 84 mPa.s. Note that the first letter of the regime identifier describes the regime and the second letter indicates the continuous phase; e.g., MW indicates a mixed flow regime with water as the continuous phase.

Arirachakaran *et al.* (1989)[56] noted that a generalized flow pattern map (one that includes all oils) for oil–water pipe flows is neither currently available nor likely to be produced in the foreseeable future because of the complex transition behaviour governed by factors such as superficial velocity, phase inversion concentration, viscosity and interfacial tension. However, the format of the flow regime map reproduced in Figure 56 is useful for comparison purposes where consistency is desired.

The oil–water experiments conducted for this project were limited in number and in terms of the range of mixture superficial velocities generated. Most of the flow regimes observed from the experiments were stratified or semi–stratified (note from Table 10 that several of the flow regimes observed appeared to be combinations of the basic regimes

described by Arirachakaran *et al.*[56] and reproduced in Figure 56). The term "semi–stratified" is used to indicate a regime intermediate to stratified and either mixed or intermittent regimes, in which phase stratification is still evident, but some degree of mixing and/or dispersion of one phase within another is also taking place. For example, in Experiments 14, 20 and 25 from Table 10 the flow regime that was observed would best be described as stratified by Arirachakaran *et al.*'s[56] definition, but the bubbly dispersed oil layer almost entirely filled the top half of the pipe, such that the regime was very close to mixed with water as the continuous phase. Another example is the stratified/intermittent combination flow regime reported here for Experiments 11, 17 and 23. During these experiments a rough, bubbly stratified flow was observed to alternate with large agglomerations of dispersed oil bubbles that would fill much but not all of the available space in the pipe as they passed. A purely intermittent flow as defined by Arirachakaran *et al.*[56], with regular, periodic and complete disruptions of the continuous phase, did not occur during the experiments. Neither were annular or purely dispersed regimes observed, but this is not surprising considering the limited number and range of experiments performed. An annular regime would not be expected to form under normal conditions for such a low viscosity oil as was used in any case.

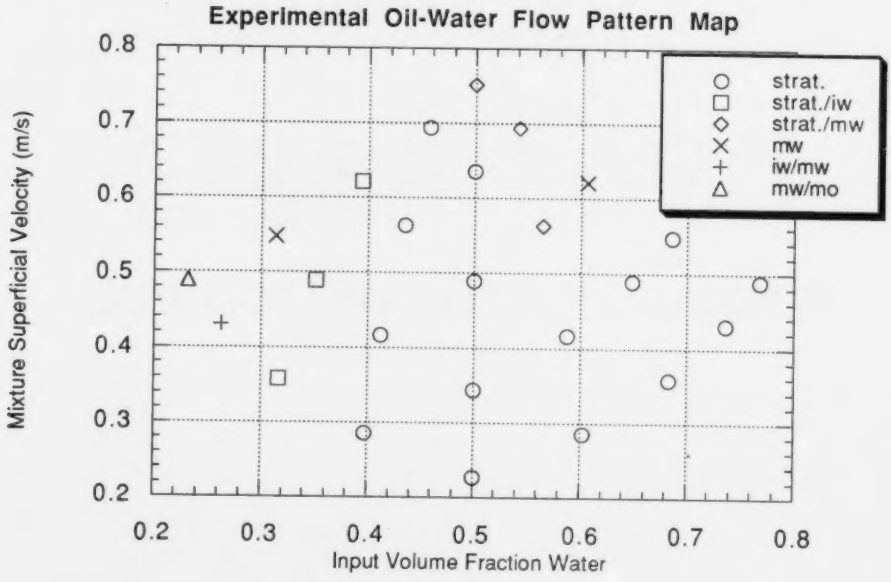

Figure 57: Experimental Oil–Water Flow Pattern Data

Figure 57 is the flow regime data plotted in the format used by Arirachakaran *et al.*[56] and other workers. No boundaries have been drawn in, but some of the regions presented in Figure 56 may be noted in comparison. Many more data points and a reliable method of determining the inversion point would be required to generate a more complete flow regime map.

6.2 Oil–Water Flow With Influx Flow Through A Perforation

For each oil–water pipe flow experiment listed in Table 10 , three additional experiments were conducted with varying water–only flow rates through a single drilled hole in the model. The following photographs are presented to illustrate the effect of the flow influx via the drilled perforation. In all the photographs the flow direction is from left to right.

Figure 58 is a photograph of Experiment 1, with oil and water–phase superficial velocities of 0.113 m/s, and no water flow through the single perforation. As noted in Table 10, the flow regime is clearly stratified with a very smooth interface between the upper (dyed) oil phase and the lower transparent water phase. Figure 59 depicts the same experimental conditions except for a water flow through a single perforation located at a position underneath the model adjacent to the left edge of the photograph. The perforation flow velocity in Figure 59 is 2.35 m/s. Note that downstream of the perforation the smooth stratified interface between the oil and water phases has disappeared, to be replaced by a mixed, turbulent phase lying between pure oil and water phases. This mixed phase continues well down the flow model (several metres) before its disappearance.

The perforation flow velocity was increased to 3.26 m/s for Figure 60. Otherwise, the experimental conditions are again the same as for the previous two figures. The perforation flow velocity is sufficiently large to completely disrupt the overlying oil phase; in turn the oil phase is constricted as it approaches the perforation, and then it expands rapidly downstream of the perforation, causing the oil to break up into bubbles and disperse within the underlying water phase.

Figure 61 is a photograph of Experiment 2, with the oil superficial velocity of 0.113 m/s, water superficial velocity equal to 0.172 m/s, and no flow through the perforation. The interface is slightly wavy and is located somewhat above the centreline of the pipe model. In Figure 62 the water flow velocity through the perforation is 3.26 m/s. Two large water bubbles dispersed in the oil are visible downstream of the perforation.
Experiment 5 is recorded in Figure 63. The oil superficial velocity is still 0.113 m/s, and the water superficial velocity is 0.376 m/s, with no flow through the perforation.

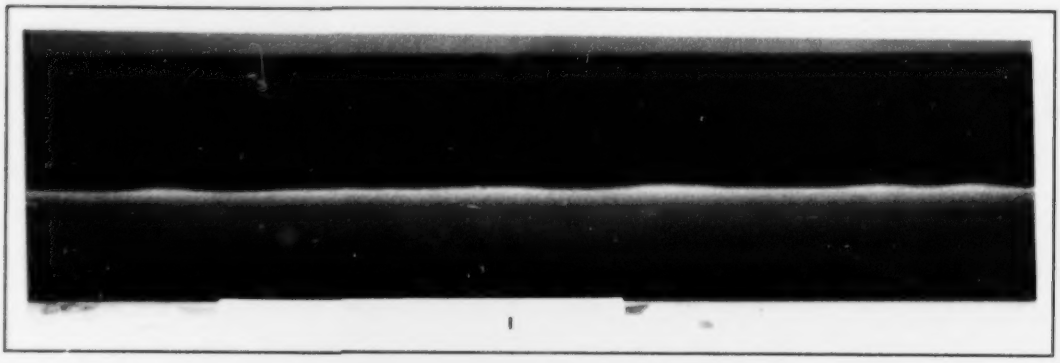

Figure 58: Oil–Water Flow Experiment 1, with no flow through perforation

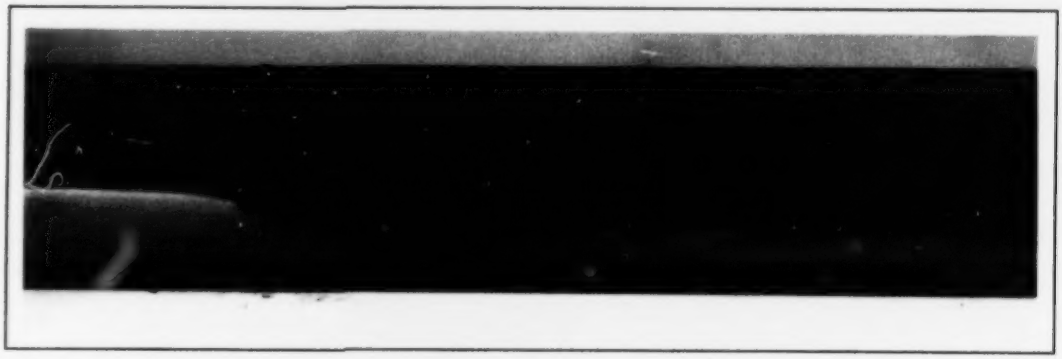

Figure 59: Oil–Water Flow Experiment 1, with water flow through perforation at 2.35 m/s

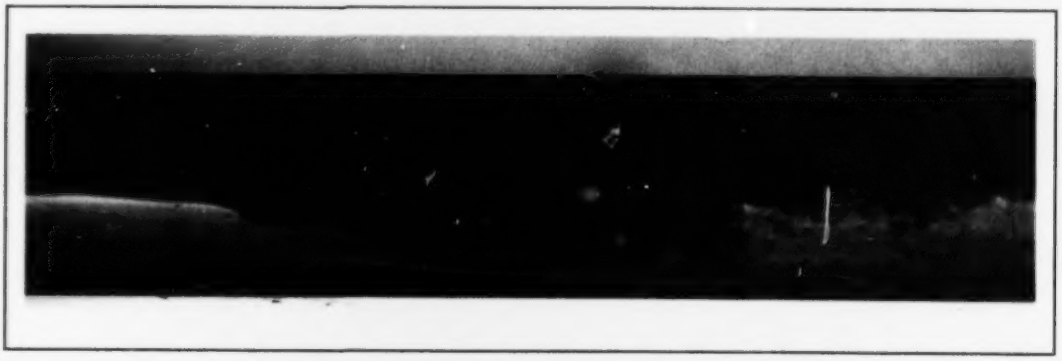

Figure 60: Oil–Water Flow Experiment 1, with water flow through perforation at 3.26 m/s

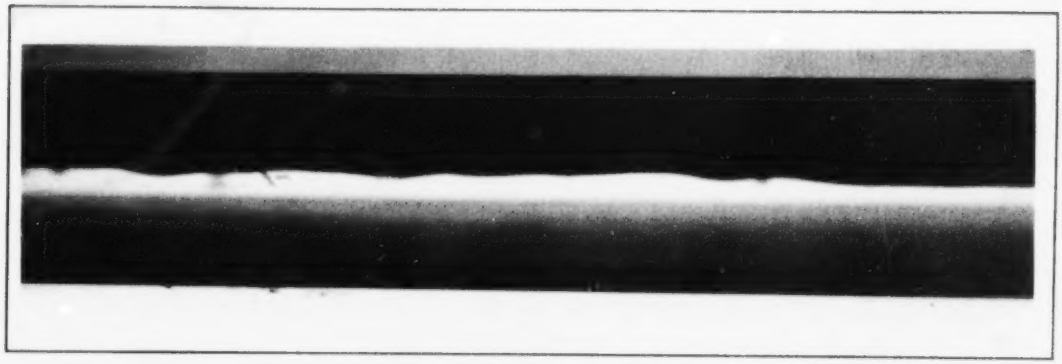

Figure 61: Oil–Water Flow Experiment 2, with no flow through perforation

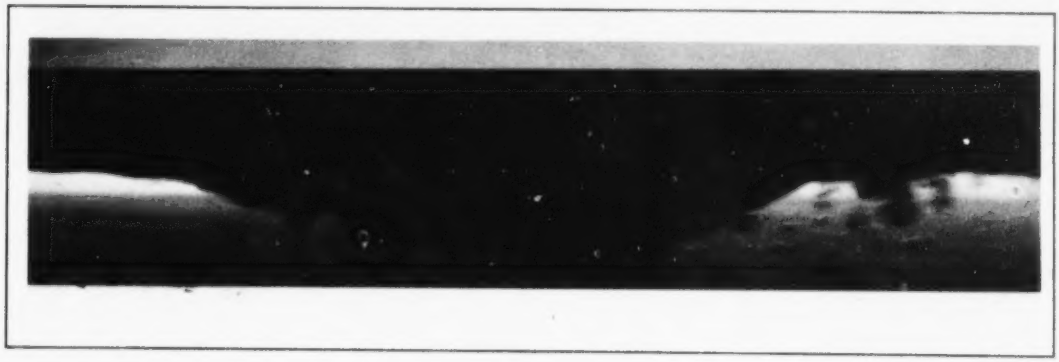

Figure 62: Oil–Water Flow Experiment 2, with water flow through perforation at 3.26 m/s

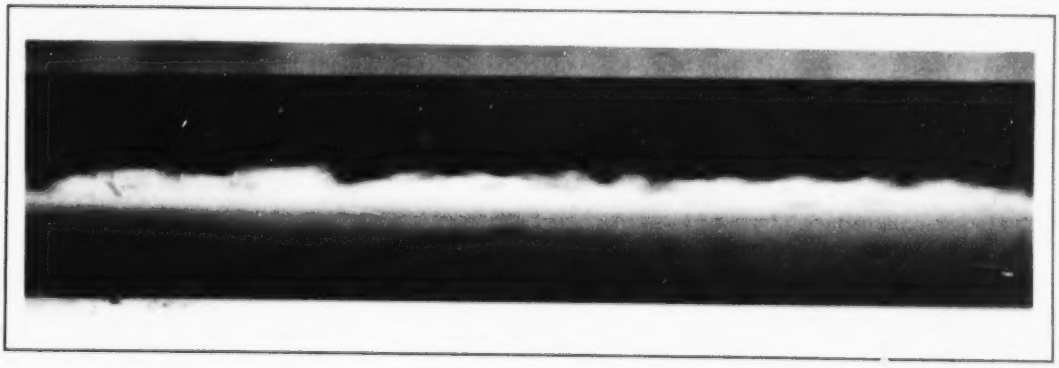

Figure 63: Oil–Water Flow Experiment 5, with no flow through perforation

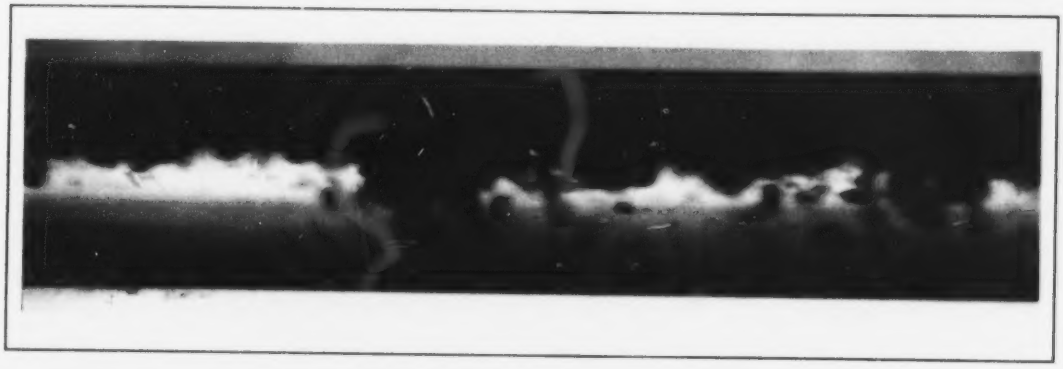

Figure 64: Oil–Water Flow Experiment 5, with water flow through perforation at 3.26 m/s

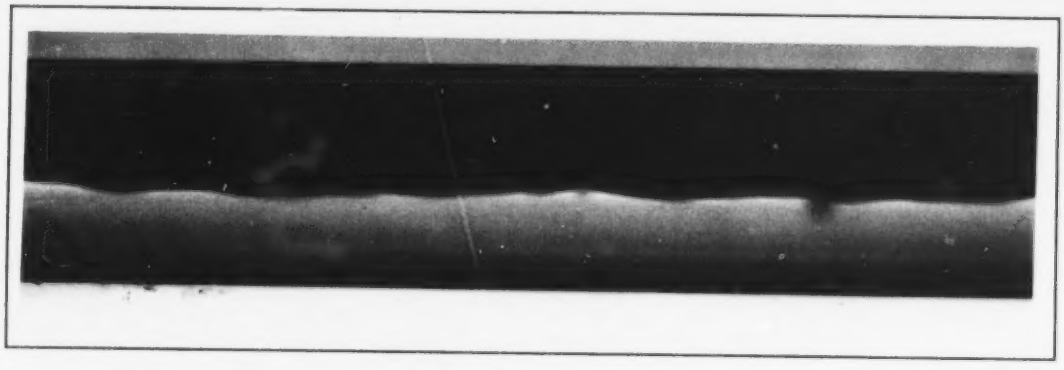

Figure 65: Oil–Water Flow Experiment 7, with no flow through perforation

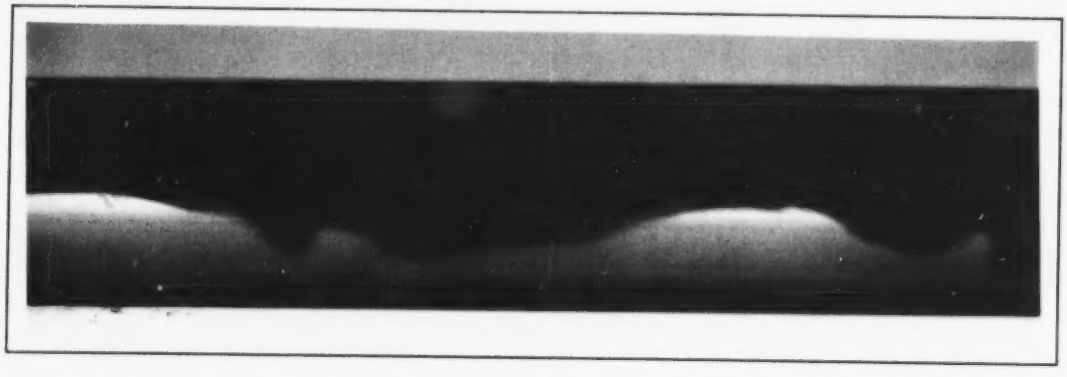

Figure 66: Oil–Water Flow Experiment 7, with water flow through perforation at 2.35 m/s

A mixed zone of disperse oil bubbles lies between pure oil and water phases. The interface is very bubbly and is located well above the centreline of the pipe model. In Figure 64, the water influx velocity through the perforation is 3.26 m/s. The oil bubbles are more numerous and have expanded greatly into the underlying water zone downstream of the perforation.

Experiment 7 is depicted in Figures 65–67. The oil and water superficial velocities for each of these figures is 0.172 m/s. In Figure 65 there is no influx flow through the perforation. The interface is slightly wavy and is located roughly in the middle of the pipe model. The occasional disperse oil bubble may be observed in the water phase near the interface. In Figure 66, water flows through the perforation at 2.35 m/s. The interface downstream of the perforation has become very wavy and uneven, with large oil bubbles displacing the water at the interface. In Figure 67, the water perforation rate has been increased to 3.26 m/s. A mixed water–in–oil phase has expanded downstream of the perforation to occupy the pipe diameter almost entirely. Medium–sized oil bubbles are freely dispersed within the water phase.

Figures 68 and 69 are for Experiment 14, in which the oil and water superficial velocities were 0.245 and 0.3175 m/s, respectively. In Figure 68 there is no flow through the perforation. A substantial mixed zone, consisting of disperse small to medium oil bubbles in water, lies between pure oil and water phases. In Figure 69 water flows through the perforation at 3.26 m/s. Note that at the higher (totaled) pipe flow rates the influx stream has a less noticeable visual effect on the flow regime. The mixed zone has expanded slightly downward, and there are more disperse oil bubbles flowing in the water phase downstream of the perforation.

Figures 70 and 71 are photographs of Experiment 18, in which the oil and water superficial velocities in the pipe were 0.245 and 0.3175 m/s, respectively. In Figure 70 there is no flow through the perforation; note the presence of medium to large–sized oil bubbles flowing in the water phase at the interface, which is mixed and wavy and is located slightly below the centreline of the pipe model. In Figure 71, the water flow rate through the perforation is 3.26 m/s. The mixed, oil–in–water zone has now expanded well below the centreline of the pipe to occupy almost the entire diameter, and more freely dispersed oil bubbles flow within the underlying water phase.

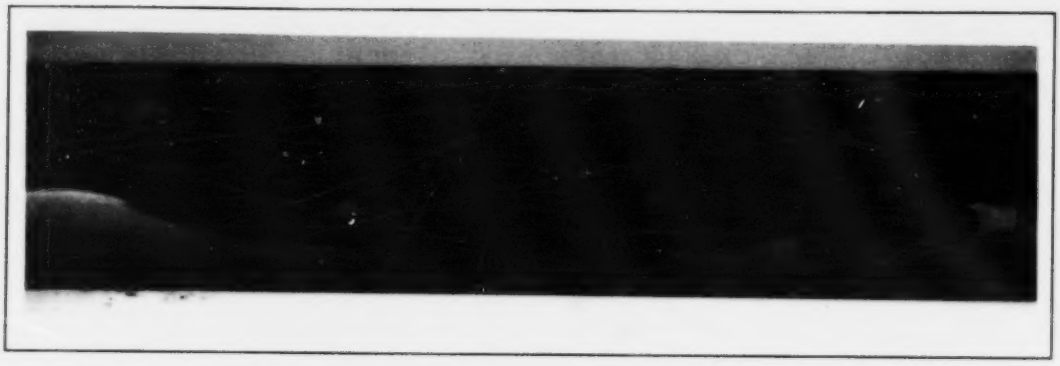

Figure 67: Oil–Water Flow Experiment 7, with water flow through perforation at 3.26 m/s

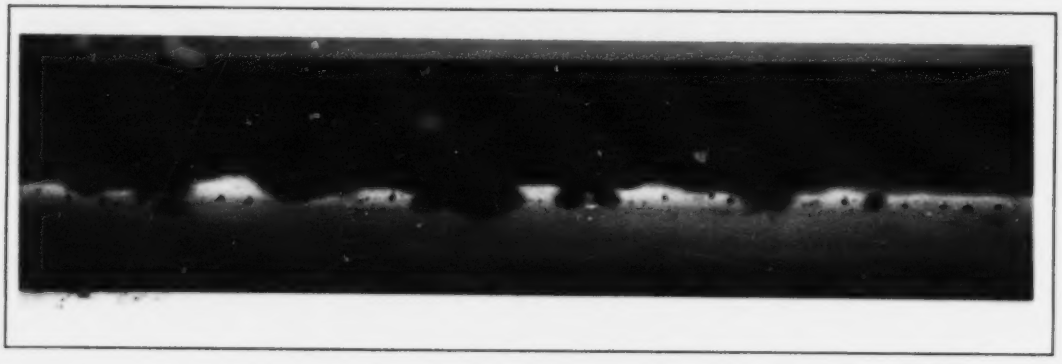

Figure 68: Oil–Water Flow Experiment 14, with no flow through perforation

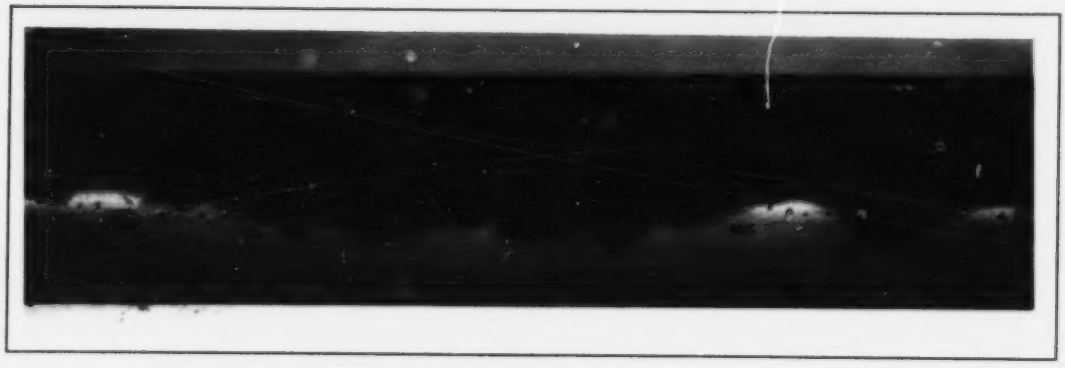

Figure 69: Oil–Water Flow Experiment 14, with water flow through perforation at 3.26 m/s

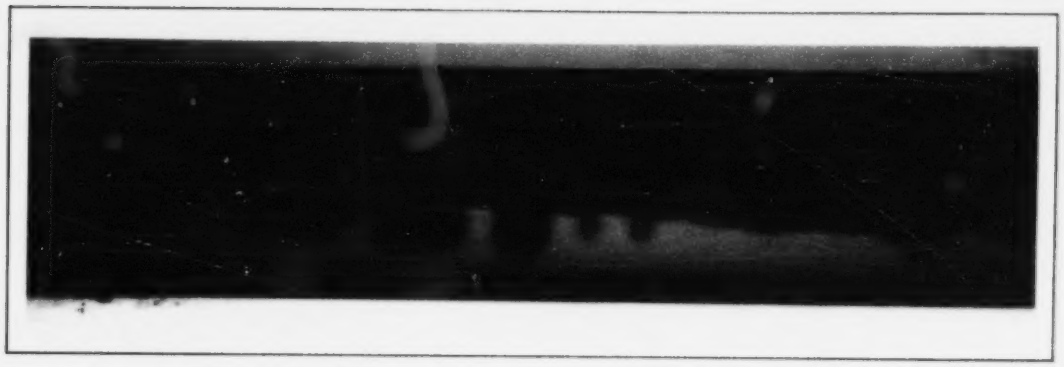

Figure 70: Oil–Water Flow Experiment 18, with no flow through perforation

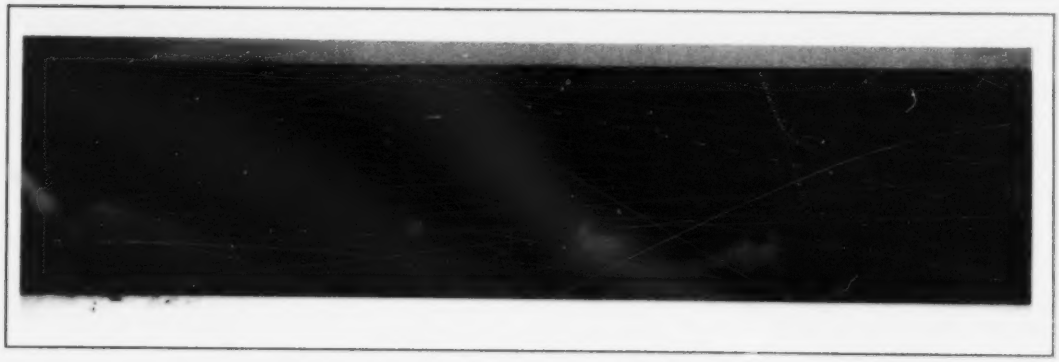

Figure 71: Oil–Water Flow Experiment 18, with water flow through perforation at 3.26 m/s

7. SUMMARY AND CONCLUSIONS

An experimental model apparatus was designed and constructed for the purpose of studying the pressure drop, holdup and flow regime behaviour of oil–water pipe flow with and without flow through a single perforation. Experiments were carried out with a light mineral oil and water and the pressure gradients were measured and analyzed. Measured data from oil–water flow experiments without influx flow through a perforation were compared with the results of two correlation methods and one numerical method of analysis. Holdup data from these experiments was taken and analyzed. Data from the oil–water flow experiments with water influx flow through a single perforation was compared with results from a correlation method modified to include the effects of confluent influx accelerational pressure drop. Numerical models were used to predict pressure drop across the length of horizontal wells under a variety of field conditions for both cased and perforated, and open–hole completions. Existing predictive numerical models were modified and improved by incorporating laminar flow and accelerational pressure drop calculations. Flow regime behaviour observations were made for all experiments, and regime data was compared with other oil–water flow regime maps. The following conclusions have been reached on the basis of the experimental observations and the numerical analyses:

1) The Beggs and Brill[6] correlation method was found to provide adequate pressure gradient predictions for the oil–water flow experiments conducted. Thus the approach taken in the correlation of averaging critical phase parameters such as viscosity and density should allow reasonable field–scale pressure gradient predictions in horizontal wells using single–phase reservoir–coupled numerical models. If greater accuracy is required, the Beggs and Brill[6] correlation may itself be coupled to a multiphase reservoir simulator.

2) The Asheim *et al.*[62] accelerational confluence model, adapted for oil–water two–phase flows, was found to be inadequate in predicting the pressure drops across a single perforation for the experiments conducted. However, this was not unexpected since the influx flow rates through the perforation were all beyond the working range specified by Asheim *et al.*[62], i.e., $u_p < 3u$.

3) At perforation influx flow velocities significantly beyond this working range, such as were encountered during the course of the experiments conducted ($3.1 \leq u_p \leq 14.4$), acceleration of the confluent flow is supplanted as the dominant factor affecting pressure drop by a constriction or venturi effect on the axial flow in combination with a disruption of the existing flow regime and boundary layer within the pipe. The pressure drops across the perforation under these flow conditions are far greater than those predicted using wall friction and/or accelerational models.

4) The Asheim *et al.*[62] accelerational confluence pressure drop model was successfully incorporated into various field–scale predictive models based on the work of Dikken[3], Landman[8], and Landman and Goldthorpe[4]. This adaptation significantly improves pressure drop predictions for these models.

5) Numerical approaches including those that are based on discretization of the pipe cross–section for stratified two–phase flows need to make use of sophisticated two–phase turbulence models in order to be effective in predicting turbulent–turbulent oil–water pressure gradient behaviour.

8. RECOMMENDATIONS FOR FURTHER RESEARCH

Based on the results of this study, the following recommendations are made to extend the scope of the research area, and to improve the quality of the data:

1) A more detailed investigation of the along wellbore pressure and flow disruption due to "confluent inflow" or influx from an opening or perforation is desirable. A simple improvement or modification to the existing model will allow this. Pressure taps drilled immediately on either side of a perforation tap and associated manometers will provide useful pressure data in this regard. This kind of experimental setup has been used for the study of two-phase air-liquid flow by Ihara and Shimizu[18].

2) The existing setup of equipment controlling the influx flow is probably inadequate in terms of both the variability of the flow rate and reliability. The influx pump is currently driven by a modified Ruska pump and its transmission. Ideally another variable speed drive should be implemented to control this pump.

3) There is room for more experiments to be performed at both higher and lower main (axial) pump rates. The latter may be accomplished with the existing equipment, but will require moving the distal pressure tap (the one nearest the separation tank) somewhat towards the centre of the model to allow for incomplete pipe filling at low rates. The former may be accomplished with a modified pulley arrangement resulting in a higher range of speeds for the main pumps. Currently the model is capable of a main flow total velocity of approximately 2.5 ft./s (0.762 m/s). Similar experiments conducted by Russell, Hodgson and Govier[36] and Arirachakaran *et al.*[56] included pipe flow velocities approaching 13 ft/s (3.96 m/s).

4) Parameters not investigated in this study, but which should be examined include perforation influx location along the well model, perforation influx fluid (oil, oil and water, etc.), viscosity of oil, etc. It should also be possible to modify the model for multiple simultaneous perforation flow. Experiments with air flow included could be conducted quite easily; Stapelberg and Mewes[57] provide a good experimental example of three–phase pipe flow experiments. It would be difficult and probably costly, but Ihara *et al.*[21] demonstrated that combining flow in porous media with an open–hole completed horizontal well model is possible.

5) It would be desirable to perform experiments using different oil-water dispersions as both the main flow and influx flow constituents, for comparison with the separate stratified oil-water flows used for these experiments. It may be possible to accurately measure the in situ viscosity of the dispersion using a capillary tube viscometer arrangement. Also, the inversion point of the dispersions may be easily determined if conductance measurements are taken across the pipe, as described by Pal[65]. Whether a dispersion flow is more accurately descriptive of actual conditions in horizontal wells flowing oil and water is open to argument, and probably varies from well to well. Arirachakaran *et al.*[56] and Cengel *et al.*[55] describe similar pipe flow experiments.

6) A superior photographic record could certainly be obtained. The oil should be dyed so as to be differentiable from the water, but also transparent enough so that oil bubbles may be easily discernible from a continuous oil phase. Alternatively, fine aluminum dust may be added to improve the clarity of the interface between phases. In the current series of experiments, it was not always easy to tell if the oil phase was entirely occupied by bubbles, due to the darkness of the dye used. Still greater clarity and contrast may be obtained, allowing sufficient detail to enable measurement of the amplitude and period of interface waves, by using stereophotogrammetry with two cameras[42]. Higher shutter speeds than those used for the current series of experiments are desirable for the higher velocity runs. A setup which employs a high speed flash (1/2000 s) would improve the results. Alternatively, a regular flash used together with flood lamps, high speed film and a camera capable of similar shutter speeds would work. Similarly, the video recordings would be greatly improved by setting up a parallel track to perform consistent tracking shots.

7) In the current series of experiments, the oil and water phases were separated by gravity in a holding tank downstream of the model, prior to being pumped back to the head of the model separately in a continuous loop. This simple setup was adequate for the experiments performed, but future experiments with other oils may require an improved separation process. Stapleberg and Mewes[57] employed a gravity separation tank in conjunction with two coalescers to separate the phases up to the limit of solubility.

8) The current experimental setup is somewhat unsafe. The variable speed drives power the main pumps via pulleys and V–belts. In order to set and check the main pump shaft speeds, the operator must work very close to the pulleys, and there is a risk of catching

a finger or hair. The pulley–belt arrangement should be covered by a guard for future experiments.

REFERENCES

1) Joshi, S., "Pressure drop through a horizontal well", ch. 10 from *Horizontal Well Technology*, pp. 379–420, Pennwell, 1991.

2) Doan, Q., Personal communication, September 1994.

3) Dikken, B.J., "Pressure drop in horizontal wells and its effect on their production performance", paper SPE 19824, presented at the 64th Annual Technical Conference and Exhibition of the Society of Petroleum Engineers, San Antonio Texas, October 8–11, 1989; also *JPT*, pp. 1426–1433, November 1990.

4) Landman, M. and Goldthorpe, W., "Optimization of perforation distribution for horizontal wells", SPE 23005, presented at the SPE Asia–Pacific Conference held in Perth, Western Australia, November 4–7, 1991.

5) Marett, B. and Landman, M., "Optimal perforation design for horizontal wells in reservoirs with boundaries", SPE 25366, presented at the SPE Asia Pacific Oil & Gas Conference & Exhibition held in Singapore, February 8–10, 1993.

6) Brill, J. and Beggs, H., *Two–Phase Flow in Pipes*, 6th Edition, University of Tulsa Press, 1994.

7) Doan, Q., "Scaled experiments of flow near and inside a horizontal well in steamflooding", M.Sc. Thesis, The University of Alberta, 1991.

8) Landman, M., "Analytical modeling of selectively perforated horizontal wells", *J. Pet. Sci.& Eng.*, pp. 179–188, 10 (1994).

9) Novy, R., "Pressure drops in horizontal wells: when can they be ignored?", SPE 24941, presented at the 67th Annual Technical Conference and Exhibition of the Society of Petroleum Engineers, Washington, D.C., October 4–7, 1992.

10) Kinney, R., "Fully developed frictional and heat–transfer characteristics of laminar flow in porous tubes", *Inter. J. of Heat and Mass Transfer*, Vol. 11, pp. 1393–1401, 1968.

11) Olson, R. and Eckert, E., "Experimental studies of turbulent flow in a porous circular tube with uniform fluid injection through the tube wall", *J. of Applied Mech.*, Vol. 33, pp. 7–17, 1966.

12) Ozkan, E., Sarica, C., Haciislamoglu, M. and Raghavan, R., "Effect of conductivity on horizontal well pressure behaviour", SPE 24683, presented at the 67th Annual Technical Conference and Exhibition of the Society of Petroleum Engineers, Washington, D.C., October 4–7, 1992.

13) Sarica, C., Ozkan, E., Haciislamoglu, M., Raghavan, R. and Brill, J., "Influence of wellbore hydraulics on pressure behaviour and productivity of horizontal gas wells", SPE 28486, presented at the SPE 69th Annual Technical Conference and Exhibition, New Orleans LA, September 25–28, 1994.

14) Tiefenthal, S., "Super–critical production from horizontal wells in oil rim reservoirs", SPE 25048, presented at the European Petroleum Conference held in Cannes, France, November 16–18, 1992.

15) Konieczek, J., "The concept of critical rate in gas coning and its use in production forecasting", SPE 20722, presented at the 65th Annual Technical Conference and Exhibition of the Society of Petroleum Engineers, New Orleans, LA, September 23–26, 1990.

16) Ihara, M., "Two–phase flow in horizontal wells", M.Sc. Thesis, University of Tulsa, Tulsa OK, 1991.

17) Ihara, M., Brill, J. and Shoham, O., "Experimental and theoretical investigation of two–phase flow in horizontal wells", SPE 24766, presented at the 67th Annual Technical Conference and Exhibition of the Society of Petroleum Engineers, Washington, D.C., October 4–7, 1992.

18) Ihara, M. and Shimizu, N., "Effect of accelerational pressure drop in a horizontal wellbore", SPE 26519, presented at the 68th Annual Technical Conference and Exhibition of the Society of Petroleum Engineers, Houston, TX, October 3–6, 1993.

19) Brekke, K. and Lien, S., "New and simple completion methods for horizontal wells improve the production performance in high–permeability, thin oil zones", SPE 24762, presented at the 67th Annual Technical Conference and Exhibition of the Society of Petroleum Engineers, Washington, D.C., October 4–7, 1992.

20) Su, Z. and Gudmundsson, J., "Friction factor of perforation roughness in pipes", SPE 26521, presented at the 68th Annual Technical Conference and Exhibition of the Society of Petroleum Engineers, Houston, TX, October 3–6, 1993.

21) Ihara, M., Kikuyama, K., Hasegawa, Y. and Mizuguchi, K., "Flow in horizontal wellbores with influx through porous walls", SPE 28485, presented at the SPE 69th Annual Technical Conference and Exhibition, New Orleans LA, September 25–28, 1994.

22) Stone, T., Edmunds, N. and Kristoff, B., "A comprehensive wellbore/reservoir simulator", SPE 18419, presented at the SPE Symposium on Reservoir Simulation, Houston TX, February 6–8, 1989.

23) Islam, M. and Chakma, A., "Comprehensive Physical and numerical modeling of a horizontal well", SPE 20627, presented at the 65th Annual Technical Conference and Exhibition of the Society of Petroleum Engineers, New Orleans, LA, September 23–26, 1990.

24) Folefac, A., Archer, J., Issa, R. and Arshad, A., "Effect of pressure drop along horizontal wellbores on well performance", SPE 23094, presented at the Offshore Europe Conference, Aberdeen, September 3–6, 1991.

25) Folefac, A., Issa, R. and Wall, C., "A computational model for two phase flow in wellbores, SPE 22233, unsolicited, 1990.

26) Wallis, G., *One–Dimensional Two–Phase Flow*, McGraw–Hill, 1969.

27) Briggs, P., "Pressure drop in horizontal well completions—is it important?", presented at JETEC 1991.

28) Collins, D., Nghiem, L., Sharma, R., Agarwal, R. and Jha, N., "Field–scale simulation of horizontal wells with hybrid grids", SPE 21218, presented at the 11th SPE Symposium on Reservoir Simulation held in Anaheim, CA, February 17–20, 1991.

29) Govier, G. and Aziz, K., *The Flow of Complex Mixtures in Pipes*, Van Nostrand Reinhold Co., 1972.

30) Nghiem, L., Collins, D. and Sharma, R., "Seventh SPE comparative solution project: modeling of horizontal wells in reservoir simulation", SPE 21221, presented at the 11th SPE Symposium on Reservoir Simulation held in Anaheim, CA, February 17–20, 1991.

31) Lien, S., Seines, K., Havig, S. and Kydland, T., "Experience from the ongoing long–term test with a horizontal well in the Troll oil zone", SPE 20715, presented at the 65th Annual Technical Conference and Exhibition of the Society of Petroleum Engineers, New Orleans, LA, September 23–26, 1990.

32) Korady, V., Renard, G. and Lemonnier, P., "Modeling of pressure drop for three–phase flow in horizontal wells", presented at the 6th European IOR Symposium, Stavenger Norway, May 21–23 1991.

33) Seines, K., Aavatsmark, I., Lien, S. and Rushworth, P., "Considering wellbore friction effects in planning horizontal wells", *JPT*, Vol. 45, No. 10, pp. 994–1000, October 1993.

34) Lockhart, R. and Martinelli, R., "Proposed correlation of data for isothermal two phase, two component flow in pipes", *Chem. Eng. Progress*, Vol. 45, pp. 39–48, 1949.

35) Clarke, K. and Shapiro, A., U.S. Patent No. 2,533,878, May 31 1949.

36) Russell, T., Hodgson, G. and Govier, G., "Horizontal pipeline flow of mixtures of oil and water", *Cdn. J. of Chem Eng.*, pp. 9–17, February 1959.

37) Russell, T. and Charles, M., "The effect of the less viscous liquid in the laminar flow of two immiscible liquids", *Cdn. J. of Chem Eng.*, pp. 18–24, February 1959.

38) Charles, M., Govier, G. and Hodgson, G., "The horizontal pipeline flow of equal density oil–water mixtures", *Cdn. J. of Chem Eng.*, pp. 27–36, February 1961.

39) Charles, M. and Redberger, P., "The reduction of pressure gradients in oil pipelines by the addition of water: numerical analysis of stratified flow", *Cdn. J. of Chem Eng.*, pp. 70–75, April 1962.

40) Gemmell, A. and Epstein, N., "Numerical analysis of stratified laminar flow of two immiscible Newtonian liquids in a circular pipe", *Cdn. J. of Chem Eng.*, pp. 215–224, October 1962.

41) Charles, M. and Lilleleht, L., "Co–current stratified laminar flow of two immiscible liquids in a rectangular conduit", *Cdn. J. of Chem Eng.*, pp. 110–116, June 1965.

42) Charles, M. and Lilleleht, L., "The application of stereophotogrammetry to the measurement of interfacial waves", *Cdn. J. of Chem Eng.*, pp. 277–279, December 1965.

43) Charles, M. and Lilleleht, L., "Correlation of pressure gradients for the stratified laminar–turbulent pipeline flow of two immiscible liquids", *Cdn. J. of Chem Eng.*, pp. 47–49, February 1966.

44) Agrawal, S., Gregory, G. and Govier, G., "An analysis of horizontal stratified two phase flow in pipes", *Cdn. J. of Chem Eng.*, Vol. 51, pp. 281–286, June, 1973.

45) Taitel, Y. and Dukler, A., "A model for predicting flow regime transitions in horizontal and near horizontal gas–liquid flow", *AIChEJ*, Vol. 22, No. 1, pp. 47–55, 1976.

46) Taitel, Y. and Dukler, A., "A theoretical approach to the Lockhart–Martinelli correlation for stratified flow", *Int. J. of Multiphase Flow*, Vol. 2, pp. 591–595, 1976.

47) Shoham, O. and Taitel, Y., "Stratified turbulent–turbulent gas–liquid flow in horizontal and inclined pipes", *AIChEJ*, Vol. 30, No. 3, pp. 377–385, May 1984.

48) Issa, R., "Prediction of turbulent, stratified, two–phase flow in inclined pipes and channels", *Int. J. of Multiphase Flow*, Vol. 14, No. 2, pp. 141–154, 1988.

49) Akai, M., Inoue, A. and Aoki, S., "The prediction of stratified two–phase flow with a two–equation model of turbulence", *Int. J. of Multiphase Flow*, Vol. 7, pp. 21–39, 1981.

50) Hall, A. and Hewitt, G., "Application of two–fluid analysis to laminar stratified oil–water flows", *Int. J. of Multiphase Flow*, Vol. 19, No. 4, pp. 711–717, 1993.

51) Barnea, D., "A unified model for predicting flow–pattern transition for the whole range of pipe inclinations", *Int. J. of Multiphase Flow*, Vol. 13, No. 1, pp. 1–12, 1987.

52) Xiao, J., Shoham, O. and Brill, J., "A comprehensive mechanistic model for two–phase flow in pipelines", SPE 20631, presented at the 65th Annual Technical Conference and Exhibition of the Society of Petroleum Engineers, New Orleans, LA, September 23–26, 1990.

53) Ansari, A., Sylvester, N., Shoham, O. and Brill, J., "A comprehensive mechanistic model for upwards two–phase flow in wellbores", SPE 20630, presented at the 65th Annual Technical Conference and Exhibition of the Society of Petroleum Engineers, New Orleans, LA, September 23–26, 1990.

54) Pucknell, J., Mason, J. and Vervest, E., "An evaluation of recent "mechanistic" models of multiphase flow for predicting pressure drops in oil and gas wells", SPE 26682, presented at the Offshore European Conference held in Aberdeen, Scotland, September 7–19, 1993.

55) Cengel, J., Faruqui, A., Finnigan, J., Wright, C. and Kundsen, J., "Laminar and turbulent flow of unstable liquid–liquid emulsions", *AIChEJ*, Vol. 8, No. 3, pp. 335–339, 1962.

56) Arirachakaran, S., Oglesby, K., Malinowsky, M., Shoham, O. and Brill, J., "An analysis of oil/water flow phenomena in horizontal pipes", SPE 18836, presented at the SPE Production Operations Symposium held in Oklahoma City, OK, March 13–14, 1989.

57) Stapelberg, H. and Mewes, D., "The pressure loss and slug frequency of liquid–liquid–gas slug flow in horizontal pipes", *Int. J. of Multiphase Flow*, Vol. 20, No. 2, pp. 285–303, 1994.

58) Mills, A., "Progressing cavity oilwell pumps — past, present and future", *J. Cdn. Pet. Tech.*, Vol. 33, No. 4, pp. 5–6, April 1994.

59) Olson, .R., *Essentials of Engineering Fluid Mechanics*, 4th Edition, Harper & Row, 1980.

60) Hein, M., "'3P' flow analyzer", *Oil & Gas J.*, pp. 132–138, Aug. 9 1982.

61) Hein, M., "3P calculator program for multiphase flow analysis in pipelines, casing and tubing", *Oil & Gas J.*, pp. 148–152, Aug. 16 1982.

62) Asheim, H., Kolnes, J. and Oudeman, P., "A flow resistance correlation for completed wellbore", *J. Pet. Sci.& Eng.*, vol. 8, no. 2, pp. 97–104, 1992.

63) Chauvel, Y., Oosthoek, P., "Production logging in horizontal wells: applications and experience to date", SPE 21094, presented at the SPE Latin American Petroleum Engineering Conference, Rio de Janeiro, October 14–19, 1990.

64) Chauvel, Y., "Quantitative three–phase profiling and flow regime characterization in a horizontal well", SPE 26520, presented at the 68th Annual Technical Conference and Exhibition of the Society of Petroleum Engineers, Houston, TX, October 3–6, 1993.

65) Pal, R., "Pipeline flow of unstable and surfactant–stabilized emulsions", *AIChEJ*, Vol. 39, No. 11, pp. 1754–1764, 1993.

66) Gerald, C. and Wheately, P., *Applied Numerical Analysis*, 4th Edition, Addison–Wesley, 1989.

APPENDIX A

A complete explanation of Dikken's[3] "Pressure Drop in Horizontal Wells and Its Effect on Their Production Performance".

Assumptions:

–single–phase incompressible liquid model
–open–hole completion
–Blasius power law friction factor used for turbulent flow
–reservoir considered homogeneous
–no along–wellbore pressure gradients allowed for in the reservoir
–well runs parallel to a constant pressure boundary such that the well has a constant productivity index per unit well length.

Please refer to Figure A1. The following equation defines the relationship between the inflow performance of a horizontal well with respect to the specific productivity index per unit length of the producing section and the drawdown at each position along the section:

$$q_s(x) = J_s\left(P_e - P_w(x)\right) \tag{A–1}$$

In this equation, $q_s(x)$ refers to the influx flow rate into the well at any position x, with x = 0 at the producing end and $x = L$ at the far end. The parameter J_s is the specific productivity index per unit length, P_e is the pressure at an assumed constant pressure boundary at some fixed distance from the well, and $P_w(x)$ is the well pressure.
The next equation is nothing more than a volume balance for the well itself. The well rate at any position x must equal the sum of the influx that has occurred up to that point. This may be expressed as

$$q_w(x) = -\int_L^x q_s(x)\ dx \tag{A–2}$$

where $q_w(x)$ is the well rate. The minus sign is necessary since we are integrating from the end of the well back to the position x, and flow is in this direction.

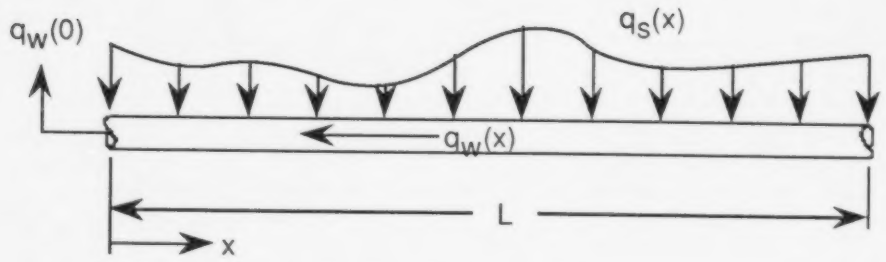

Figure A1: Influx and Well Flow in Horizontal Well

Equation (A–2) may be written in differential form:

$$\frac{d}{dx}q_w(x) = -q_s(x) \tag{A–3}$$

A dimensional analysis of wall friction in turbulent single–phase flow in a circular pipe produces the following equation for the pipe wall or "Moody's" friction factor (Olson, 1980)[59]:

$$f = \frac{\Delta P 2D}{L\rho u^2} \tag{A–4}$$

where u is the velocity of the flow in the pipe, D is the pipe diameter, ρ is the fluid density and $\Delta P = P_w(L) - P_w(0)$. Now considering a thin element of the well (or pipe) and taking the limit as $\Delta x \longrightarrow 0$

$$f = \frac{2D}{\rho u^2}\frac{d}{dx}P_w(x) \tag{A–5}$$

or

$$\frac{d}{dx}P_w(x) = \frac{f\rho u^2}{2D} \tag{A–6}$$

The following equation is Blasius' correlation for single–phase flow in circular pipes:

$$f = 0.3164\,\mathrm{Re}^{-\alpha} \tag{A–7}$$

where the exponent α is equal to 0.25 for turbulent flow in smooth pipes, decreasing with increasing roughness. Re is the Reynolds number for the flow, defined as

$$\mathrm{Re} = \frac{\rho u D}{\mu} \tag{A–8}$$

where the term in the denominator is the fluid viscosity. Upon substitution for f and Re, along with the definition of the flow velocity u in terms of the volumetric flow rate q and the area of the pipe, Equation (A–6) becomes:

$$\frac{d}{dx}P_w(x) = \frac{0.3164\,\mathrm{Re}^{-\alpha}\rho u^2}{2D}$$

$$= \frac{0.3164\left(\frac{\rho u D}{\mu}\right)^{-\alpha}\rho u^2}{2D}$$

$$= 0.3164\left(\frac{\mu\pi D}{4\rho q_w(x)}\right)^{\alpha}\frac{\rho 8 q_w(x)^2}{\pi^2 D^5}$$

$$= R_w q_w(x)^{2-\alpha} \tag{A–9}$$

where

$$R_w = 0.3164\left(\frac{\mu\pi D}{4\rho}\right)^{\alpha}\frac{8\rho}{\pi^2 D^5} \tag{A–10}$$

An equation coupling steady reservoir flow and the flow in the horizontal wellbore is arrived at by again differentiating Equation (A–3) and substituting Equations (A–1) and (A–9):

$$\frac{d^2}{dx^2}q_w(x) = J_s R_w q_w(x)^{2-\alpha} \tag{A–11}$$

Solutions to Equation (A–11) are provided for each of laminar and turbulent flow, in both semi–infinite well length and finite well length cases. Recall that α = 1 for laminar flow,

and that $0.0 \le \alpha \le 0.25$ for turbulent flow, with 0.25 being the limiting value for smooth pipes. For laminar flow the coefficient is 64 instead of 0.3164.

A.1 Semi-Infinite Well Case

The well is considered to be infinite in the increasing x direction. For this case the boundary conditions are as follows:

$$\lim_{x\to\infty} P_w(x) = P_e \Rightarrow \lim_{x\to\infty} \frac{d}{dx} q_w(x) = 0 \qquad \text{(A–12)}$$

Upon integration, the latter expression becomes,

$$\lim_{x\to\infty} q_w(x) = 0 \qquad \text{(A–13)}$$

if inflow into the well end is neglected (no inflow should occur here because there is complete penetration of the reservoir). The other boundary condition is:

$$\lim_{x\to 0} P_w(x) = P_w(0) \Rightarrow \lim_{x\to 0} \frac{d}{dx} q_w(x) = -J_s\left(P_e - P_w(0)\right) \qquad \text{(A–14)}$$

Substituting Equation (A–3) in the latter expression above yields

$$\lim_{x\to 0} q_s(x) = J_s\left[P_e - P_w(0)\right] \qquad \text{(A–15)}$$

A.1.1 Laminar Flow

For the case of laminar flow, the α exponent in Equation (A–11) is equal to 1 and the equation becomes a linear second order ordinary differential equation with general solution:

$$q_w(x) = c_1 e^{\sqrt{J_s R_w}\, x} + c_2 e^{-\sqrt{J_s R_w}\, x} \qquad \text{(A–16)}$$

in which the c terms are constants, evaluated by applying the boundary conditions. As x approaches infinity,

$$0 = c_1 e^{\infty} + c_2 e^{-\infty} \Rightarrow c_1 = 0$$

and

$$q_w(x) = c_2 e^{-\sqrt{J_s R_w}\, x}$$

Taking the derivative and letting x approach 0:

$$\frac{d}{dx} q_w(x) = -q_s(x) = -\sqrt{J_s R_w}\, c_2 e^{-\sqrt{J_s R_w}\,(x)}$$

$$J_s\left[P_e - P_w(0)\right] = \sqrt{J_s R_w}\, c_2 e^{-\sqrt{J_s R_w}\,(0)}$$

$$c_2 = \frac{J_s\left[P_e - P_w(0)\right]}{\sqrt{J_s R_w}} = \sqrt{\frac{J_s}{R_w}}\left[P_e - P_w(0)\right]$$

and therefore

$$q_w(x) = \sqrt{\frac{J_s}{R_w}}\left[P_e - P_w(0)\right] e^{-\sqrt{J_s R_w}\, x} \qquad \text{(A–17)}$$

This equation may be differentiated in order to solve for the pressure drop in the well:

$$\frac{d}{dx} q_w(x) = -q_s(x) = -\sqrt{J_s R_w}\sqrt{\frac{J_s}{R_w}}\left[P_e - P_w(0)\right] e^{-\sqrt{J_s R_w}\,(x)}$$

$$= -J_s\left[P_e - P_w(0)\right] e^{-\sqrt{J_s R_w}\, x}$$

$$P_e - P_w(x) = \frac{q_s(x)}{J_s} = \left[P_e - P_w(0)\right] e^{-\sqrt{J_s R_w}\, x} \qquad \text{(A–18)}$$

A.1.2 Turbulent Flow

Beginning again with Equation (A–11):

$$\frac{d^2}{dx^2} q_w(x) = J_s R_w q_w(x)^{2-\alpha} \qquad \text{(A–11)}$$

This equation is solved by first multiplying both sides by the derivative of the well rate and then integrating:

$$\int \frac{dq_w(x)}{dx}\frac{d^2q_w(x)}{dx^2}dx = \int \frac{dq_w(x)}{dx} J_s R_w q_w(x)^{2-\alpha} dx$$

$$\frac{1}{2}\left(\frac{dq_w(x)}{dx}\right)^2 = \frac{J_s R_w}{3-\alpha} q_w(x)^{3-\alpha} + K'$$

$$\frac{dq_w}{dx} = \pm\sqrt{\frac{2J_s R_w}{3-\alpha}}\sqrt{q_w(x)^{3-\alpha} + K'} \qquad \text{(A–19)}$$

where K' is a constant of integration. The positive solution is immediately rejected since the flow rate always increases as x decreases. This leaves

$$\frac{dq_w}{dx} = -\sqrt{\frac{2J_s R_w}{3-\alpha}}\sqrt{q_w(x)^{3-\alpha} + K'}$$

and now a boundary conditions is applied. As x approaches 0,

$$0 = -\sqrt{\frac{2J_s R_w}{3-\alpha}}\sqrt{0^{3-\alpha} + K'} \Rightarrow K' = 0$$

so that

$$\frac{dq_w}{dx} = -\sqrt{\frac{2J_s R_w}{3-\alpha}}\sqrt{q_w(x)^{3-\alpha}} \qquad \text{(A–20)}$$

Now integrating again in order to obtain an expression for the well rate:

$$\int \frac{dq_w}{q_w(x)^{\frac{3-\alpha}{2}}} = \int -\sqrt{\frac{2J_s R_w}{3-\alpha}}dx$$

$$\frac{2}{\alpha-1} q_w(x)^{\frac{\alpha-1}{2}} = -\sqrt{\frac{2J_s R_w}{3-\alpha}}x + K$$

$$q_w(x) = \left(K + \frac{1-\alpha}{2}\sqrt{\frac{2J_sR_w}{3-\alpha}}x \right)^{\frac{2}{\alpha-1}} \tag{A–21}$$

where K is again a constant of integration. Applying the boundary condition as x approaches 0,

$$\frac{dq_w(x)}{dx} = \frac{2}{\alpha-1}\left(K + \frac{1-\alpha}{2}\sqrt{\frac{2J_sR_w}{3-\alpha}}x \right)^{\frac{3-\alpha}{\alpha-1}}\left(\frac{1-\alpha}{2}\sqrt{\frac{2J_sR_w}{3-\alpha}} \right)$$

$$J_s[P_e - P_w(0)] = \frac{2}{\alpha-1}\left(K + \frac{1-\alpha}{2}\sqrt{\frac{2J_sR_w}{3-\alpha}}(0) \right)^{\frac{3-\alpha}{\alpha-1}}\left(\frac{1-\alpha}{2}\sqrt{\frac{2J_sR_w}{3-\alpha}} \right)$$

$$= \frac{2}{\alpha-1}(K)^{\frac{3-\alpha}{\alpha-1}}\left(\frac{1-\alpha}{2}\sqrt{\frac{2J_sR_w}{3-\alpha}} \right)$$

$$K = \left(\sqrt{\frac{J_s(3-\alpha)}{2R_w}}[P_e - P_w(0)] \right)^{\frac{\alpha-1}{3-\alpha}}$$

so that

$$q_w(x) = \left[\left(\sqrt{\frac{J_s(3-\alpha)}{2R_w}}[P_e - P_w(0)] \right)^{\frac{\alpha-1}{3-\alpha}} + \frac{1-\alpha}{2}\sqrt{\frac{2J_sR_w}{3-\alpha}}x \right]^{\frac{2}{\alpha-1}} \tag{A–22}$$

Dikken[3] defined the following dimensionless variables:

$$\tilde{x} = \frac{1-\alpha}{2K}\sqrt{\frac{2J_sR_w}{3-\alpha}}x \tag{A–23}$$

$$\tilde{q}_w(\tilde{x}) = K^{\frac{2}{\alpha-1}}q_w \tag{A–24}$$

$$\Delta\tilde{P}_w(\tilde{x}) = \frac{P_w(x) - P_w(0)}{P_e - P_w(0)} \tag{A–25}$$

then

$$\tilde{q}_w(\tilde{x}) = (1+\tilde{x})^{\frac{2}{\alpha-1}} \tag{A–26}$$

$$\frac{d}{d\tilde{x}}\tilde{q}_w(\tilde{x}) = \frac{2}{\alpha-1}(1+\tilde{x})^{\frac{3-\alpha}{\alpha-1}} \tag{A–27}$$

and

$$\Delta\tilde{P}_w(\tilde{x}) = 1-(1+\tilde{x})^{\frac{3-\alpha}{\alpha-1}} \tag{A–28}$$

$$= 1-\frac{\alpha-1}{2}\frac{d}{d\tilde{x}}\tilde{q}_w(\tilde{x}) \tag{A–29}$$

If some dimensionless position $\tilde{x} = \tilde{L}_s$ is specified, the total dimensionless well rate may be calculated for a horizontal well of dimensionless length $\tilde{L}_s$ as follows:

$$\tilde{q}_t(\tilde{L}_s) = \tilde{q}_w(0) - \tilde{q}_w(\tilde{L}_s)$$

$$= 1-(1+\tilde{L}_s)^{\frac{2}{\alpha-1}} \tag{A–30}$$

Similarly, the incremental rate may be defined as:

$$\frac{d}{d\tilde{x}}\tilde{q}_t(\tilde{L}_s) = \frac{2}{1-\alpha}(1+\tilde{L}_s)^{\frac{3-\alpha}{\alpha-1}} \tag{A–31}$$

Figure A2 indicates that 80% of the total well production will come from a total dimensionless length of only 0.7 – 1.2, depending on the value of alpha, for the semi–infinite well case. There is little benefit to be gained, therefore, by drilling beyond this length.

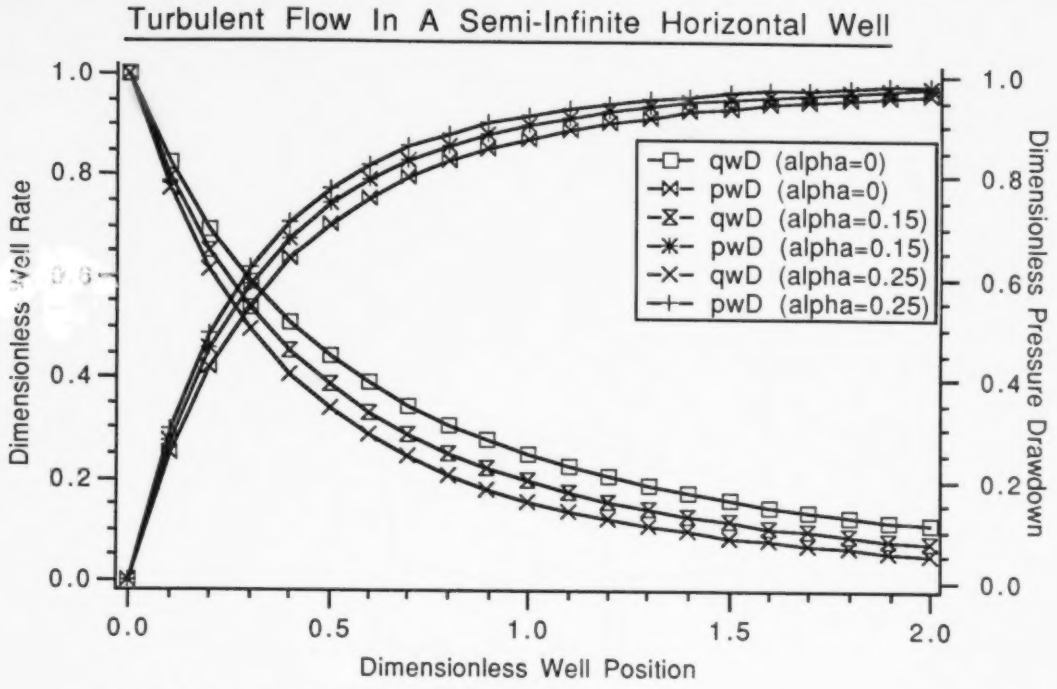

Figure A2: Turbulent Flow in a Semi–Infinite Horizontal Well

A.2 Finite Well Case

A.2.1 Laminar Flow

Beginning with the general solution:

$$q_w(x) = c_1 e^{\sqrt{J_s R_w}\,x} + c_2 e^{-\sqrt{J_s R_w}\,x} \tag{A–16}$$

This may be re–written as:

$$q_w(x) = c_1 \cosh\left[\sqrt{J_s R_w}\,x\right] + c_2 \sinh\left[\sqrt{J_s R_w}\,x\right] \tag{A–32}$$

The boundary conditions for the case of a finite well are, at $x = L$:

$$q_w(L) = 0 \tag{A–33}$$

and at $x = 0$:

$$\frac{d}{dx}q_w(0) = -J_s[P_e - P_w(0)] \qquad \text{(A–34)}$$

Applying the first boundary condition to the first term of Equation (A–32):

$$0 = c_1 \cosh\left[\sqrt{J_s R_w}L\right] \Rightarrow c_1 = 0$$

and

$$q_w(x) = c_2 \sinh\left[\sqrt{J_s R_w}x\right]$$

This equation is expanded as follows:

$$q_w(x) = c_2 \sinh\left[\sqrt{J_s R_w}(L-(L-x))\right]$$

$$= c_3 \sinh\left[\sqrt{J_s R_w}L\right]\cosh\left[\sqrt{J_s R_w}(L-x)\right] - c_4 \cosh\left[\sqrt{J_s R_w}L\right]\sinh\left[\sqrt{J_s R_w}(L-x)\right]$$

Again applying the first boundary condition to the first term:

$$0 = c_3 \sinh\left[\sqrt{J_s R_w}L\right]\cosh\left[\sqrt{J_s R_w}(L-L)\right] \Rightarrow c_3 = 0$$

so that

$$q_w(x) = -c_4 \cosh\left[\sqrt{J_s R_w}L\right]\sinh\left[\sqrt{J_s R_w}(L-x)\right]$$

Now taking the derivative:

$$\frac{d}{dx}q_w(x) = -c_4 \cosh\left[\sqrt{J_s R_w}L\right]\left(-\sqrt{J_s R_w}\right)\cosh\left[\sqrt{J_s R_w}(L-x)\right]$$

and applying the second boundary condition:

$$-J_s[P_e - P_w(0)] = c_4\sqrt{J_s R_w}\cosh\left[\sqrt{J_s R_w}L\right]\cosh\left[\sqrt{J_s R_w}(L-0)\right]$$

$$= c_4\sqrt{J_s R_w}\cosh^2\left[\sqrt{J_s R_w}L\right]$$

therefore

$$c_4 = \frac{-J_s[P_e - P_w(0)]}{\sqrt{J_s R_w}\cosh^2\left[\sqrt{J_s R_w}L\right]}$$

$$= \frac{-\sqrt{\frac{J_s}{R_w}}[P_e - P_w(0)]}{\cosh^2\left[\sqrt{J_s R_w}L\right]}$$

and

$$q_w(x) = \frac{\sqrt{\frac{J_s}{R_w}}[P_e - P_w(0)]}{\cosh^2\left[\sqrt{J_s R_w}L\right]}\cosh\left[\sqrt{J_s R_w}L\right]\sinh\left[\sqrt{J_s R_w}(L-x)\right]$$

$$= \sqrt{\frac{J_s}{R_w}}[P_e - P_w(0)]\frac{\sinh\left[\sqrt{J_s R_w}(L-x)\right]}{\cosh\left[\sqrt{J_s R_w}L\right]} \qquad \text{(A–35)}$$

A.2.2 Turbulent Flow

Recall from the infinite well case the following equations in dimensionless form:

$$\tilde{q}_w(\tilde{x}) = (1+\tilde{x})^{\frac{2}{\alpha-1}} \qquad \text{(A–26)}$$

$$\frac{d}{d\tilde{x}}\tilde{q}_w(\tilde{x}) = \frac{2}{\alpha-1}(1+\tilde{x})^{\frac{3-\alpha}{\alpha-1}} \qquad \text{(A–27)}$$

Now taking the second derivative:

$$\frac{d^2}{d\tilde{x}^2}\tilde{q}_w(\tilde{x}) = \frac{6-2\alpha}{(\alpha-1)^2}(1+\tilde{x})^{\frac{4-2\alpha}{\alpha-1}}$$

$$= \frac{6-2\alpha}{(\alpha-1)^2}\tilde{q}_w(\tilde{x})^{2-\alpha} \qquad \text{(A–36)}$$

The boundary conditions for the finite well case in dimensionless form are:

$$\tilde{q}_w\left(\tilde{L}\right)=0 \tag{A–37}$$

and

$$\frac{d}{d\tilde{x}}\tilde{q}_w(0)=\frac{2}{\alpha-1} \tag{A–38}$$

The problem is simplified by the replacement of the first boundary condition with a second condition at the heel or producing end of the horizontal well:

$$\tilde{q}_w(0)=\tilde{q}_t \ , \ \ 0\le\tilde{q}_t\le 1 \tag{A–39}$$

i.e., the dimensionless well length associated with the specified total well rate is found where the dimensionless well rate reaches zero with increasing dimensionless distance.

$$\tilde{q}_w(\tilde{x})=0\Rightarrow\tilde{x}=\tilde{L}$$

Equation (A–36) is solved by first replacing it with two first order ordinary differential equations:

$$\frac{d}{d\tilde{x}}\eta=\xi \tag{A–40}$$

$$\frac{d}{d\tilde{x}}\xi=\frac{6-2\alpha}{(\alpha-1)^2}\eta^{2-\alpha} \tag{A–41}$$

with boundary conditions:

$$\eta(0)=\tilde{q}_t \ , \ \ 0\le\tilde{q}_t\le 1 \tag{A–42}$$

$$\xi(0)=\frac{2}{\alpha-1} \tag{A–43}$$

Dikken[3] found the solution to these equations using a predictor–corrector numerical method. A modified Euler predictor–corrector method of solution is described here.[66] Letting the step length $\Delta\tilde{x} = h$, the following equations constitute the predictor set:

$$\eta_{p_{\tilde{x}+h}} = \eta_{p_{\tilde{x}}} + h\xi_{p_{\tilde{x}}} \tag{A–44}$$

$$\xi_{p_{\tilde{x}+h}} = \xi_{p_{\tilde{x}}} + h\left[\frac{6-2\alpha}{(\alpha-1)^2}\eta_{p_{\tilde{x}}}^{2-\alpha}\right] \tag{A–45}$$

The corrector set of equations is:

$$\eta_{c_{\tilde{x}+h}} = \eta_{p_{\tilde{x}}} + h\left[\frac{\xi_{p_{\tilde{x}}} + \xi_{p_{\tilde{x}+h}}}{2}\right] \tag{A–46}$$

$$\xi_{c_{\tilde{x}+h}} = \xi_{p_{\tilde{x}}} + 0.5h\left[\frac{6-2\alpha}{(\alpha-1)^2}\eta_{p_{\tilde{x}}}^{2-\alpha} + \frac{6-2\alpha}{(\alpha-1)^2}\eta_{c_{\tilde{x}+h}}^{2-\alpha}\right] \tag{A–47}$$

The routine calculates the predictor values for the first position, $\tilde{x} = 0$, then corrects and recorrects up to 10 times before advancing to the next dimensionless well position. The last obtained (the most corrected) values for each position are:

$$\eta_c = \tilde{q}_w \text{ and } \xi_c = \frac{d}{d\tilde{x}}\tilde{q}_w(\tilde{x})$$

The dimensionless well position $\tilde{x}$ advances until $\eta_c = \tilde{q}_w = 0$, at which point $\tilde{x} = \tilde{L}$. Please refer to the following Fortran program listing, PEULER.F.

Figure A3 was generated using this program. The figure demonstrates in general dimensionless terms the effect of increasing turbulent flow pressure drop on production in a horizontal well. It may be observed that for a well with $\alpha = 0.15$ to achieve the same total dimensionless flow rate (0.75 for the example above) as a well with $\alpha = 0.25$ (corresponding with smooth wellbore walls) an additional 13% of well length would have to be drilled. A well with $\alpha = 0.0$ would require an additional 33% of well length to match this output.

```
C       PROGRAM PEULER.F
C       THIS PROGRAM USES A MODIFIED EULER PREDICTOR–CORRECTOR
C       METHOD TO SOLVE A SECOND ORDER NON–LINEAR ORDINARY
C       DIFFERENTIAL EQUATION WITH TWO INITIAL CONDITIONS
C
      REAL ETA,ZI,XD,ALPHA,ETA0,ZI0,XD0,XDEND,H,TOL,
     +     ZIP,ZIC,ETAP,ETAC,Z,LD,QTD,DETA0,DZI0
      INTEGER I
      FCN1(ETA,ZI,XD)=ZI
      FCN2(ETA,ZI,XD)=((6.0–2.0*ALPHA)/(1.0–ALPHA)**2.0)
     +              *(ETA)**(2.0–ALPHA)
      QTD=1.0
      ALPHA=0.0
      ETA0=QTD
      ZI0=2.0/(ALPHA–1.0)
      DATA XD0,XDEND,H,TOL/0.0,2.0,0.005,0.001/
      PRINT 190, QTD,ALPHA
      PRINT 200
      PRINT 201, XD0,ETA0,ZI0
5     IF(XD0 .LT. XDEND .AND. ETA0 .GT. 0.0) THEN
        DETA0=FCN1(ETA0,ZI0,XD0)
        ETAP=ETA0+H*DETA0
        DZI0=FCN2(ETA0,ZI0,XD0)
        ZIP=ZI0+H*DZI0
C
      DO 10 I=1,10
        ETAC=ETA0+H*(DETA0+FCN1(ETAP,ZIP,XD0+H))/2.0
        ZIC=ZI0+H*(DZI0+FCN2(ETAC,ZIP,XD0+H))/2.0
        Z=(ABS(ETAC–ETAP)+ABS(ZIC–ZIP))/2.0
        IF(Z .LE. TOL) GO TO 20
        ETAP=ETAC
        ZIP=ZIC
10    CONTINUE
      LD=XD0+H
      PRINT 202, LD
20    XD0=XD0+H
```

```
      PRINT 201, XD0,ETAC,ZIC
      ETA0=ETAC
      ZI0=ZIC
      GO TO 5
      END IF
190   FORMAT(1X,'QTD = ',F5.2,5X,'ALPHA = ',F5.2)
200   FORMAT(///4X,'XD',13X,'ETA',21X,'ZI'/)
201    FORMAT(1X,F5.3,6X,F10.7,12X,F13.7)
202   FORMAT(1X,'AT XD = ',F5.2,' TOLERANCE NOT MET ',
     +    'WITHIN 10 RECORRECTIONS ')
      STOP
      END
```

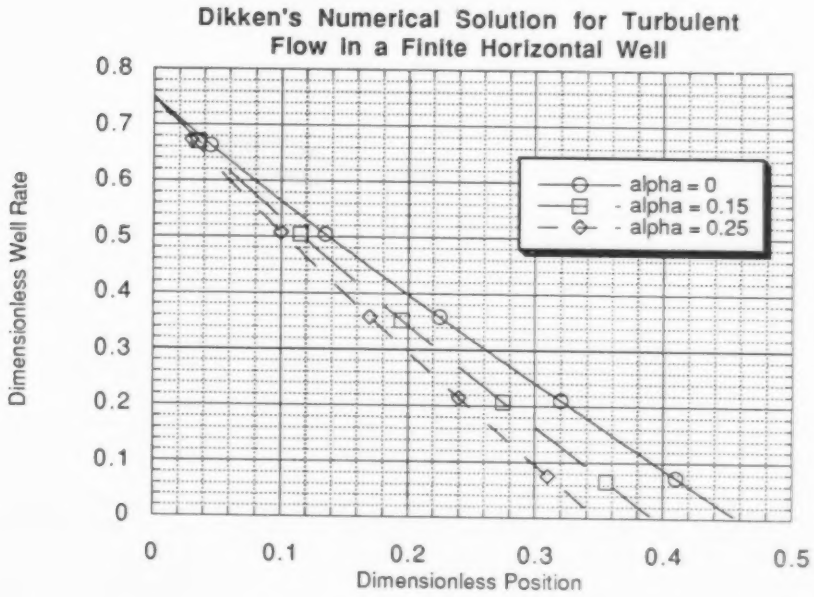

Figure A3: Numerical Solution for Turbulent Flow in Finite Horizontal Well

APPENDIX B

Bipolar Co-ordinate Transformation for Numerical Analysis of Stratified Oil–Water Flows

One of the chief difficulties in numerical solutions to the problem of stratified two–phase flow in pipes is caused by the inhomogeneity of the boundaries, which consist of a circular surface (the pipe wall) and a plane (the interface between the phases). This difficulty may be alleviated by choosing a bipolar co-ordinate system. This set of co-ordinates enables the computing mesh to be fitted to the wall of the pipe and to the rectilinear interface simultaneously. As noted in 3. Literature Review, this method has been employed as part of a numerical solution of stratified two–phase pipe flow by Shoham and Taitel (1984)[47], Issa (1987)[48] and by Hall and Hewitt (1993)[50].

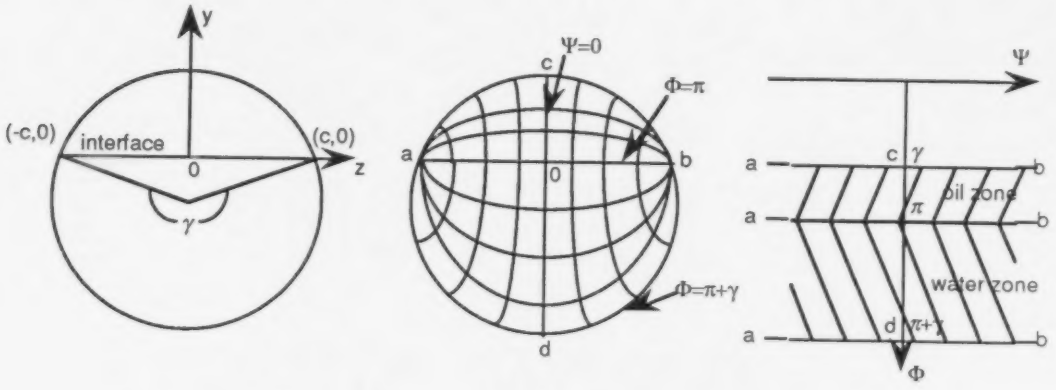

Figure B1: Bipolar Co-oridinate Transformation using Conformal Mapping

If the intersection points are (–c,0) and (c,0) as in the above figure, the conformal transformation which defines the bipolar coordinates is

$$z = ic\cot\left(\frac{\omega}{2}\right) \qquad \text{(B–1)}$$

where,

$w = z + iy$ defines the Cartesian coordinate plane, with z and y as coordinates

$\omega = \Phi + i\Psi$ defines the bipolar coordinate plane, with Φ and Ψ as coordinates

and, $i = \sqrt{-1}$

This conformal mapping allows the transformation of the oil and water cross sections into two infinite strips (as in Figure B1, above), where

$\gamma < \Psi < \pi$ and $-\infty < \Phi < \infty$ for the oil

$\pi < \Psi < \pi + \gamma$ and $-\infty < \Phi < \infty$ for the water

Now solving Equation (B–1) for z and y:

$$z + iy = ic\cot\left(\frac{\Phi + i\Psi}{2}\right)$$

$$= ic\left[\frac{\cos\left(\frac{\Phi}{2} + \frac{i\Psi}{2}\right)}{\sin\left(\frac{\Phi}{2} + \frac{i\Psi}{2}\right)}\right]$$

$$= ic\left[\frac{\cos\left(\frac{\Phi}{2}\right)\cos\left(\frac{i\Psi}{2}\right) - \sin\left(\frac{\Phi}{2}\right)\sin\left(\frac{i\Psi}{2}\right)}{\sin\left(\frac{\Phi}{2}\right)\cos\left(\frac{i\Psi}{2}\right) + \cos\left(\frac{\Phi}{2}\right)\sin\left(\frac{i\Psi}{2}\right)}\right]$$

$$= ic\left[\frac{\cos\left(\frac{\Phi}{2}\right)\cosh\left(\frac{\Psi}{2}\right) - i\sin\left(\frac{\Phi}{2}\right)\sinh\left(\frac{\Psi}{2}\right)}{\sin\left(\frac{\Phi}{2}\right)\cosh\left(\frac{\Psi}{2}\right) + i\cos\left(\frac{\Phi}{2}\right)\sinh\left(\frac{\Psi}{2}\right)}\right]$$

$$\times\left[\frac{\sin\left(\frac{\Phi}{2}\right)\cosh\left(\frac{\Psi}{2}\right) - i\cos\left(\frac{\Phi}{2}\right)\sinh\left(\frac{\Psi}{2}\right)}{\sin\left(\frac{\Phi}{2}\right)\cosh\left(\frac{\Psi}{2}\right) - i\cos\left(\frac{\Phi}{2}\right)\sinh\left(\frac{\Psi}{2}\right)}\right]$$

$$= ic\left[\frac{\cos\left(\frac{\Phi}{2}\right)\cosh^2\left(\frac{\Psi}{2}\right)\sin\left(\frac{\Phi}{2}\right)-\sin\left(\frac{\Phi}{2}\right)\cos\left(\frac{\Phi}{2}\right)\sinh^2\left(\frac{\Psi}{2}\right)}{\sin^2\left(\frac{\Phi}{2}\right)\cosh^2\left(\frac{\Psi}{2}\right)+\cos^2\left(\frac{\Phi}{2}\right)\sinh^2\left(\frac{\Psi}{2}\right)}\right]$$

$$-ic\left[\frac{i\left(\sin^2\left(\frac{\Phi}{2}\right)\sinh\left(\frac{\Psi}{2}\right)\cosh\left(\frac{\Psi}{2}\right)+\cos^2\left(\frac{\Phi}{2}\right)\sinh\left(\frac{\Psi}{2}\right)\cosh\left(\frac{\Psi}{2}\right)\right)}{\sin^2\left(\frac{\Phi}{2}\right)\cosh^2\left(\frac{\Psi}{2}\right)+\cos^2\left(\frac{\Phi}{2}\right)\sinh^2\left(\frac{\Psi}{2}\right)}\right]$$

$$= ic\left[\frac{\sin\left(\frac{\Phi}{2}\right)\cos\left(\frac{\Phi}{2}\right)\left\{\cosh^2\left(\frac{\Psi}{2}\right)-\sinh^2\left(\frac{\Psi}{2}\right)\right\}-i\left\{\sinh\left(\frac{\Psi}{2}\right)\cosh\left(\frac{\Psi}{2}\right)\left[\sin^2\left(\frac{\Phi}{2}\right)+\cos^2\left(\frac{\Phi}{2}\right)\right]\right\}}{\sin^2\left(\frac{\Phi}{2}\right)\cosh^2\left(\frac{\Psi}{2}\right)+\left\{\cos^2\left(\frac{\Phi}{2}\right)\cosh^2\left(\frac{\Psi}{2}\right)-\cos^2\left(\frac{\Phi}{2}\right)\cosh^2\left(\frac{\Psi}{2}\right)\right\}+\cos^2\left(\frac{\Phi}{2}\right)\sinh^2\left(\frac{\Psi}{2}\right)}\right]$$

$$= ic\left[\frac{\sin\left(\frac{\Phi}{2}\right)\cos\left(\frac{\Phi}{2}\right)-i\left\{\sinh\left(\frac{\Psi}{2}\right)\cosh\left(\frac{\Psi}{2}\right)\right\}}{\cosh^2\left(\frac{\Psi}{2}\right)\left\{\sin^2\left(\frac{\Phi}{2}\right)+\cos^2\left(\frac{\Phi}{2}\right)\right\}-\cos^2\left(\frac{\Phi}{2}\right)\left\{\cosh^2\left(\frac{\Psi}{2}\right)-\sinh^2\left(\frac{\Psi}{2}\right)\right\}}\right]$$

$$= ic\left[\frac{\sin\left(\frac{\Phi}{2}\right)\cos\left(\frac{\Phi}{2}\right)-i\left\{\sinh\left(\frac{\Psi}{2}\right)\cosh\left(\frac{\Psi}{2}\right)\right\}}{\cosh^2\left(\frac{\Psi}{2}\right)-\cos^2\left(\frac{\Phi}{2}\right)}\right]$$

$$= ic\left[\frac{2\sin\left(\frac{\Phi}{2}\right)\cos\left(\frac{\Phi}{2}\right)-i2\left\{\sinh\left(\frac{\Psi}{2}\right)\cosh\left(\frac{\Psi}{2}\right)\right\}}{2\cosh^2\left(\frac{\Psi}{2}\right)-2\cos^2\left(\frac{\Phi}{2}\right)}\right]$$

$$= ic\left[\frac{\sin(\Phi)-i\sinh(\Psi)}{2\cosh^2\left(\frac{\Psi}{2}\right)-2\cos^2\left(\frac{\Phi}{2}\right)}\right]$$

$$= ic\left[\frac{\sin(\Phi)-i\sinh(\Psi)}{-\{\cos(\Phi)+1\}+\{\cosh(\Psi)+1\}}\right]$$

$$= ic\left[\frac{\sin(\Phi) - i\sinh(\Psi)}{\cosh(\Psi) - \cos(\Phi)}\right]$$

$$= \frac{ic\sin(\Phi) + c\sinh(\Psi)}{\cosh(\Psi) - \cos(\Phi)} \qquad \text{(B–2)}$$

and therefore,

$$z = \frac{c\sinh(\Psi)}{\cosh(\Psi) - \cos(\Phi)} \quad \text{and} \quad y = \frac{c\sin(\Phi)}{\cosh(\Psi) - \cos(\Phi)} \qquad \text{(B–3)}$$

The metric coefficients defining the arc lengths along the Φ and Ψ co-ordinate lines may be derived from

$$l_\Phi = \sqrt{\left(\frac{\partial z}{\partial \Phi}\right)^2 + \left(\frac{\partial y}{\partial \Phi}\right)^2} \quad \text{and} \quad l_\Psi = \sqrt{\left(\frac{\partial z}{\partial \Psi}\right)^2 + \left(\frac{\partial y}{\partial \Psi}\right)^2} \qquad \text{(B–4)}$$

Finding the values of the partial derivatives used in these two equations from the equations for z and y (B–3) leads to

$$l_\Phi = l_\Psi = \frac{|c|}{\cosh(\Psi) - \cos(\Phi)} \qquad \text{(B–5)}$$

The numerical grid mesh is defined by the specification of the arc lengths of the faces of each grid cell. These are denoted by

$$\Delta\Phi = l_\Phi d\Phi \quad \text{and} \quad \Delta\Psi = l_\Psi d\Psi \qquad \text{(B–6)}$$

The arc length along Φ direction lines is given by

$$\Delta\Phi = \int_{\Phi_1}^{\Phi_2} l_\Phi d\Phi = \int_{\Phi_1}^{\Phi_2} \frac{|c|}{\cosh(\Psi) - \cos(\Phi)} d\Phi \qquad \text{(B–7)}$$

Integration gives:

$$\Delta\Phi = \frac{2|c|}{\sinh(\Psi)}\left[\tan^{-1}\left(\sqrt{\frac{\cosh(\Psi)+1}{\cosh(\Psi)-1}}\tan\left(\frac{\Phi}{2}\right)\right)\right]_{\Phi_1}^{\Phi_2} \quad \text{for} \quad \cosh(\Psi) \neq 1 \qquad \text{(B–8)}$$

and

$$\Delta\Phi = -|c|\left[\operatorname{cotan}\left(\frac{\Phi}{2}\right)\right]_{\Phi_1}^{\Phi_2} \quad \text{for } \cosh(\Psi) = 1 \qquad \text{(B–9)}$$

This case corresponds with the vertical diameter, i.e. $z = 0$. The arc length along the Ψ direction lines is given by

$$\Delta\Psi = \int_{\Psi_1}^{\Psi_2} l_\Psi d\Psi = \int_{\Psi_1}^{\Psi_2} \frac{|c|}{\cosh(\Psi)-\cos(\Phi)} d\Psi \qquad \text{(B–10)}$$

Integration gives:

$$\Delta\Psi = \frac{2|c|}{\sin(\Phi)}\left[\tan^{-1}\left(\sqrt{\frac{\cos(\Phi)+1}{1-\cos(\Phi)}}\tanh\left(\frac{\Psi}{2}\right)\right)\right]_{\Psi_1}^{\Psi_2} \quad \text{for} \quad \cos(\Phi) \neq -1 \qquad \text{(B–11)}$$

and

$$\Delta\Psi = |c|\left[\tanh\left(\frac{\Psi}{2}\right)\right]_{\Psi_1}^{\Psi_2} \quad \text{for } \cos(\Phi) = -1 \qquad \text{(B–12)}$$

which corresponds to the interface position, i.e. y = 0.

The grid distribution in the Ψ direction is therefore determined by specification of Ψ_1 , Ψ_2, etc. on the interface, while the definition of Φ_1 , Φ_2, etc. on the vertical diameter determines the mesh distribution in the Φ direction. The arc lengths are then calculated as above.

The Navier–Stokes equations for each phase may now be written in a general curvilinear orthogonal form. They are, for the water:

$$\frac{1}{l_\Phi l_\Psi}\frac{\partial}{\partial\Psi}\left(\mu_w\frac{l_\Phi}{l_\Psi}\frac{\partial u_w}{\partial\Psi}\right)+\frac{1}{l_\Phi l_\Psi}\frac{\partial}{\partial\Phi}\left(\mu_w\frac{l_\Psi}{l_\Phi}\frac{\partial u_w}{\partial\Phi}\right)-\frac{dP}{dx}=0 \qquad \text{(B–13)}$$

and for the oil:

$$\frac{1}{l_\Phi l_\Psi}\frac{\partial}{\partial\Psi}\left(\mu_o\frac{l_\Phi}{l_\Psi}\frac{\partial u_o}{\partial\Psi}\right)+\frac{1}{l_\Phi l_\Psi}\frac{\partial}{\partial\Phi}\left(\mu_o\frac{l_\Psi}{l_\Phi}\frac{\partial u_o}{\partial\Phi}\right)-\frac{dP}{dx}=0 \qquad \text{(B–14)}$$

The boundary conditions similarly transformed to the ω plane are:

1) At $\Phi=\pi+\gamma$, $u_w=0$ (no slip condition at pipe wall)
2) At $\Phi=\gamma$, $u_o=0$ (same as above)
3) At $\Phi=\pi$, $\frac{\mu_w}{l_\Phi}\frac{\partial u_w}{\partial\Phi}=\frac{\mu_o}{l_\Phi}\frac{\partial u_o}{\partial\Phi}$ (interfacial shear stress condition)
4) At $\Psi=0$, $\frac{\partial u_w}{\partial\Psi}=\frac{\partial u_o}{\partial\Psi}=0$ (symmetry condition)
5) As $\Psi\to\infty$, $u_w=u_o=0$ (no slip condition at wall–interface junction).

The discretized form of the Navier-Stokes Equation (B–13 or B–14) is:

$$\left[\left(\mu\frac{\Delta\Phi}{\Delta\Psi}\right)_2(u_2-u_0)-\left(\mu\frac{\Delta\Phi}{\Delta\Psi}\right)_4(u_0-u_4)\right]+\left[\left(\mu\frac{\Delta\Psi}{\Delta\Phi}\right)_3(u_3-u_0)-\left(\mu\frac{\Delta\Psi}{\Delta\Phi}\right)_1(u_0-u_1)\right]$$

$$-(\Delta\Psi\Delta\Phi)_0\left(\frac{dP}{dx}\right)=0 \qquad \text{(B–15)}$$

The viscosity values apply to each cell face indicated by the subscript and are obtained by interpolation from the nodal values.

This equation may be applied for the case of each liquid phase, and may be re-written implicitly as

$$K_0u_0=K_1u_1+K_2u_2+K_3u_3+K_4u_4+S_0 \qquad \text{(B–16)}$$

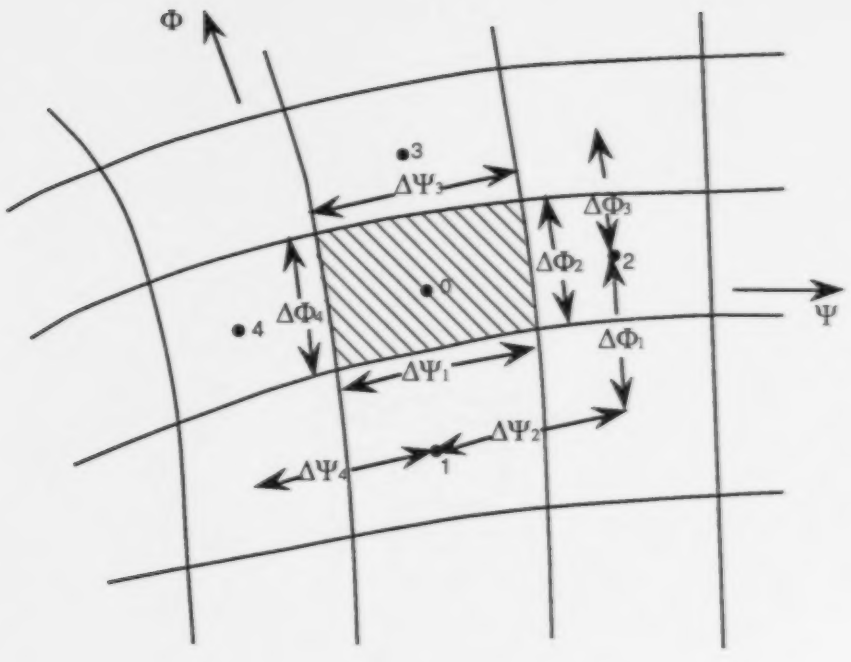

Figure B2: Typical Node in the Numerical Grid

where

$$K_1 = \left(\mu \frac{\Delta\Psi}{\Delta\Phi}\right)_1 \tag{B–17}$$

with similar expressions for the other coefficients on the RHS, and with the source term given by

$$S_0 = -(\Delta\Psi\Delta\Phi)_0\left(\frac{dP}{dx}\right) \tag{B–18}$$

The coefficient for the node we are solving for is given by

$$K_0 = K_1 + K_2 + K_3 + K_4 \tag{B–19}$$

Equation (B–16) is symmetric and therefore may be solved using any normal method of solving sets of linear equations. This set of equations must be solved iteratively, because neither the height of the interface h, nor the pressure gradient dP/dx is known before hand.

Both these quantities must be estimated initially. The velocities for each node over the entire cross section are then obtained by solving the system of equations. This velocity field will not give the correct total flow rate unless the solution has converged, since the pressure gradient used is only an estimate (there is no associated error in matching the grid to the cross section as there was with the Cartesian grid case). The pressure gradient is then adjusted so as to satisfy the overall continuity. This is in itself an iterative or trial–and–error process of modifying the pressure gradient such that the new velocity matrix satisfies the overall flow rate:

$$\sum_{w+o} A_0 u_0 = Q_w + Q_o \qquad \text{(B–20)}$$

where A_0 is the cell cross sectional area, Q_w and Q_o are the flow rates of the water and oil phases, respectively, and the summation is over all the grid cells in the pipe cross section.

Finally, the interface height is dealt with. Again, unless the solution has converged, the velocity and flow cross sectional area of each phase (which is dependent on h) will not satisfy the overall flow rate of that phase. For example, for the oil phase h is adjusted until

$$\sum_{o} A_0 u_0 = Q_o \qquad \text{(B–21)}$$

When this equation is satisfied, so must the corresponding equation for the water phase be satisfied.

APPENDIX C

C.1 Colebrook and White Correlation C Program Listing

The following C program listing solves for the single–phase Colebrook and White friction factor, given the viscosity, density, pipe diameter, roughness, and flow rate.

```
/* This program uses the Colebrook and White friction factor corelation to calculate the
friction factor for values of dimensional roughness (k) between 1.5e-6 and 1.5e-3, for
single-phase turbulent pipe flow over the whole range of turbulent Reynolds Numbers. */

# include <stdio.h>
# include <math.h>
# define M 10

main()
{
float d,rho,mu,pi,k,temp,err;
float f[M],fnew[M],re[M],q[M];
int i,j,iteration;

pi=3.1415926;
d=0.0261239;
rho=845.1;
mu=0.0024;
k=1.5e-6;

q[0]= 6.0783086e-5 ;
q[1]= 9.204008e-5 ;
q[2]= 1.311132e-4 ;
q[3]=1.701825565e-4 ;
q[4]= 2.0143955e-4 ;

do
{
printf("k=%e\n", k);
for(i=0; i<=4; i++)
{
iteration=0;
re[i]=(4*rho*q[i])/(pi*d*mu);
f[i]=fnew[i]=0.5;

do
{
temp=err=0.0;
f[i]=fnew[i];
temp=1.74-2.0*log10((2.0*k)/d+18.7/(re[i]*sqrt(f[i])));
fnew[i]=1.0/(temp*temp);
```

```
iteration++;
err=(fnew[i]-f[i]);
if (err<0.0) err=-err;
/* printf("err=%f\n",err); */
if(iteration>100) printf("iterations > 100\n");
} while(err>1.0e-7 && iteration<105);
printf("f=%.9f\titeration=%d\n", fnew[i],iteration);
}
k=k+5.0e-6;
} while(k<1.5e-4);
}
```

C.2 Gemmell and Epstein[40] Stratified Model

The following C program listing may be used to determine the two–phase liquid–liquid pressure drop if the single–phase pressure drop behaviour of one of the phases and the interface height (in situ volume fraction) are known beforehand.

```
/* This program uses the theory outlined in "Numerical analysis of stratified laminar flow
of two immiscible newtonian liquids in a circular pipe", by Gemmell & Epstein, Can. J. of
Chem. Engg., Oct. 1962[40]. The assumptions are perfectly stratified, laminar two–phase
liquid–liquid pipe flow, with no slip at the pipe walls or the interface. vfrf, or the factor by
which the flow rate of an oil may be increased for the same pressure gradient by the
addition of a second liquid (water, say) to the flow stream, is calculated. The program
divides the cross-section of the pipe into a Cartesian grid depending on the desired density
(NDIV). The number of nodes is counted and then the velocity at each node for both
phases and the interface is calculated. These velocities are averaged to then calculate the
vfrf, which then may be used to calculate dimensional pressure drops outside the program.
*/

#include <stdio.h>
#include <math.h>
#define MAX 1440
#define NDIV 30
float r;
void solution();
int max,myabs();
float eqn[MAX][MAX];
float rhs[MAX],soln[MAX];
float soln1[MAX];
float sumA;
float sumB, soln2[MAX], ivr;
float vfrf, vfrb;
int count=0,level,B_lev;


int Arr_i[MAX];
int Arr_j[MAX];
int myabs(k)
```

```
int k;
{
if (k <0) return(-k);
 else return (k);
}
float dist(i,j)
int i,j;
{
return(sqrt(myabs(i-NDIV)*myabs(i-NDIV)*r*r/(NDIV*NDIV)
+j*j*r*r/(NDIV*NDIV)));
}

main()
{
int i,j,c,c1;
int counter[MAX][MAX];
int i_cnt[MAX];
float t,muprime;
printf("Give the length of the radius:\n");
scanf("%f",&r);
printf("Give the level of B liquid from bottom(in terms of divisions):\n");
scanf("%d",&level);
printf("Give muprime:\n");
scanf("%f",&muprime);

for (i=0;i<=2*NDIV;i++)
{
i_cnt[i]=0;
        for(j=0;j<=NDIV;j++)
                if (dist(i,j)<r) {          Arr_i[count]=i;
                                            Arr_j[count]=j;
                                    counter[i][j]=count; count++;
                                            i_cnt[i]+=1;
                        }
}
max = count-1;
B_lev=2*NDIV-level;
for(c=0;c <=max;c++)
for (c1=0;c1<=max;c1++) eqn[c][c1] =0;

for (c=0;c <=max;c++)
{
  i=Arr_i[c];
  j=Arr_j[c];
  if (i != B_lev)  {
          if (i < B_lev) rhs[c]= -8 /* * (1/NDIV)*(1/NDIV)*/;
            else rhs[c]= -8 * muprime/* * (1/NDIV)*(1/NDIV)*muprime*/;
              if (j < (i_cnt[i]-1)) {
          if (i>0)
{
        if (j <= i_cnt[i-1]-1)

                                eqn[c][counter[i-1][j]]=1;
```

```
else  if (j !=0){
                        t=r*r;
t-= (myabs((i-1)-NDIV)*myabs((i-1)-NDIV)*r*r/(NDIV*NDIV));
                    t=sqrt(t);
                    t= t - i_cnt[i-1]*r/NDIV + r/NDIV;
                    eqn[c][counter[i-1][j-1]]=- (r/NDIV -t)/t;
}
}
              if (j>0)
                    eqn[c][counter[i][j-1]]=1;
           if (j!=0)
                    eqn[c][counter[i][j+1]]=1;
                    else eqn[c][counter[i][j+1]]=2;
            if (j <= i_cnt[i+1]-1)
                                    eqn[c][counter[i+1][j]]=1;

else if (j!=0){
                        t=r*r;
t-= (myabs((i+1)-NDIV)*myabs((i+1)-NDIV)*r*r/(NDIV*NDIV));
                    t=sqrt(t);
                    t= t - i_cnt[i+1]*r/NDIV + r/NDIV;
                    eqn[c][counter[i+1][j-1]]=- (r/NDIV -t)/t;
}
                    eqn[c][c]=-4;
                                    }
                    else if (j == (i_cnt[i]-1)) {


              if (i>0)
{
           if (j <= i_cnt[i-1]-1)
                                    eqn[c][counter[i-1][j]]=1;

else if (j!=0) {
                        t=r*r;
t-= (myabs((i-1)-NDIV)*myabs((i-1)-NDIV)*r*r/(NDIV*NDIV));
                    t=sqrt(t);
                    t= t - i_cnt[i-1]*r/NDIV + r/NDIV;
                    eqn[c][counter[i-1][j-1]]=- (r/NDIV -t)/t;
}
}
           if (j <= i_cnt[i+1]-1)
                                    eqn[c][counter[i+1][j]]=1;

else if (j!=0) {
                        t=r*r;
t-= (myabs((i+1)-NDIV)*myabs((i+1)-NDIV)*r*r/(NDIV*NDIV));
                    t=sqrt(t);
                    t= t - i_cnt[i+1]*r/NDIV + r/NDIV;
                    eqn[c][counter[i+1][j-1]]=- (r/NDIV -t)/t;
}
              if (j>0)
                    eqn[c][counter[i][j-1]]=1;
                    eqn[c][counter[i+1][j]]=1;
```

```
                        t=r*r;
t-= (myabs(i-NDIV)*myabs(i-NDIV)*r*r/(NDIV*NDIV));
                    t=sqrt(t);
                    t= t - i_cnt[i]*r/NDIV + r/NDIV;
                    eqn[c][c]=-4- (r/NDIV -t)/t;
                  }
                  }
        else {
            rhs[c]=-16*muprime/(muprime +1) /* *(1/NDIV)*(1/NDIV)*/;
          if (j < i_cnt[i]-1) {

if (i>0)                    eqn[c][counter[i-1][j]]=2*muprime/(muprime +1);
                    if (j>0) eqn[c][counter[i][j-1]]=1;
          if (j!=0)
                    eqn[c][counter[i][j+1]]=1;
      else                eqn[c][counter[i][j+1]]=2;
                    eqn[c][counter[i+1][j]]=2/(muprime +1);
                    eqn[c][c]=-4;
                                }
                    else if (j == (i_cnt[i]-1)) {
                    eqn[c][counter[i-1][j]]=2*muprime/(muprime +1);
                    eqn[c][counter[i][j-1]]=1;
                    eqn[c][counter[i+1][j]]=2/(muprime +1);
                        t=sqrt(r*r- (myabs(i-NDIV)*myabs(i-NDIV)*r*r/(NDIV*NDIV)));
                    t= t - i_cnt[i]*r/NDIV + r/NDIV;
                    eqn[c][c]=-4- (r/NDIV -t)/t;
              }
            }
}
/* code for solver with eqn as max X max aray and rhs as max X 1 array of rhs
*/


solution();

/* the following calculates the volumetric flow rate factor, which is identical
        to the pressure gradient reduction factor        */

vfrf=2.0*(sumA/3.1415926);
vfrb=2.0*(sumB/3.1415926);
ivr=sumA/sumB;      /*  this is the input volume ratio  */
printf("vfrf=%f\n",vfrf);
printf("vfrb=%f\n",vfrb);
printf("ivr=%f\n",ivr);

}


void solution()
{
/* THIS FUNCTION IS THE GAUSS ELIMINATION METHOD TO SOLVE FOR
DELP  */

int  n,m,n1,k1,k2,i,j,k,i1,j1;
```

```
float eqn2[MAX][MAX],eqn1[MAX][MAX],x[MAX];
float b0,b1,ccc,s,y;
float bbb[MAX];
sumA=0.0;
sumB=0.0;

n=max;
for(i=0;i<=n;++i)
eqn[i][n+1]=rhs[i];

m=m+1;
n=n+1;
m=n+1;
for(i=1;i<=n;++i)
for(j=1;j<=m;++j)
{
eqn1[i][j]=eqn[i-1][j-1];
eqn2[i][j]=eqn[i-1][j-1];
}
/*---------------------------*/
n1=n-1;
for(k=1;k<=n1;++k)
{
k1=k+1;
k2=k;
b0=myabs(eqn2[k][k]);
for(i=k1;i<=n;++i)
{
b1=myabs(eqn2[i][k]);
if((b0-b1)<0)
{
b0=b1;
k2=i;
}
}
if((k2-k) != 0)
{
/* interchange rows to obtain the largest pivot element */
for (j=k;j<=m;++j)
ccc=eqn2[k2][j];
eqn2[k2][j]=eqn2[k][j];
eqn2[k][j]=ccc;
}
for(i=k1;i<=n;++i)
{
for(j=k1;j<=m;++j)
eqn2[i][j]=eqn2[i][j]-eqn2[i][k]*eqn2[k][j]/eqn2[k][k];
eqn2[i][k]=0.0;
}
}

/* Apply back substitution */
```

```
x[n]=eqn2[n][m]/eqn2[n][n];

for(i1=1;i1<=n1;++i1)
{
i=n-i1;
s=0.0;
j1=i+1;
for(j=j1;j<=n;++j)
s=s+eqn2[i][j]*x[j];
x[i]=(eqn2[i][j]-s)/eqn2[i][i];


}

/* printing data */


/* checking */
for(i=1;i<=n;++i)
{
y=0.0;
for(j=1;j<=n;++j)
y=y+x[j]*eqn1[i][j];

/* printf("y=%f rhs=%f\n",y,rhs[i-1]) ; */

}
/* for (i=1;i<=max;i++)  printf("%f\n",x[i]); */
/*for this program only */
n-=1;
/* for (i=0;i<=n;++i)
for (j=0;j<=n;j++)
if (eqn[i][j] != 0)  printf("i=%d,j=%d and
[%d,%d]=%f\n",Arr_i[i],Arr_j[i],Arr_i[j],Arr_j[j],eqn[i][j]); */

for(i=0,i<=n;++i)
{
soln[i]=x[i+1]/(NDIV*NDIV);
/*printf("node = %d \t value =%f corresponds to i=%d and
j=%d\n",i,soln[i],Arr_i[i],Arr_j[i]);
*/

if (Arr_i[i]<B_lev){
soln1[i]=soln[i]/(NDIV*NDIV);
sumA+=soln1[i];
}
else if (Arr_i[i]>B_lev)  {
soln2[i]=soln[i]/(NDIV*NDIV);
sumB+=soln2[i];
}

}
}/* soln ends here */
```

C.3 Field–Scale Predictive Models

C.3.1 Non–Reservoir–Coupled Constant Influx Model

The following Mathematica program listing solves for the pressure profile along a open–hole completed horizontal well with known constant influx rate. It is not coupled to reservoir flow.

```
(* Mathematica program listing Lopen.m

This program assumes a constant influx and solves for open hole completions divided into
n segments. The procedure is not coupled to reservoir flow and therefore is non–iterative.
*)

n=4000;
l=1000;
q=2000; (* This is the specified flowrate, m3/day  *)
mu=N[ 5/10000,32];
rho=N[750,32];
d=N[125/1000,32];
area=N[(Pi d^2)/4,32];
kappa=N[2/100,32];
pd=1000000;
pp=Array[p,{n}]; Do[pp[[i]]=pd,{i,n}];
Do[y[i]=(i)(l/(n)),{i,n}];
qw=Array[h,{n}];re=Array[m,{n}];ff=Array[o,{n}];
qq=Array[b,{n}];ffw=Array[s,{n}];ffa=Array[t,{n}];
qw[[1]]=q/(24 3600);
Do[qq[[i]]=qw[[1]]/n, {i,n}];

        Do[qw[[i]]=N[Sum[qq[[j]],{j,i,n,1}],16],{i,n}];
        Do[re[[i]]=N[(rho d qw[[i]])/(2 mu area), 16],{i,n}];
        Do[ffw[[i]]=N[If[re[[i]] < 2300, 64/re[[i]], (1/4)
                (Log[10,(kappa/((37/10)d))+((574/100)/(re[[i]]^
                (9/10)))])^-2], 16],{i,n}];
        Do[ffa[[i]]=N[((2 d)/(l/n))(2(qq[[i]])/(qw[[i+1]])+
                (qq[[i]]/qw[[i+1]])^2), 16], {i,n-1}];
        ffa[[n]]=0;
        Do[ff[[i]]=N[ffw[[i]]+ffa[[i]], 16], {i,n}];
        Do[pp[[i+1]]=N[pp[[i]]+((rho ff[[i+1]] qw[[i+1]]^2)/(2 d area^2))
                Abs[y[i+1]-y[i]], 16],{i,n-1}];

Print[pp[[1]]]
Do[Print[FortranForm[pp[[i]]]], {i,2,n,(n/80)}]
Print[FortranForm[pp[[n]]]]
```

C.3.2 Landman and Goldthorpe[4] Cased and Perforated Model

The following Mathematica program listing is based on work by Landman and Goldthorpe[4], and incorporates the Asheim *et al.*[62] accelerational pressure drop model. The pressure profile of a cased and perforated horizontal well located in an infinite and homogeneous reservoir is solved for iteratively. A matrix of dimension nxn, where n is the number of perforations specified, must be inverted as part of the solution.

```
(* LANDMAN SIMULATOR FOR MATHEMATICA *)

(* The following code is written for Mathematica. It is based on a numerical method described by
Landman and Goldthorpe, "Optimization of perforation distribution for horizontal wells", SPE
23005, presented at the SPE Asia-Pacific Conference, Nov. 1991[4] . The model couples the Darcy
flow into each perforation with the one-dimensional momentum equations for pipe flow. It is
strictly single phase, incompressible. All units are standard SI unless otherwise noted. Please
note that the calculation time and storage requirements depend exponentially on the number of
perforations specified, n, as an nxn matrix must be inverted. *)

n=500;
l=200;
mu=N[2/1000,32];
rho=N[750,32];
d=N[125/1000,32];
area=N[(Pi d^2)/4,32];
kappa=N[1/1000,32];
delta=N[1/100,32];
a=N[35/100,32];
k=N[(75/100)(9869)/(10^16),32];
c:=N[mu/(4 Pi k),32];
pd=1000000;
pp=Array[p,{n}]; Do[pp[[i]]=pd,{i,n}];
ppnew=Array[v,{n}]; Do[ppnew[[i]]=pd,{i,n}];
ppdif=Array[w,{n}];
test=10000;
toler:=pd/(10^5);
Do[y[i]=(i)(l/(n)),{i,n}];
q = Array[ h,{n}];
re = Array[ m,{n}];
ff = Array[ o,{n}];
ffw = Array[ s,{n}];
ffa = Array[ t,{n}];
aa=Array[f,{n,n}];
Do[aa[[i,j]]=If[i==j,c(-2/a)Log[delta/a],c/Abs[y[i]-y[j]]],{i,n},{j,n}];
aA=Inverse[aa]; (*aa.aA*)

While[ test > toler,
        qq=aA . pp; (*N[qq]*)
```

```
    Do[ q[[i]] = Sum[qq[[j]],{j,i,n,1}],{i,n}];
    Do[ re[[i]] = (rho d q[[i]])/(2 mu area),{i,n}];
    Do[ ffw[[i]] = If[ re[[i]] < 2300, 64/re[[i]],
          (1/4)(Log[10,(kappa/((37/10)d))+((574/100)/
          (re[[i]]^(9/10)))])^-2],{i,n}];
    Do[ffa[[i]] =((2 d)/(l/n))((2 qq[[i]]/q[[i+1]]) + (qq[[i]]/q[[i+1]])^2),
          {i,n-1}];
    ffa[[n]]=0;
    Do[ ff[[i]] = ffw[[i]] + ffa[[i]], {i,n}];
    Do[ppnew[[i+1]] = ppnew[[i]]+((rho ff[[i+1]] q[[i+1]]^2)/(2 d area^2))
          Abs[y[i+1]-y[i]],{i,n-1}];
    Do[ppdif[[i]]=Abs[ppnew[[i]]-pp[[i]]], {i,n}];
  test = Max[ppdif];
    Do[pp[[i]] = ppnew[[i]],{i,n}];
];

Print[FortranForm[ppnew[[1]]]]
Do[Print[FortranForm[ppnew[[i]]]], {i,2,n,(n/50)}]
Print[FortranForm[ppnew[[n]]]]
```

C.3.3 Landman[8] Hypergeometric Model

The following Mathematica program listing was developed from Landman's[8] hypergeometric model for open–hole completed horizontal wells (coupled to reservoir flow as in the cased and perforated model), modified to include the effects of accelerational pressure drop[62] and laminar flow. Landman's[8] original hypergeometric model is based on Dikken's[3] work and produces results practically identical to those of the Dikken's (see Appendix A).

```
(*Program Lhyper1.m

This program uses the Gauss hypergeometric function in conjunction with
Mathematica's root finding algorithm to solve for the pressure drop along
an open–completed horizontal wellbore. *)

(*<<Statistics.m*)
Off[FindRoot::frmp]; (* shutting off annoying messages *)
Off[ReplaceAll::reps];
(* Off[Nsum::nsnum]; *)
Off[Part::partw];
alpha=0.23; (* Blasius exponent *)
cc=0.3164;  (* Blasius constant *)
n=200;
l=500;
rho=850;
d=0.20;
r=d/2;
mu= 2 10^-3;
```

```
k=986.9 10^-15;
qpd=500;  (* flowrate of well in m3/d *)
qps=qpd/(24 3600);
(*js=400 10^-12;*)
jjs=Array[jj,{n}];
Do[y[i]=(i)(l/(n)),{i,n}];
Do[jjs[[i]]=(4 Pi k/mu)(Log[(l-y[i]+Sqrt[(l-y[i])^2+r^2])/(-y[i]+
      Sqrt[y[i]^2+r^2])])^-1, {i,n}];
(*js=Mean[jjs];*)  (* finding an approximation of the specific *)
js=Sum[jjs[[i]], {i,1,n}]/n;  (* productivity index, Js  *)
a=0.5;
b=1/(3-alpha);
c=(4-alpha)/(3-alpha);
z=(-qps^(3-alpha))/kk;
rw=((8 cc rho)/(Pi^2 d^5)) ((Pi d mu)/(4 rho))^alpha;
hh=Hypergeometric2F1[a,b,c,z];

kk1=kk /. FindRoot[l==Sqrt[(3-alpha)/(2 js rw)] qps hh (1/Sqrt[kk]),
      {kk, {10,20}}, MaxIterations -> 100];

pd=N[Sqrt[(kk1+qps^(3-alpha))(2 rw)(1/(js (3-alpha)))]]; (*drawdown*)

qq = Array[p,{n}];
qq1 = Array[g,{n}];
hh1 = Array[e,{n}];
z1 = Array[m,{n}];
Do[z1[[i]]=(-qq[[i]]^(3-alpha))/kk1, {i,n}];
Do[hh1[[i]]=Hypergeometric2F1[a,b,c,z1[[i]]], {i,n}];
Do[qq1[[i]]=qq[[i]] /. FindRoot[l-y[i]==Sqrt[(3-alpha)/(2 js rw)] qq[[i]]
      hh1[[i]] (1/Sqrt[kk1]),Evaluate[{qq[[i]], {0,1}}],
      MaxIterations->100],{i,n}]; (* well rates *)

pp=Array[u,{n}];
pe=pd; (* equate press. at res. boundary with drawdown at well heel *)
Do[pp[[i]]=pe-(Sqrt[(2 rw)/((3-alpha)js)])(Sqrt[qq1[[i]]^(3-alpha)+kk1]),
      {i,n}]; (* well pressures *)
qqs=Array[o,{n}];
Do[qqs[[i]]=js*(pe-pp[[i]]), {i,n}];  (* influx rate per unit length *)
deltapw=pp[[n]]-pp[[1]];
lambda = qps*((2 rw)/((3-alpha)js pd^2))^(1/(3-alpha));


(*
      Here the calculated influx rate per unit length vector is used
as input to a simple routine to determine separately the wall and
accelerational friction factors for the given well flow.  These are in
turn used to calculate the pressure drop across the well. In certain
situations the accelerational friction factor and/or the laminar flow
friction factor may be significant in terms of the pressure drop.
*)

area=N[(Pi d^2)/4,32];
kappa=N[8/100000,32];  (* well roughness *)
pp2=Array[t,{n}]; Do[pp2[[i]]=0,{i,n}];
```

```
pp3=Array[vv,{n}];
re=Array[mm,{n}];ff=Array[oo,{n}];
ffw=Array[ss,{n}];ffa=Array[tt,{n}];
qq2=Array[uu,{n}];ffw1=Array[bb,{n}];

h=l/n;
Do[re[[i]]=N[(rho d qq1[[i]])/(2 mu area), 16],{i,n}];(*Reynolds Numbers*)
Do[ffw[[i]]=N[(1/4)
        (Log[10,(kappa/((37/10)d))+((574/100)/(re[[i]]^
        (9/10)))])^-2, 16],{i,n-1}];
(*      Do[ffw[[i]]=N[cc*re[[i]]^
                (-alpha),16], {i,n-1}];*)
        Do[ffw1[[i]]=N[If[re[[i]] < 2300, 64/re[[i]],(1/4)
                (Log[10,(kappa/((37/10)d))+((574/100)/(re[[i]]^
                (9/10)))])^-2], 16],{i,n-1}];
        ffw[[n]]=ffw1[[n]]=ffa[[n]]=0;
        Do[ffa[[i]]=N[((2 d)/h)(2*h(qqs[[i]])/(qq1[[i]])+
                ((h*qqs[[i]])/qq1[[i]])^2), 16], {i,n-1}];
        Do[ff[[i]]=N[ffw1[[i]]+ffa[[i]], 16], {i,n}];
        pp2[[1]]=pp3[[1]]=pp[[1]];
        Do[pp2[[i+1]]=(pp2[[i]]+((rho ffw[[i]] qq1[[i]]^2)/
                (2 d area^2)) Abs[y[i+1]-y[i]]),{i,n-1}];
        Do[pp3[[i+1]]=(pp3[[i]]+((rho ff[[i]] qq1[[i]]^2)/
          (2 d area^2)) Abs[y[i+1]-y[i]]),{i,n-1}];

Print[l]
Print[n]
Print[FortranForm[N[qpd]]]
Print[FortranForm[N[js]]]
Print[FortranForm[N[pd]]]
Print[N[pp[[1]],8]," ",N[pp2[[1]],8]," ",
N[pp3[[1]],8]," ",FortranForm[N[qqs[[1]]]]]
Do[Print[N[FortranForm[pp[[i]]],8]," ",N[pp2[[i]],8]," ",
N[pp3[[i]],8]," ",FortranForm[N[qqs[[i]]]]],
        {i,2,n,(n/50)}]
Print[N[FortranForm[pp[[n]]],8]," ",N[pp2[[n]],8]," ",
N[pp3[[n]],8]," ",FortranForm[N[qqs[[n]]]]]
```